

GRAIN PACKING RESISTANCE TO PARTICLE MOBILITY AND THE INFLUENCE
OF SALMON SPAWNING ON STREAM BED STABILITY AND STORAGE AND
EXCHANGE OF MARINE NUTRIENTS IN STREAM CHANNELS

A Dissertation

Presented in Partial Fulfillment of the Requirements for the

Degree of Doctorate of Philosophy

with a

Major in Water Resources

in the

College of Graduate Studies

University of Idaho

by

Todd H. Buxton

June 2014

Major Professors: Elowyn M. Yager, Ph.D and Alexander K. Fremier, Ph.D.

Authorization to Submit Dissertation

This dissertation of Todd H. Buxton, submitted for the degree of Doctor of Philosophy with a major in Water Resources and titled “Grain Packing Resistance to Particle Mobility and the Influence of Salmon Spawning on Stream Bed Stability and Storage and Exchange of Marine Derived Nutrients in Stream Channels” has been reviewed in final form. Permission, as indicated by the signatures and dates below, is now granted to submit final copies to the College of Graduate Studies for approval.

Major Professors:

_____ Date: _____
Elowyn M. Yager

_____ Date: _____
Alexander K. Fremier

Committee
Members:

_____ Date: _____
John M. Buffington

_____ Date: _____
Marwan A. Hassan

Department
Administrator:

_____ Date: _____
Jan Boll

College of Natural
Resources Dean:

_____ Date: _____
Kurt Pregitzer

Final Approval and Acceptance by the Dean of the College of Graduate Studies:

_____ Date: _____
Jie Chen

Abstract

Pacific salmon (*Oncorhynchus spp.*) influence the structure and productivity of stream ecosystems by altering the stability of river beds during spawning and delivering marine derived nutrients (MDN) to watersheds. Although much has been learned about the physical and ecological roles of salmon in streams, it remains unclear how spawning modifies grain packing, streambed stability, and the residence time and exchange of MDN in streambeds.

A female salmon modifies streambeds by using rapid undulations of her tail to build a nest (redd) for spawning. During redd construction, streambed sediments are mixed, fines are winnowed, and grain packing is loosened as the female moves sediment into a dune-like mound (tailspill) while digging a pit in which to deposit her eggs. This process was simulated on water-worked beds composed of mixed-grain sizes in a laboratory flume, and measurements on simulated redds and bed surfaces undisturbed by spawning were used to quantify grain packing resistance to particle motion and the relative stability of redds and unspawned beds.

Grain packing resistance was determined as the difference between the total resistance to granular motion (measured with a load cell) and that due to pocket resistance (measured with a tilt board) on the flat portion of simulated redds and planar unspawned beds. Packing was the primary form of resistance to grain motion, exceeding pocket resistance by as much as 80%. Packing also increased calculations of critical bed shear stress and Shields stress and decreased the exponent in a grain hiding function, promoting conditions that tend toward equal mobility.

Experiments determining packing resistance were expanded to the entire redd structure, and the stability of redds and unspawned beds was assessed with calculations of critical shear stress, estimates of boundary shear stress, visual measurements of sediment mobility, and bedload transport measurements. Findings indicate packing resistance to grain motion was up to 39% lower on redds, which resulted in lower critical shear stress on spawned surfaces. This in combination with flow convergence elevating boundary shear stress on the tailspill led to incipient motion being observed at a bed-average shear stress that was 22% lower on a redd. Visual observations were confirmed as the average mass transport rate of sediment per unit bed area was nearly 5 times higher on a redd than unspawned bed. The finding that redds are unstable compared to unspawned beds suggests a linkage between salmon spawning and streambed mobility that may have implications for the formation and maintenance of fish habitats in salmon-bearing streams.

The residence time of MDN delivered to streams by salmon influences stream productivity since biochemical processing requires a certain amount of time to occur. Salmon spawning winnows fine sediment and loosens packing, which increase sediment porosity and hydraulic conductivity. This combined with topographically-forced pressure variations pumping water through redds may elevate hyporheic exchange and decrease the residence time ($=\text{hyporheic volume}/\text{hyporheic exchange flux}$) of MDN in the bed. An evaluation of these influences indicates the residency of MDN decreases with increased proportions of a planar bed surface occupied by redds, from 5.79 h on an unspawned bed to 0.03 h for a mass spawned bed (1.0 spawning). Shorter residence times with increased spawning results from hyporheic exchange rising over four orders of magnitude with spawning while hyporheic volume increased less than an order of magnitude. High hyporheic exchange associated with

redds increases nutrient storage compared to the exchange that occurs in unspawned beds, suggesting a positive feedback between spawning activity and nutrient uptake that may promote salmon reproduction and future returns of adult salmon.

Acknowledgements

I would like to thank my committee for their help in accomplishing this work. Special thanks to Alex Fremier for his persistent and ultimately successful push to fund this project. Special thanks also to Marwan Hassan for his enthusiasm and support throughout this project. I am also indebted to Elowyn Yager and John Buffington for sharing their keen knowledge of rivers and for their dogged editing of my writing. Witnessing Drs. Yager and Buffington's scientific prowess and calm, careful guidance was itself an education.

It takes a community to accomplish research. Heidi Schott loaned her load cell and Chris Cochella provided advice for measuring grain resistance to movement with load cells. Tom Quinn and Smokey Pittman shared data on redds in streams, and Adam Dresser and Mark Wattier provided feedback on several ideas in this study. Thanks to Jan Boll for securing funding to complete my work, and to Kurt Pregitzer for granting it through a U.S.

Department of Agriculture - McIntire-Stennis Federal appropriation to the University of Idaho. Funding was also provided by a U.S. Geologic Survey S-104B grant to Alex Fremier. Thanks also to Dillon Wardwell and Dave Johnson for help with math. Rick Healy helped with VS2DTI and Daniele Tonina aided my understanding of hyperheic flow in Chapter 4. I appreciate Bob Basham and Ralph Budwig's guidance in the flume. Special thanks to Eric Beach of the Green Diamond Resource Company in Shelton, WA for providing access to Kennedy Creek, to Chris Olberding for housing during fieldwork on Kennedy Creek, and to Sister Louise Olberding for her interest in rivers and my research in them.

Above all, I am indebted to my fiancé Cindy Adams for her support during this project and for her assistance in the flume. I could not have accomplished this work without her.

Dedications

Mom

(Kathy M. Buxton)

(1944 – 2009)

Scooby Buxton

(1991 – 2011)

Table of Contents

Authorization to Submit Dissertation	ii
Abstract.....	iii
Acknowledgements.....	vi
Dedication.....	vii
Table of Contents.....	viii
List of Figures.....	xii
List of Tables	xx
Chapter 1: General Introduction	1
1.1 References.....	5
Chapter 2: Grain Packing Resistance to Particle Mobility	9
2.1 Abstract.....	9
2.2 Introduction.....	10
2.3 Materials and Methods	13
2.3.1 Experimental Setup.....	13
2.3.2 Redd Construction... ..	15
2.3.3 Framework for Determining Packing Resistance	16
2.3.4 Total Resistance Force Measurements	18
2.3.5 Pocket Resistance Measurements	19
2.3.6 Equivalence of Methods	21
2.3.7 Monte Carlo Simulations.....	22
2.3.8 Embeddedness	23
2.4 Results.....	25

2.4.1	Grain Size Distributions, Protrusion, Embeddedness.....	25
2.4.2	Packing Friction Coefficients	27
2.4.3	Predictive Equation for Packing Friction Coefficients.....	34
2.4.4	Critical Boundary Shear Stress	38
2.4.5	Grain Hiding Function and Shields Stress.....	41
2.5	Discussion.....	44
2.6	Summary.....	47
2.7	References.....	50
Chapter 3: The Relative Stability of Salmon Redds and Unspawned Streambeds.....		58
3.1	Abstract.....	58
3.2	Introduction.....	59
3.3	Materials and Methods	62
3.3.1	Overview.....	62
3.3.2	Field Measurements.....	63
3.3.3	Experimental Scaling.....	64
3.3.4	Experimental Layouts	68
3.3.5	Bed Construction	70
3.3.6	Evaluation of Simulated Spawning	71
3.3.7	Experiment 1: Grain Packing Resistance and Critical Shear Stress ...	72
3.3.7.1	Mathematical Framework	71
3.3.7.2	Total Resistance Force Measurements	74
3.3.7.3	Pocket Resistance Measurements	76
3.3.7.4	Monte Carlo Simulations.....	76

3.3.7.5 Critical Shear Stress Calculations.....	77
3.3.8 Experiment 2: Boundary Shear Stress	78
3.3.9 Experiment 3: Measurements of Grain Mobility.....	79
3.4 Results.....	81
3.4.1 Simulated Spawning, Redds, and Unspawned Beds	81
3.4.2 Packing Friction Coefficients	83
3.4.3 Critical Shear Stress.....	87
3.4.4 Boundary Shear Stress.....	90
3.4.5 Mobility Experiment.....	92
3.5 Discussion.....	95
3.6 Summary.....	103
3.7 References.....	105

Chapter 4: The Influence of Salmon Spawning on the Residence Time and Exchange of

Marine Derived Nutrients in Streambeds	118
4.1 Abstract.....	118
4.2 Introduction.....	119
4.3 Methods	123
4.3.1 Overview.....	123
4.3.2 Field Site.....	125
4.3.3 Redds and Unspawned beds in VS2DTI	125
4.3.4 Hyporheic Flow Simulations	130
4.3.5 Hyporheic Flux and Residence Time of MDN.....	133
4.4 Results.....	135

4.4.1 Base Simulation135

4.4.2 Sensitivity Runs140

4.5 Discussion and Conclusions143

4.6 References.....149

Appendix A: Shear Stress Partitioning162

List of Figures

Figure 2.1: Bulk grain-size distributions before water working and surface grain-size distributions after water working for each sediment mixture and bed (US=unspawned, LB=left bank redd, RB=right bank redd). The bulk sample from Kennedy Creek is included for comparison.....	14
Figure 2.2: Side- and planview of a redd in the flume [<i>Buxton et al.</i> , submitted].....	15
Figure 2.3: Schematic of load cell and tilt board measurements and forces	17
Figure 2.4: Paired pocket friction coefficients (measured with the load cell and tilt board for grains placed in similar orientations on the left bank redd composed of sediment mix 2. A simple linear regression of the data ($R^2=0.74$, not shown) exhibits a slope of 0.9 and intercept of 0.2	22
Figure 2.5: Example of embeddedness calculated with Equation (2.5) for a 10 mm diameter sphere with variable protrusion	24
Figure 2.6: Measured (A.) grain protrusion and calculated (B.) embeddedness (Equation (2.5)) as a function of apparent diameter on glued bed surfaces (all data combined). Symbols and colors represent half-phi size classes (lower bin size reported in figure key)	26
Figure 2.7: Cumulative distributions of packing friction coefficients (μ_{pack}) for grain-size classes on the unspawned beds (US), left bank redds (LB) and right bank redds (RB) for sediment mixtures 1-3. Lines represent half-phi size classes (lower bin size reported in figure key) for each bed	28

Figure 2.8: Packing friction coefficient (μ_{pack}) as a function of (A.) embeddedness (E) and (B.) grain diameter (D) for unspawned beds (US), left bank redds (LB) and right bank redds (RB) for sediment mixtures 1-3. The solid curves are power regressions of all data in (A.) and (B.). Dotted curves in (A.) are power regressions corresponding to individual beds by color. Friction coefficients and values of E are averaged by grain-size class. Grain diameter represents the lower bin size for classes in half-phi size intervals for each bed. The unspawned bed and left bank redd are labeled in (A.) for reference in Figure 2.9.32

Figure 2.9: Power law coefficients (α) and exponents (β) for regressions of packing friction coefficients (μ_{pack}) and embeddedness (E) for individual beds in Figure 2.8a as a function of the skewness (S) and median grain size (D_{50}) of the bed surface grain-size distributions. Coefficients for the unspawned bed and LB redd composed of sediment mix 1 are shown in the figure, but excluded from the linear regression because they were outliers33

Figure 2.10: Bed average packing (μ_{pack}) as a function of skewness of the bed surface grain-size distributions.....34

Figure 2.11: Plots of packing predicted with Equation (2.12) versus modeled in Monte Carlo simulations. Symbols and colors represent half-phi size classes (lower bin size reported in figure key) for each bed37

Figure 2.12: Difference in (A.) critical bed shear stress (τ_c) calculated with the total angle of resistance and pocket angle of resistance and (B.) critical bed shear stress calculated for total resistance for grain-size classes on unspawned beds (US) and left bank (LB) and right bank (RB) redds. Values of τ_c computed for the 5.7 mm grains on the LB redd composed of sediment mixes 1 and 2 are not plotted because they far exceeded the other values. Numbers indicate sediment mixtures composing the beds. Grain diameter represents the lower bin size for half-phi size intervals for each40

Figure 2.13: Critical dimensionless shear stress (τ_{ci}^*) for grain-size fractions (D_i) calculated with the 10th percentiles of the total resistance angle (A.) and pocket resistance angles (B.) versus relative grain size (D_i/D_{50}) for the unspawned beds (US) and left bank (LB) and right bank (RB) redds composed of sediment mixtures 1-3. Inset tables in both figures indicate critical dimensionless shear stress values for the median grain size (τ_{c50}^*) and the b -exponent in Equation (2.13), which is included in (B.) for reference. The percent increase in τ_{c50}^* and decrease in b due to packing are respectively shown in (A.).....43

Figure 2.14: Critical dimensionless shear stress for median grain sizes (τ_{c50}^*) versus the critical boundary Reynolds number (Re_c^*) in this study and others. Values obtained from Tables 1a-c in *Buffington and Montgomery (1997)* were measured by visual, reference transport, and competence methods in streams and laboratory channels. Theoretical values for packed and unpacked grains were calculated with Equation (2.13). The critical boundary Reynolds number is defined as $u_c^* D_{50} / \nu$, where u_c^* is the critical shear velocity at incipient motion ($u_c^* \equiv \sqrt{\tau_c / \rho}$) and ν is kinematic viscosity44

Figure 3.1: Side and planview of a salmon redd modified from <i>Buxton et al.</i> [submitted] ...	61
Figure 3.2: Cumulative percentiles for bulk sediment mixtures 1-4 used in the flume experiments (scaled values shown)	67
Figure 3.3: Redds and unspawned beds used for (A.) total resistance measurements (F_t) (sediment mix 1 shown), (B.) flow velocity measurements with particle image velocimetry (PIV) and (C.) visual measurements of grain mobility and bed load capture. Beds are spray painted blue in (A.) to discern surface grains from subsurface particles during total resistance measurements; black in (B.) to reduce PIV laser refraction; and in (C.) the redd is painted orange and the unspawned bed is painted black to aide observations of grain mobility and to allow the origin of surface grains to be distinguished in bed load traps that are shown in the upper portion of the figure. The bed in (B.) is shown after removal from the flume, with the outline of the redd and location of PIV transects in yellow (transect on the right is for the unspawned bed). The unspawned bed in (A.) is shown before it was painted to distinguish it from redds in this figure	69
Figure 3.4: Schematic of load cell and tilt board measurements and forces [modified from <i>Buxton et al.</i> , submitted]	74
Figure 3.5: Median grain size (D_{50} in A.) and (B.) sorting parameters (σ , <i>Blatt et al.</i> , 1980) measured on redds in the flume and on Pacific salmon redds in several Washington and Idaho streams. Median grain sizes in the flume are scaled larger by a factor of 3 for comparison to values of D_{50} in streams	82

- Figure 3.6: Redd dimensions in the flume compared to dimensions of chum salmon redds in Kennedy Creek near Olympia, WA, Herman Creek near Haines, Alaska, and Lilliwaup Creek at Lilliwaup, WA. Redd dimensions in the flume are scaled larger by a factor of 3 in these comparisons83
- Figure 3.7: Cumulative distributions of packing friction coefficients (μ_{pack}) for grain-size classes (lower bin size reported in figures) on the unspawned beds (US) and redds composed of sediment mixtures 1-385
- Figure 3.8: Cumulative distributions of critical shear stress (τ_c) grouped by bed surface and plotted for grain-size classes in half-phi intervals (lower bound of each bin size reported in figure key) on redds and unspawned (US) beds composed of sediment mix 1-3.....89
- Figure 3.9: Boundary shear stress (τ_b ; solid line) estimated on a redd (A. and B.) and unspawned bed (C. and D.) with the law of the wall using flow velocity profiles measured with Particle Image Velocimetry at flow rates of $0.32 \text{ m}^3 \text{ s}^{-1}$ and $0.64 \text{ m}^3 \text{ s}^{-1}$ in the flume. Values are averaged on both structures (dotted lines). Negative horizontal distances are in the upstream direction. The horizontal distance of the tailspill flat in Figure 3-9a-b is located from 0 to -15.1 cm, and the tailspill slope is located from -15.1 to -36.2 cm91
- Figure 3-10: Visual measurements of grain mobility on a redd and unspawned bed. Bed-average shear stress is plotted as a function of discharge in the flume for reference94

Figure 3-11: Mass transport rates of surface grains mobilized from the spawned and unspawned bed areas in experiment 3. Data labels are values of bed average shear stress (τ_{avg}) in pascals.....	95
Figure 3-12: Stratigraphy of sediment in a dewatered chum salmon redd in Kennedy Creek, WA.....	99
Figure 4-1: Side- and planview diagram of a redd modified from <i>Buxton et al.</i> [submitted].....	122
Figure 4.2: Site map for the study reach on Herman Creek near Haines, Alaska	124
Figure 4.3: Depiction of a redd showing the distribution of total water pressure head for base simulations (A.) and in sensitivity runs with half (B.) and twice (C.) the number of . total water pressure head values as in the base simulation. Water pressure head was determined by adding the average water depth (0.25 m) to the dynamic pressure head. Dynamic pressure was estimated as h_m (Figure 4.3a) with Equation (4.1) and sinusoidally distributed with Equation (4.2). In the base simulation dynamic pressures were spatially averaged over topographic elements of the redd, including the pot (0.255 m), upstream tailspill slope (0.260 m), tailspill flat (0.249 m), and downstream tailspill slope (0.243 m).....	129

Figure 4.4: Dimensions of the model domain and several parameters included in the simulations. Red areas in the domain represent salmon redds that extend 0.20 m into and above the unspawned area of the domain (grey colored) and exhibit higher hydraulic conductivity (K_{sp}) and porosity (n_{sp}) than unspawned beds (K_{us} and n_{us} , respectively). The lower boundary of the domain represents an impermeable layer. Total pressure head acts on the inlet and outlet boundaries (elevation head+static water head) and on the top boundary as depicted for redds (see Figure 4.3a) and unspawned portions of the bed. Nodes on the pressure inlet boundary are points between which water pressure head is designated in the model.....131

Figure 4.5: Contour plots of solute concentration (indicated in figure key, where 1.0 is 100% concentration) entering the top surface of the domain and exiting the downstream boundary in simulations with an unspawned bed and beds with variable proportions of the surface occupied by redds. Depth of alluvium is 3 m at the upstream (left) end of the domains and 2.82 m at the downstream (right) end of domains. The length of the domains is 60 m, and the width is 1 m134

Figure 4.6: Storage duration (hrs) of MDN versus the proportion of the bed surface occupied by redds (P). The curve is a linear regression of the data, indicating an inverse relationship between storage duration and the proportion of the bed surface occupied by redds.....136

- Figure 4.7: Hyporheic flux and volume plotted against the proportion of the bed surface occupied by redds (P). The curves are polynomials that demonstrate the rapid increase in exchange flux and volume from that for an unspawned bed ($P=0$) with the presence of a single redd ($P=0.05$). Thereafter, exchange flux and volume increase linearly with spawning density (P).....136
- Figure 4.8: Contour plots of hyporheic flow speeds (indicated in m s^{-1} in figure key) in simulations with an unspawned bed and beds with variable proportions of the surface occupied by redds.....138
- Figure 4.9: Contour plots of hyporheic flux (indicated in $\text{m}^3 \text{s}^{-1}$ in figure key) in simulations with an unspawned bed and beds with variable proportions of the surface occupied by redds.....139
- Figure 4.10: Contour plots of solute concentration (indicated in figure key, where 1.0 is 100% concentration) in sensitivity runs with two (A.) and eight total head values on redds (B.)141

List of Tables

Table 2.1: Approximate equivalence of characteristics of grains used for total resistance measurements and pocket resistance measurements	19
Table 2.2: Characteristics of grain size distributions on unspawned beds (US) and the flat portion of left bank (LB) and right bank (RB) redd tailspills	25
Table 2.3: Average friction coefficients for total resistance (μ_t), pocket angle resistance (μ_p), and packing resistance (μ_{pack}), and the standard error of the average μ_{pack} by each grain-size class (lower bin size shown) and bed.....	29
Table 2.4: Coefficients (α) and exponents (β) for power law regressions ($\alpha(E)^\beta$) of packing friction coefficients as a function of grain embeddedness (E) for individual beds (see Figure 2.8a)	32
Table 2.5: Multiple linear regressions ^a of percentiles (n) of packing distributions for all beds combined. The standard error (SE) for regression intercept (ω), embeddedness (E , dimensionless), grain diameter (D , mm), and skewness of the grain-size distributions (S) are listed along with the correlation coefficient (R^2) for each parameter	36
Table 3.1: Scaled redd dimensions and median grain sizes (D_{50}) and sorting parameters (σ ; Blatt <i>et al.</i> , 1980) for surface particles on redds and unspawned beds (US) in flume experiments 1-3	66
Table 3.2: Approximate equivalence of characteristics of grains used for total resistance measurements and pocket resistance measurements	77

Table 3.3: Average friction coefficients for total resistance (μ_t), pocket angle resistance (μ_p), and packing resistance (μ_{pack}), and the standard error of the average μ_{pack} by each grain-size class (lower bin size shown) and bed. Values of bed average μ_{pack} are also listed	86
Table 3.4: Critical shear stress averaged within grain-size classes (lower bin size shown) and used to calculate the weighted average (by grain size frequency) for each bed.	88
Table 4.1: Parameters in base simulations of hyporheic flow	132
Table 4.2: Model results from the base simulations	135

Chapter 1. General Introduction

Pacific salmon (*Oncorhynchus* spp.) are a keystone species in stream ecosystems because they physically alter river beds [Montgomery *et al.*, 1996; Gottesfeld *et al.*, 2004, 2008] and deliver marine derived nutrients (MDN) to watersheds [Schindler *et al.*, 2003]. Although much has been learned about the physical and ecological roles of salmon in streams [see reviews by Gende *et al.*, 2002; Schindler *et al.*, 2003; Naiman *et al.*, 2009; and DeVries, 2012], it remains unclear how spawning modifies grain packing, stream bed stability, and the residence time and flux of MDN in hyporheic zones.

Background. Salmon hatch from nests (redds) in streambeds and rear for up to three years before migrating to sea, where they spend at least half of their life and gain around 95% of their body mass before returning to natal areas to construct redds and spawn [Groot and Margolis, 1991; Naiman *et al.*, 2002]. Male salmon assist in redd construction [Hartman *et al.*, 1964; Crisp and Carling, 1989], but the majority of work is performed by the female using rapid undulations of her tail to dig a pit, which moves sediment a short distance downstream into a tailspill mound and modifies grain sizes composing the bed. Once the pit is sufficiently deep (0.10 to 0.50 m; DeVries, 1997), the female deposits a portion of her eggs for fertilization by the male. After fertilization, eggs are covered with material excavated just upstream of the pit. This sequence is repeated until the female spawns her brood and the redd exhibits several egg pits, a tailspill, and pot depression. Salmon die after spawning, leaving nutrients that facilitate trophic interactions that feedback to benefit salmon reproduction [Gende *et al.*, 2002].

Chapter 2. Researchers have long acknowledged that grain packing influences particle mobility [Kirchner *et al.*, 1990; Buffington *et al.*, 1992] and that the spawning action

of salmonids disrupts packing [Montgomery *et al.*, 1996]. Despite this recognition, packing resistance to particle motion has remained unquantified due to difficulty in isolating it from other forms of resistance acting on grains. Previous mechanistic studies of incipient motion in gravel-bed rivers have quantified resistance to motion in terms of friction angles that describe the angle through which a grain must pivot to move from its resting pocket [Miller and Byrne, 1966; Li and Komar, 1986; Wiberg and Smith, 1987; Kirchner *et al.*, 1990; Buffington *et al.*, 1992; McEwan and Heald, 2001]. Friction angle studies treat surface grains as resting in open pockets. However, natural streambeds commonly exhibit some degree of grain burial and packing by surrounding grains [Yalin, 1972], which has been identified as a missing component of resistance in mechanistic studies of grain motion [Buffington *et al.*, 1992].

To quantify packing resistance, I simulated spawning in a laboratory flume and measured the total resistance and pocket resistance to grain motion on the flat portion of simulated redds and planar water-worked bed surfaces undisturbed by spawning. Total resistance to motion was measured with a load cell on half of each bed before gluing the undisturbed halves and measuring pocket resistance with a tilt board. From these measurements, I produced distributions of total resistance and pocket resistance for grain-size classes and used Monte Carlo simulations to randomly pair percentiles from each distribution. From these pairings, I determined packing resistance distributions by subtracting total resistance from pocket resistance for grain-size classes on each bed. Results indicated packing resistance varies with grain size, embeddedness, and skewness of the grain-size distribution. From this, I present an empirical equation for predicting packing resistance as a function of these factors. I also show that packing substantially increases

predicted values of critical shear stress and Shields stress. Packing also promotes bed conditions that are closer to exhibiting equal mobility of grain-size fractions.

Chapter 3. Spawning alters stream beds in ways that benefit salmon reproduction by promoting hyporheic flow through redds [Zimmermann and Lapointe, 2005; Tonina and Buffington, 2009] and protecting embryos from predation and damage by bed scour, disputably at the cost of stability of the redd structure. Theoretical calculations by Montgomery *et al.* [1996] indicate critical conditions for sediment entrainment on solitary redds is nearly double that for unspawned beds. Montgomery *et al.* [1996] also calculated that bed stability is increased an additional 64% by form drag generated by topographic roughness from redds in clusters. These findings have not been supported by field observations of mobility of solitary redds [Lisle, 1989; Bigelow, 2003] or redds in high densities [Rennie and Millar, 2000], or in numerical models of mass spawned reaches [Hassan and Tonina, in review].

I investigated the relative stability of redds and unspawned beds by expanding experiments in Chapter 1 in the flume. Packing resistance to grain motion was quantified on the entire redd and unspawned bed surfaces using methods presented above. The stability of redds and unspawned beds was also assessed with calculations of critical shear stress, estimates of boundary shear stress, visual measurements of sediment mobility, and bedload transport measurements on spawned and unspawned surfaces. Results from these complementary assessments suggest redds are unstable compared to unspawned beds, indicating the need for additional research investigating linkages between spawning disturbance and stream bed mobility that may have implications for formation and maintenance of fish habitats in salmon-bearing streams.

Chapter 4. Marine nutrients are delivered to streams by salmon but only a portion are retained long enough in hyporheic areas of streambeds to facilitate biochemical uptake [Johnson *et al.*, 2004; Mitchell and Lamberti, 2005; Moore *et al.*, 2007; Marzadri *et al.*, 2012, Rinella *et al.*, 2013]. Nutrient retention in hyporheic zones is affected by spawning winnowing fines and increasing sediment porosity and hydraulic conductivity and divergent pressure pumping water through redds. I evaluated these influences on the residence time ($=\text{hyporheic volume}/\text{hyporheic exchange flux}$) and hyporheic exchange of MDN using a two-dimensional groundwater model with variable proportions of a planar stream bed surface occupied by redds. Predictions indicated hyporheic exchange increased rapidly with spawning compared to an unspawned bed without comparably increasing hyporheic volume. As a result, residence times of MDN decreased as a linear function of increasing proportions of the streambed surface occupied by redds. Given the considerable influence of spawning on hyporheic flow, additional research is needed to determine conditions under which uptake of MDN is limited by hyporheic exchange governing the supply of nutrients to the bed and residence time allowing biochemical uptake of nutrients to occur.

1.1 References

- Bigelow, P. E. (2003), Scour, fill, and salmon spawning in a northern California coastal stream, M.S. thesis, Dept. of Geol., Humboldt State Univ., Arcata, CA.
- Buffington, J. M., W. E. Dietrich, and J. W. Kirchner (1992), Friction angle measurements on a naturally formed gravel streambed: implications for critical boundary shear stress, *Water Resour. Res.*, 28, 411-425.
- Crisp, D. T. and P. A. Carling (1989), Observations on siting, dimensions, and structure of salmonid redds, *J. Fish. Biol.*, 34, 119-134.
- DeVries, P. (2012), Salmonid influences on rivers: a geomorphic fish tail, *Geomorphology*, 157, 66-74.
- DeVries, P. (1997), Riverine salmonid egg burial depths: review of published data and implications for scour studies, *Can. J. Fish. Aquat. Sci.*, 54, 1685-1698.
- Gende, S. M., E. D. Edwards, M. F. Willson, and M. S. Wipfli (2002), Pacific salmon in aquatic and terrestrial ecosystems, *BioScience*, 52, 917-928.
- Gottesfeld, A. S., M. A. Hassan, J. F. Tunnicliffe, and R. W. Poirer (2004), Sediment dispersion in salmon spawning streams: the influence of floods and salmon redd construction, *J. Am. Water Res. Assoc.*, 40, 1071-1086.
- Gottesfeld, A. S., M. A. Hassan, and J. F. Tunnicliffe (2008), Salmon bioturbation and stream Processes, *Am. Fish. Soc. Sym.*, 65, pp 1-19.
- Groot, C. and L. Margolis (1991), Pacific Salmon Life Histories. UBC Press, Vancouver, BC, 564 pp.
- Hartman, W. L., T. R. Merrell, and R. Painter (1964), Mass spawning behavior of sockeye salmon in Brooks River, Alaska, *Copeia*, 2, 362-368.

- Hassan, M. A. and D. Tonina (In review) Does sockeye salmon spawning activity enhance bed mobility in small creeks? *J. Geophys. Res.–Earth Sci.*
- Johnson, N. T., E. A. Macisaac, P. J. Tschaplinski, and K. J. Hall (2004), Effects of the abundance of spawning sockeye salmon (*Oncorhynchus nerka*) on nutrients and algal biomass in forested streams, *Can. J. Fish. Aq. Sci.*, 403, 384-403.
- Kirchner, J. W., W. E. Dietrich, F. Iseya, and H. Ikeda (1990), The variability of critical shear stress, friction angle, and grain protrusion in water worked sediments, *Sedimentology*, 37, 647-672.
- Li, Z. and P. D. Komar (1986), Laboratory measurements of pivoting angles for applications to selective entrainment of gravel in a current, *Sedimentology*, 33, 413-423.
- Lisle, T. E. (1989), Sediment transport and resulting deposition in spawning gravels, North Coastal California, *Water Res. Research*, 25, 1303-1319.
- Manning, R. (1891), On the flow of water in open channels and pipes, *Trans. Inst. Civ. Eng. of Ireland*, 20, 161-207.
- Marzadri, A., D. Tonina, and A. Bellin (2012), Morphodynamic controls on redox conditions and on nitrogen dynamics within the hyporheic zone: Application to gravel bed rivers with alternate-bar morphology, *J. Geophys. Res.–Biogeosci.*, 117, G3.
- McEwan, I. and J. Heald (2001), Discrete particle modeling of entrainment from flat uniformly sized sediment beds, *J. Hydraul. Eng.*, 127, 588-597.
- Miller, R. L. and R. J. Byrne (1966), The angle of repose for a single grain on a fixed rough bed, *Sedimentology*, 6, 303-314.

- Mitchell, N. L. and G. A. Lamberti (2005), Responses in dissolved nutrients and epilithon abundance to spawning salmon in southeast Alaska streams, *Limn. Oceanography*, 50, 217-227.
- Montgomery, D. R., J. M. Buffington, N. P. Peterson, D. Schuett-Hames, and T. P. Quinn (1996), Stream-bed scour, egg burial depths, and the influence of salmonid spawning on bed surface mobility and embryo survival, *Can. J. Fish. Aquat. Sci.*, 53, 1061-1070.
- Moore, J. W., D. E. Schindler, J. L. Carter, J. Fox, J. Griffiths, and G. W. Holtgrieve (2007), Biotic control of stream fluxes: spawning salmon drive nutrient and matter export, *Ecology*, 88, 1278-1291.
- Naiman, R. J., R. E. Bilby, D. E. Schindler, and J. M. Helfield (2002), Pacific salmon, nutrients, and the dynamics of freshwater and riparian ecosystems, *Ecosystems*, 5, 399-417.
- Naiman, R. J., J. M. Helfield, K. K. Bartz, D. C. Drake, and J. M. Honea (2009), Pacific salmon, marine-derived nutrients, and the characteristics of aquatic and riparian ecosystems, *Am. Fish. Soc. Sym.*, 69, 395-425.
- Rennie, C. D. and R. G. Millar (2000), Spatial variability of stream bed scour and fill: a comparison of scour depth in chum salmon (*Oncorhynchus keta*) redds and adjacent bed, *Can. J. Fish. Aquat. Sci.*, 57, 928-938.
- Rinella, D. J., M. S. Wipfli, C. M. Walker, C. A. Stricker, and R. A. Heintz (2013), Seasonal persistence of marine-derived nutrients in south-central Alaskan salmon streams, *Ecosphere*, 4, 1-18.

Schindler, D. E., M. D. Scheuerell, J. W. Moore, S. M. Gende, T. B. Francis, and W. J.

Palen (2003), Pacific salmon and the ecology of coastal ecosystems, *Frontiers Ecol. Env. 1*, 31-37.

Tonina, D. and J. M. Buffington (2009), A three-dimensional model for analyzing the effects of salmon redds on hyporheic exchange and egg pocket habitat, *Can. J. Fish. Aquat. Sci.*, 66, 2157-2173.

Wiberg, P. L. and J. D. Smith (1987), Calculations of the critical shear stress for motion of uniform and heterogeneous sediments, *Water Resour. Res.*, 23, 1971-1480.

Yalin, M. S. (1972), *Mechanics of sediment transport*. Benjamin Press, New York, 290 pp.

Zimmermann, A. E. and M. F. Lapointe (2005), Intergranular flow velocity through salmonid redds: sensitivity to fines infiltration from low intensity sediment transport events, *Riv. Res. Appl.*, 21, 865-881.

Chapter 2. Grain Packing Resistance to Particle Mobility¹

2.1 Abstract

We report the first measurements of grain packing resistance to particle motion for water worked, mixed-grain sediment surfaces. Packing resistance was determined as the difference between the total resistance to motion (measured with a load cell) and that due to pocket angles (measured with a tilt board). Because paired measurements of these values were not available, Monte Carlo simulations were used to develop distributions of packing resistance from observed distributions of total and pocket angle resistance. Expressed as a coefficient of friction, packing resistance increased with decreasing grain size and was almost 18 times higher for smaller grains (26.3 for the 5.7 mm size class) than larger grains (1.5 for the 22.6 mm size class). This occurs because small grains tend to be more angular and embedded, which increases the extent of packing by surrounding grains and intergranular jamming. Packing resistance can be expressed as a function of grain size, embeddedness, and skewness of the grain-size distribution because a grain's contact and friction with the bed are regulated by these parameters. Including packing in calculations of critical bed shear stress increased values up to 72% (30% on average) over those calculated with pocket angles alone. Similarly, critical Shields stresses with packing resistance were up to 73% (37% on average) higher than values calculated without packing. These findings have implications for bed load transport predictions, which are typically nonlinear functions of the difference between applied and critical shear stresses; as such, small differences in critical shear stress can cause large prediction errors. Packing also decreased the exponent in a grain hiding function by up to 43% (average 14%), reducing the tendency for size-

selective transport and promoting conditions that tend toward equal mobility. Given the potential importance of packing resistance, future studies are needed to better understand physical and biological controls on packing, and the mechanics of packing resistance.

¹ Chapters 2-4 are written in the plural “we” for submittal to peer-reviewed journals with co-authors Elowyn M. Yager, John M. Buffington, Marwan A. Hassan, and Alexander K. Fremier.

2.2 Introduction

Previous mechanistic studies of incipient motion in gravel-bed rivers quantify resistance to motion in terms of friction angles that describe either the angle that a grain must pivot to move from its resting pocket or the frictional resistance that must be overcome if a grain slides out of its pocket [Miller and Byrne, 1966; Li and Komar, 1986; Wiberg and Smith, 1987; Kirchner *et al.*, 1990; Buffington *et al.*, 1992; McEwan and Heald, 2001]. These studies treat surface grains as resting in open pockets. However, natural streambeds commonly exhibit some degree of grain burial and packing by surrounding grains [Yalin, 1972], which has been identified as a missing component of resistance in mechanistic studies of incipient motion [Buffington *et al.*, 1992]. For example, recent work by Hodge *et al.* [2013] documented friction angles for *in situ* grains that were substantially higher than those previously reported, which may, in part, reflect added resistance due to packing.

Packing resistance can result from a variety of processes, such as settling of small grains around larger ones during active transport of all particle sizes, selective trapping of fine material in high friction areas when coarse grains are immobile, and deposition of framework grains on top of one another, resulting in partial burial and imbrication. Packing may also occur in sediment mixtures that are positively skewed, indicating an abundance of

relatively small material that is available for percolating into the bed [*Reid et al.*, 1985; *Allan and Frostick*, 1999; *Frings et al.*, 2008], thereby raising the bulk density [*Sohn and Moreland*, 1968] and tightness of the bed [*Haynes and Pender*, 2007]. High bulk densities also occur in mixtures of non-spherical grains because they tend to orient with smaller voids between them [*Brouwers*, 2006], and in beds with a stress history that has shifted grains into tight matrices [*Ockelford and Haynes*, 2013]. For example, erosion rates measured by *Jepson et al.* [1997] were a negative power function of bulk density, perhaps because grain packing stabilized particles in their mixtures.

The mechanics of packing resistance are poorly understood and may include a combination of loading/imbrication (weight of packing material on an individual grain), jamming (wedging of packing material around a grain), cohesion and mortaring (binding due to silt and clay-sized packing material), static friction (between a grain at rest and its packing material), and dynamic friction (between a mobile grain and its packing material). Regardless of the specific mechanics, we hypothesize that packing resistance will be a function of the degree that a grain is in contact with the surrounding bed material [*Sanguinito and Johnson*, 2012]. This, in turn, depends on embeddedness (the proportion of the grain below the bed surface), particle size (the surface area of the grain available for contact with neighboring particles is a function of grain radius squared), and skewness of the grain-size distribution (positive skewness indicates an abundance of smaller grains for minimizing void space in a grain mixture). However, it is unclear how grain size, embeddedness, and skewness interact to control packing resistance to grain mobility.

Although the effects of packing resistance on particle mobility have been documented, prior studies typically describe packing in qualitative terms [e.g., *Church*,

1978; *Carling and Reader*, 1982; *Hassan*, 1992; *Downes et al.*, 1998; *Heritage and Milan*, 2009]. For instance, *Powell and Ashworth* [1995] report that critical boundary shear stress for a tightly packed bed was up to seven times higher than a loosely packed bed. Similarly, *Barzilai et al.* [2012] found that critical boundary shear stress more than doubled after silt and clay-sized material deposited among framework gravels and mortared the bed with cohesive grains. Despite the recognized importance of packing resistance, it remains a qualitative factor (e.g., loose vs. tightly packed) in bed mobility studies.

To address the above issues, we measured packing resistance on water-worked beds constructed with mixed-grain sizes in a laboratory flume. The data are derived from a larger study examining the effects of salmonid spawning on bed structure and mobility. During construction of their nests (redds), salmon winnow fines and loosen the streambed, altering both the sorting and packing of the bed [*Montgomery et al.*, 1996]. We simulated redd construction in the flume and made measurements on both simulated redds and bed surfaces undisturbed by spawning, which represented a range of bed conditions for quantifying packing resistance. Here, we focus on packing resistance in general and examine the effects of salmonid spawning in more detail in a companion study. Results show that packing resistance varies with grain size, embeddedness, and skewness of the grain-size distribution, from which we develop an empirical equation for predicting packing resistance as a function of these factors. We also show that packing reduces size-selective transport and substantially increases predicted values of both the critical shear stress and critical Shields stress compared to those determined from pivot angles alone.

2.3 Materials and Methods

2.3.1 Experimental Setup

Measurements were conducted in a 20 m long, 2 m wide, 1.5 m deep flume at the Center for Ecohydraulics Research at the University of Idaho in Boise, USA. Flow straighteners were installed at the upstream end of the flume to quell flow surges before flow moved up an inclined ramp onto fixed beds of sediment. Fixed beds were installed in the upper 12 m of the flume to generate uniformly rough flow using gravel and sand-sized grains glued to plywood with contact cement. A lumber crib supported the fixed beds 0.14 m above the flume bottom so that sediment mixtures for the test beds could be placed to this depth in three wooden boxes (1.0 m long, 0.64 m wide), which were installed across the flume downstream of the fixed bed. The boxes allowed the test beds to be lifted from the flume without damage. A fixed bed was also installed for 2 m downstream of the boxes to generate roughness that prevented flow from accelerating from the test beds.

Three sediment mixtures were used in the laboratory experiments and were modeled after a bulk sediment sample collected from Kennedy Creek near Olympia, Washington where chum salmon (*Oncorhynchus keta*) spawn and build redds (Figure 2.1). The bulk sample was a composite of surface and subsurface material. The maximum particle size in the bulk sample (90.5 mm) was about 1.5% of the total sample weight, which is close to the 1% criterion recommended by *Church et al.* [1987] for requisite sample size. Sampled grains were sieved in half-phi intervals from -1 to -6 (2 to 64 mm) and the resulting size distribution was scaled smaller by a factor of three. The scaling factor of three was chosen to reduce redd dimensions to fit within the wooden boxes. The middle box held an unspawned

bed (US), while spawned beds were constructed in the two adjacent boxes, hereafter referred to as left bank (LB) and right bank (RB) redds. We varied the size distribution of the scaled bulk sample to create three experimental sediment mixtures (mix 1, 2, and 3) that allowed us to measure grain packing resistance on bed surfaces with different sediment compositions (Figure 2.1). One grain mixture was placed in the boxes at a time and screeded flat with a shovel before the flume slope was set to 0.5%, the thalweg slope of Kennedy Creek where the bulk sample was collected. Flow was then started in the flume to wet the beds before discharge was increased until five or more grains (usually sand and small gravel) were visually observed to move a downstream distance approximately equal to their diameter. Water working then proceeded for two hours by increasing discharge in increments to sustain a low rate of sediment transport.

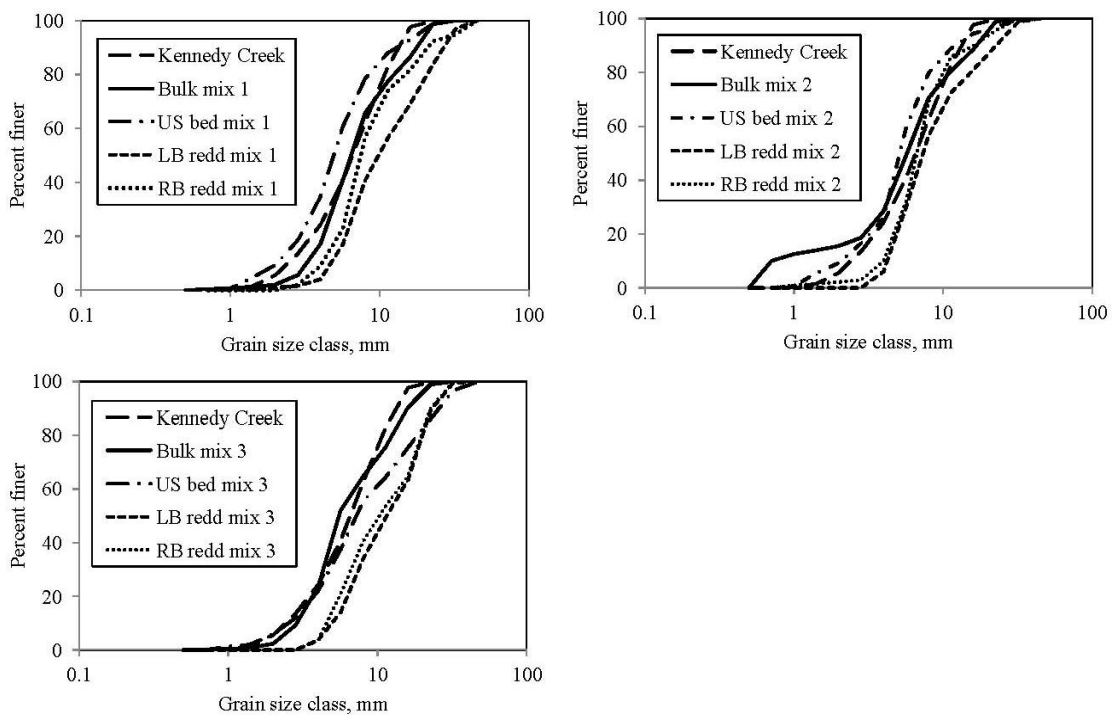


Figure 2.1. Bulk grain-size distributions before water working and surface grain-size distributions after water working for each sediment mixture and bed (US=unspawned, LB=left bank redd, RB=right bank redd). The bulk sample from Kennedy Creek is included for comparison.

2.3.2 Redd Construction

Flow was reduced after water working to generate Froude-scaled flow velocities and depths typical of those used by chum salmon during spawning [Bjornn and Reiser, 1991]. Scaled flows were sufficient to transport silt and fine sand flushed into the water column during simulated redd construction, but were too low to mobilize grains on the bed. We simulated spawning using a metal spatula to mimic the construction of redds by female salmonids, whereby rapid undulations of the tail excavate a pit for depositing eggs [Groot and Margolis, 1991; Quinn, 2005]. Successive episodes of pit excavation and filling proceeded in the upstream direction and flushed fine sediment from larger grains and loosened the bed. As in nature, completed redds were dune-like features that are composed of a depression (pot), upstream sloping tailspill, and a flat area on the tailspill (Figure 2.2). In this study, we avoided differences in bed slope affecting resistance forces by restricting measurements to planar unspawned beds and the flat portion of redd tailspills (Figure 2.2).

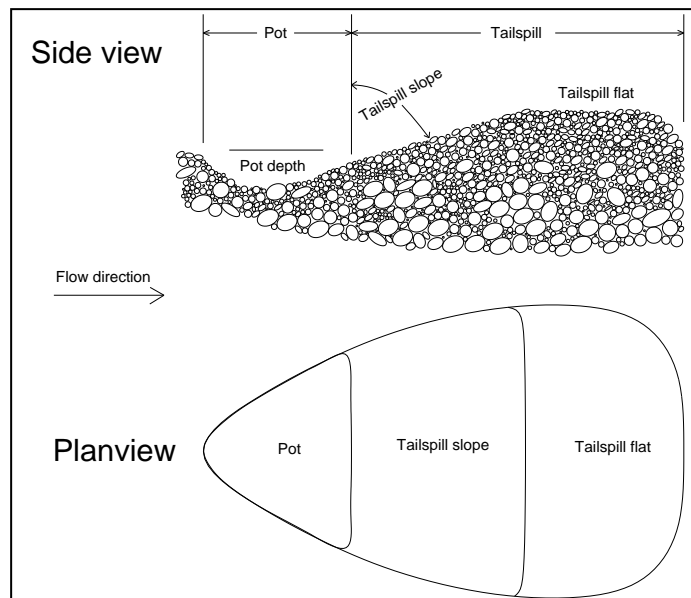


Figure 2.2. Side- and planview diagram of a redd in the flume [Buxton *et al.*, submitted]

2.3.3 Framework for Determining Packing Resistance

To isolate packing resistance on grains, we assume that forces resisting grain motion are linearly additive

$$F_t = F_{pack} + F_p = F_{pack} + F_n \tan \phi_p \quad (2.1)$$

where F_t is the total resistance force, F_{pack} is the packing resistance force, F_p is the friction force due to a grain's pocket angle, ϕ_p is the pocket friction angle, and F_n is the normal force on the grain, which for level, dewatered surfaces is the grain weight (mass times gravity).

Because it is unclear how the mechanics of F_t and F_{pack} should be defined, for simplicity and for comparison with F_p , we treat them as friction forces

$$F_t = \mu_t F_n \quad (2.2a)$$

$$F_{pack} = \mu_{pack} F_n \quad (2.2b)$$

where μ_t and μ_{pack} are, respectively, friction coefficients for the total and packing resistance.

To isolate the component of resistance due to packing, we divide the forces by F_n to eliminate the effect of grain weight and rearrange (1) to solve for μ_{pack}

$$\mu_{pack} = \frac{F_t - F_n \tan \phi_p}{F_n} = \frac{F_t}{F_n} - \tan \phi_p = \mu_t - \mu_p \quad (2.3)$$

where $\tan \phi_p$ is equal to the friction coefficient for pocket resistance, μ_p . We use friction coefficients instead of friction angles to avoid interpreting resistance to motion as a simple pivot angle and to express our results across a broader range of values than 0-90°, as dictated by the inverse tangent function.

With this framework, we determined packing resistance as the difference between the total resistance (measured with a load cell) and the pocket resistance (measured as an angle of resistance with a tilt board). Because total resistance measurements disrupt the bed and alter the initial pocket geometry, it is not possible to make paired measurements of total and pocket resistance. Consequently, total resistance measurements were made on half of each bed before gluing the undisturbed halves and measuring pocket angles (Figure 2.3). From these measurements, we produce distributions of total resistance and pocket resistance for grain sizes classed in half-phi intervals from -2.5 to -4.5 (5.7 to 22.6 mm). We then use Monte Carlo simulations to randomly pair percentiles from each distribution to determine packing resistance distributions with Equation (2.3) for grain-size classes on each bed.

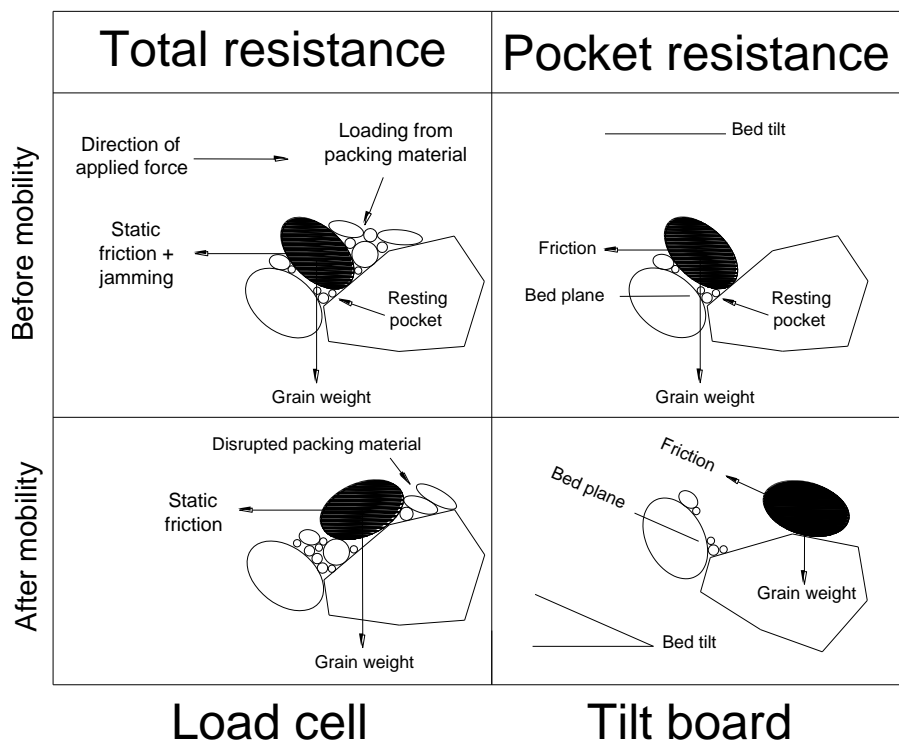


Figure 2.3. Schematic of load cell and tilt board measurements and forces [Buxton *et al.*, submitted].

2.3.4 Total Resistance Force Measurements

While laying on a platform over the beds, total resistance forces were measured by applying a push force with a load cell in a downstream and bed-parallel direction at the midpoint of the exposed frontal area of the grain [Johnston *et al.*, 1998]. With the slope of the flume set to zero, enough force was applied to push grains a distance approximately equal to their intermediate axis (hereafter grain diameter or D), which defined grain movement in our study. Distances of grain movement were approximate because measurements of D could not be made *a priori* without disturbing the grain. Resistance forces were measured with a Futek LSB210 load cell that was connected to a laptop computer with a Futek USB210 that detected the peak applied force at 10 Hz with a nominal accuracy of 0.001% (as specified by the manufacturer). The load cell was drilled and tapped for inserting a 3 mm diameter post for applying a push force to grains that extended at least partially above the local bed surface. Additional criteria were that grains had to be surrounded by undisturbed sediment and were not disrupted by prior measurements. We measured total resistance forces for every grain that met these criteria. Measurements proceeded by mobilizing individual grains with the load cell, noting the type of movement (sliding, pivoting/rolling, or tilling), extracting the grain for determining its weight, classifying angularity with the Powers [1953] roundness scale, and measuring the three major axes of the grain with digital calipers to the nearest 0.1 mm for characterizing grain shape with the Corey [1949] shape factor (CSF, Table 2.1). We excluded tilling motions (movement that plowed neighboring grains) because grains in natural channels predominantly move in a sliding or pivoting/rolling motion, or some combination of the two [Francis, 1973; Komar and Li, 1988; Ling, 1995]. We restricted our analysis to grains in the

5.7 to 22.6 mm size classes since pocket resistance measurements were limited to these grain sizes, as discussed below. The number of total resistance measurements made within grain-size classes varied with the bed area available for measurement and the coarseness of the bed, since large diameter grains cover a relatively large area of the bed compared to small grains. In addition, because tailspill flats were coarser and smaller in area compared to unspawned beds, fewer measurements were made on individual redds (73 to 196) than unspawned beds (259 to 268).

Table 2.1. Approximate equivalence of characteristics of grains used for total resistance measurements and pocket resistance measurements.

Size class (mm)	Diameter (mm)		Grain weight (grams force)		CSF ^b (dimensionless)		Angularity ^c	
	Total ^a	Pocket	Total ^a	Pocket	Total ^a	Pocket	Total ^a	Pocket
22.6	25.8	28.8	20.9	22.6	0.58	0.56	4.6	4.0
16.0	19.0	19.8	9.2	11.0	0.60	0.60	4.0	4.0
11.3	13.7	15.9	3.9	4.6	0.63	0.60	4.0	4.0
8.0	9.3	8.6	1.1	1.1	0.62	0.69	3.7	3.0
5.7	7.2	7.1	0.6	0.7	0.65	0.78	3.3	3.0

^aValues are means computed from particles used in total resistance measurements.

^bGrain shape classified with Corey Shape Factor (CSF) = $d_s/\sqrt{d_L d_i}$ where d_s , d_L , and d_i are the short, long, and intermediate grain axes. A value of 1.0 designates a sphere and <1 indicates departure from sphericity.

^cAngularity classified with the Powers [1953] roundness scale, where 3 indicates a sub-angular grain, 4 a sub-rounded grain, and 5 a rounded grain.

2.3.5 Pocket Resistance Measurements

Upon completion of the total resistance measurements, contact glue was poured on the beds to fix the undisturbed halves for removal from the flume to measure surface grain-size distributions and pocket resistance angles. Glue cemented the bed surfaces without pooling and modifying grain pocket geometries. Glued beds were lifted in their boxes with

an overhead crane onto a table for conducting *Wolman* [1954] pebble counts. Grains were selected by lowering a small pointed stick while looking away, and the apparent diameter of the particle was measured with digital calipers to the nearest 0.1 mm. Diameters were apparent because grains were sometimes partially buried and fixed on the bed. *Wolman* samples were used to determine the median grain size (D_{50}) and standard deviation of grain diameters (σ), and to calculate skewness (S) as the third moment of the grain-size distribution

$$S = \frac{N}{(N-1)(N-2)} \sum_{i=1}^N \left(\frac{D - D_{50}}{\sigma} \right)^3 \quad (2.4)$$

where N is sample size and D is the measured intermediate grain diameter. After *Wolman* samples were taken, beds were mounted on a tilt board for measuring pocket resistance angles with test grains. The tilt board was similar to those used by other researchers [*Miller and Byrne*, 1966; *Li and Komar*, 1986; *Kirchner et al.*, 1990; *Buffington et al.*, 1992; *Johnston et al.*, 1998] except it was counterbalanced and used with a block and tackle to provide slow, steady lift with a small electric hoist. Test grains were chosen from the unused portions of the experimental grain mixtures to approximate the average CSF, angularity, and diameter of grains for which total resistance measurements were made (Table 2.1).

Pocket resistance angles were measured by dropping a test grain from a short distance on to random locations of the glued surface and increasing the angle of tilt until grain movement occurred. Critical angles (ϕ) were measured to the nearest degree with an electronic level. Pocket resistance measurements were limited to angles less than 90° because $\tan \phi$ is asymptotic at 90° and because obtuse angles represent test grains entrapped by overhanging grains that would likely prevent grain movement in nature. The percentage

of such cases was higher for smaller grains and decreased from 19% for the 5.7 mm test grain to 0% for the 22.6 mm test grain. Only one test grain was placed on the bed at a time to enable accurate observations of entrainment. Approximately 50 pocket angles were measured with each test grain on each bed. On redds, the 50 measurements were apportioned by area between the pot, tailspill slope, and tailspill flat (only the latter are used here). This made as few as 12 and as many as 31 measurements available for defining pocket angle distributions within each size class on the tailspill flat of redds.

2.3.6 Equivalence of Methods

Calculating packing resistance as the difference between total resistance and pocket angle resistance requires equivalence of load cell and tilt board methods. Equivalence was established by *Johnston et al.* [1998] for a grain's first detectable movement. Because we used a somewhat different definition of motion (when a grain moves its diameter downstream), a separate test for equivalence was needed. We tested for equivalence by applying load cell and tilt board methods to test grains placed on one of our glued beds (LB redd, sediment mix 2). A test grain was placed on the surface and the pocket resistance force (F_p) was measured with the load cell before the grain was replaced on the bed and the pocket angle (ϕ_p) was measured by tilting the bed. The load cell force was converted to a friction coefficient with Equation (2.2a); the pocket angle was converted to a friction coefficient with $\tan \phi_p$. We did not expect perfect agreement between methods because it was impossible to replace grains in the same exact orientation in a given pocket. Even so, 84% of paired measurements exhibited less than a $\pm 30\%$ difference and, on average, displayed a

nearly 1:1 relationship (Figure 2.4). Paired two-sample t -tests further indicate that the approaches are statistically similar within the error of our measurements ($\alpha=0.05$).

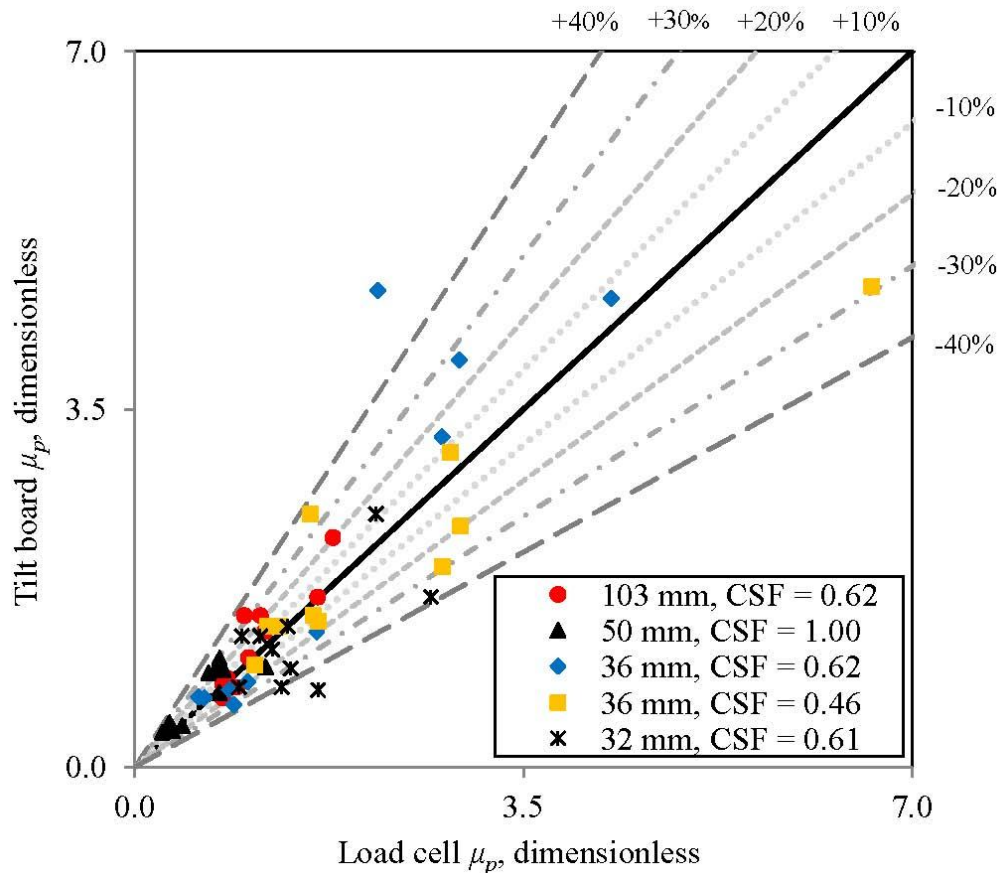


Figure 2.4. Paired pocket friction coefficients measured with the load cell and tilt board for grains placed in similar orientations on the left bank redd composed of sediment mix 2. A simple linear regression of the data ($R^2=0.74$, not shown) exhibits a slope of 0.9 and intercept of 0.2.

2.3.7 Monte Carlo Simulations

Monte Carlo simulations were used to randomly pair percentiles of total resistance and pocket resistance coefficients for determining packing resistance with Equation (2.3).

Measured μ_t and μ_p distributions were truncated at the 30th and 70th percentiles to avoid

unrealistic pairings during the simulations; for example, it is unlikely that a grain in a shallow pocket in a mixed-grain bed would have significant packing or that a grain in a deep pocket would have little packing. Normal distributions of μ for the simulations were obtained through \log_{10} transformations of measured μ_t and μ_p values. Initial testing showed that Monte Carlo simulations could reproduce the mean of measured μ_t and μ_p distributions to within $\pm 5\%$, indicating that μ_t and μ_p could be modeled with acceptable accuracy with log-normal distributions. One thousand individual pairings of μ_t and μ_p (referred to as trials) were used to determine distributions of μ_{pack} for each grain-size class on each bed. Trials yielding negative values of μ_{pack} for cases of $\mu_p > \mu_t$ were discarded, leaving between 944 and 1000 trials for grain-size classes on each bed.

2.3.8 Embeddedness

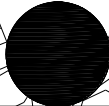
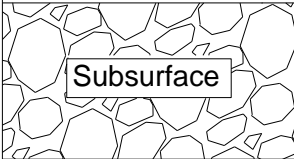
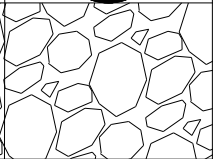
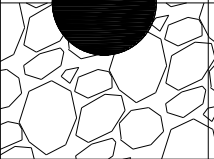
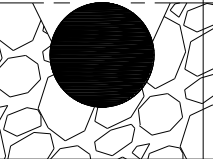
We calculated grain embeddedness using measurements of grain protrusion and diameter to relate packing resistance to grain burial. We defined embeddedness (E) as the proportion of a grain below the average bed surface (Figure 2.5), which can be inferred from grain protrusion (P) and measured grain diameter (D) using a modification of *Bunte and Abt's* [2001] equation

$$E = (D - P) / D = 1 - (P / D) \quad (2.5)$$

Because grains could not be extracted from the glued beds for directly measuring embeddedness, we define D as the apparent intermediate diameter (that visible on the surface). This likely overestimates the true vertical dimension of the grain, particularly if the grain is oriented with its short axis near vertical, and may overestimate E . Given that the short, intermediate, and long axes are related for a given sediment, our approach likely

introduces bias, but should preserve the functional trend in any relations between embeddedness, grain size, and packing resistance. Paired values of P and D were measured on the glued halves of each bed with a ruler and digital calipers, respectively. We used *Kirchner et al.*'s [1990] definition of protrusion, measuring the vertical height that a grain extends above the local mean bed elevation (interpolated by eye) within a radius equal to the D_{84} on the bed. In this approach, the use of a relative datum (local mean bed elevation) can produce negative values of protrusion when grains reside in deep pockets with their tops below the average bed elevation (Figure 2.5). Values of P and D were measured for all grains in a streamwise transect on each bed and on 4 to 7 randomly located cross-sectional transects. As with pocket angle and total resistance measurements, analyses were limited to the 5.7 to 22.6 mm size classes, for which 54 to 192 values of P were measured on each bed. From these measurements, distributions of embeddedness were determined from Equation (2.5) for each grain-size class and bed surface. These values, in turn, were used to investigate the effect of embeddedness on packing resistance.

Figure 2.5. Example of embeddedness calculated with Equation (2.5) for a 10 mm diameter sphere with variable protrusion.

Bed surface				
Subsurface				
Protrusion, mm	10	5	0	< 0
Embeddedness	0	0.5	1.0	>1.0

2.4 Results

2.4.1 Grain Size Distributions, Protrusion, and Embeddedness

Water working and simulated spawning produced surface grain-size distributions on unspawned beds and redds that differed in several key ways. Winnowing of sand during simulated spawning increased bed coarseness (D_{50}) on all redds more than water working alone (Figure 2.1, Table 2.2). Unspawned grain-size distributions were better sorted (lower σ) compared to redds for sediment mixes 1 and 2 (Table 2.2). Higher σ values were measured on redds because a portion of fines winnowed during redd building deposited on the tailspill flat and combined with coarse grains to increase σ over that on unspawned beds. This was not observed for sediment mix 3 because it contained a lower proportion of small grains (≤ 5.7 mm) than mixtures 1 and 2. Grain-size distributions on all beds were positively skewed, indicating fine sediments composed a higher proportion of the size distribution (by count) than larger grains, especially on unspawned beds. Skewness of the grain-size distributions was sufficiently high on five of the nine beds for σ to be $\geq D_{50}$ (Table 2.2).

Table 2.2. Characteristics of grain-size distributions on unspawned beds (US) and the flat portion of left bank (LB) and right bank (RB) redd tailspills.

Sediment mix	1			2			3		
	US	LB redd	RB redd	US	LB redd	RB redd	US	LB redd	RB redd
Sample size	150	100	100	150	164	100	150	100	100
D_{50}^1 (mm)	5.0	9.7	7.3	5.1	7.3	6.8	7.4	12.4	10.0
σ^a (mm)	5.1	8.4	7.8	5.5	7.3	5.7	9.4	7.3	7.1
Skewness	2.0	1.0	1.8	2.9	1.6	2.2	1.6	0.5	0.5
Embeddedness ^b	1.14	1.22	0.99	1.12	1.14	1.00	1.11	1.07	0.86

^a D_{50} is the median grain size and σ is the standard deviation of grain sizes.

^bEmbeddedness is averaged for each bed by weighting the mean embeddedness within size classes by the proportion of each grain size on the bed.

Protrusion and embeddedness displayed a range of values for each grain size for the ensemble data (Figure 2.6). As expected, values of protrusion increased with grain diameter (Figure 2.6a) and embeddedness was larger and varied more widely for smaller grains (Figure 2.6b) because they tend to deposit in resting pockets that are deep relative to their diameter, especially on surfaces that are relatively coarse, such as redds.

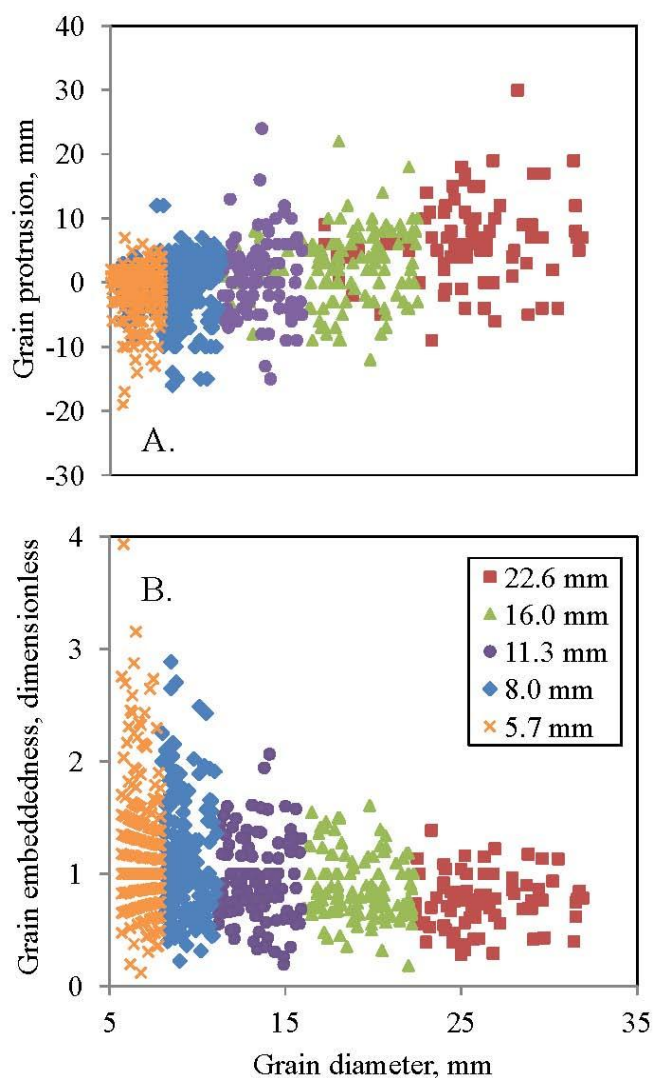


Figure 2.6. Measured (A.) grain protrusion and calculated (B.) embeddedness (Equation (2.5)) as a function of apparent diameter on glued bed surfaces (all data combined). Symbols and colors represent half-phi size classes (lower bin size reported in figure key).

2.4.2 Packing Friction Coefficients

The results of Monte Carlo simulations for each bed are presented as cumulative distributions of packing resistance (μ_{pack} , Figure 2.7) and as values for each source of resistance (μ_t , μ_{pack} , and μ_p) averaged within size classes (Table 2.3). Packing was the primary form of resistance to grain motion in nearly all size classes on all beds and exceeded pocket angle resistance (μ_p) by as much as 88% (Table 2.3). Exceptions where μ_p exceeded μ_{pack} occurred in the 22.6 mm size class on the RB redd composed of mix 3 because one pocket angle measurement was made near 90°. Another exception occurred in the 16.0 mm size class on the LB redd composed of mix 1 because few measurements were available for averaging. The median packing friction coefficient for redds (7.1) was 13% lower than for unspawned beds (8.0) as a result of spawning winnowing fines and loosening the beds. Average values of μ_t and μ_{pack} increased sharply with decreasing grain size, whereas μ_p varied little and unsystematically (Table 2.3). Somewhat constant values of μ_p contradict prior pocket angle studies and resulted from averaging within size classes, only considering angles <90°, and differences in how entrainment was defined [Kirchner *et al.*, 1990; Buffington *et al.*, 1992]. However, our bed-average values of total resistance and pocket resistance expressed as friction angles (80-82° and 45-60°, respectively) were comparable to those reported by others [e.g., Johnston *et al.*, 1998; Hodge *et al.*, 2013]. Standard errors of μ_{pack} averaged within grain-size classes were high (Table 2.3) due to the variability in μ_t and μ_p within grain-size classes and the low number of μ_t and μ_p measurements for calculating μ_{pack} . Additionally, standard errors generally increased with decreasing grain size in

reflection of high variation of embeddedness (Figure 2.6b) and because the mean μ_{pack} was higher for smaller grains.

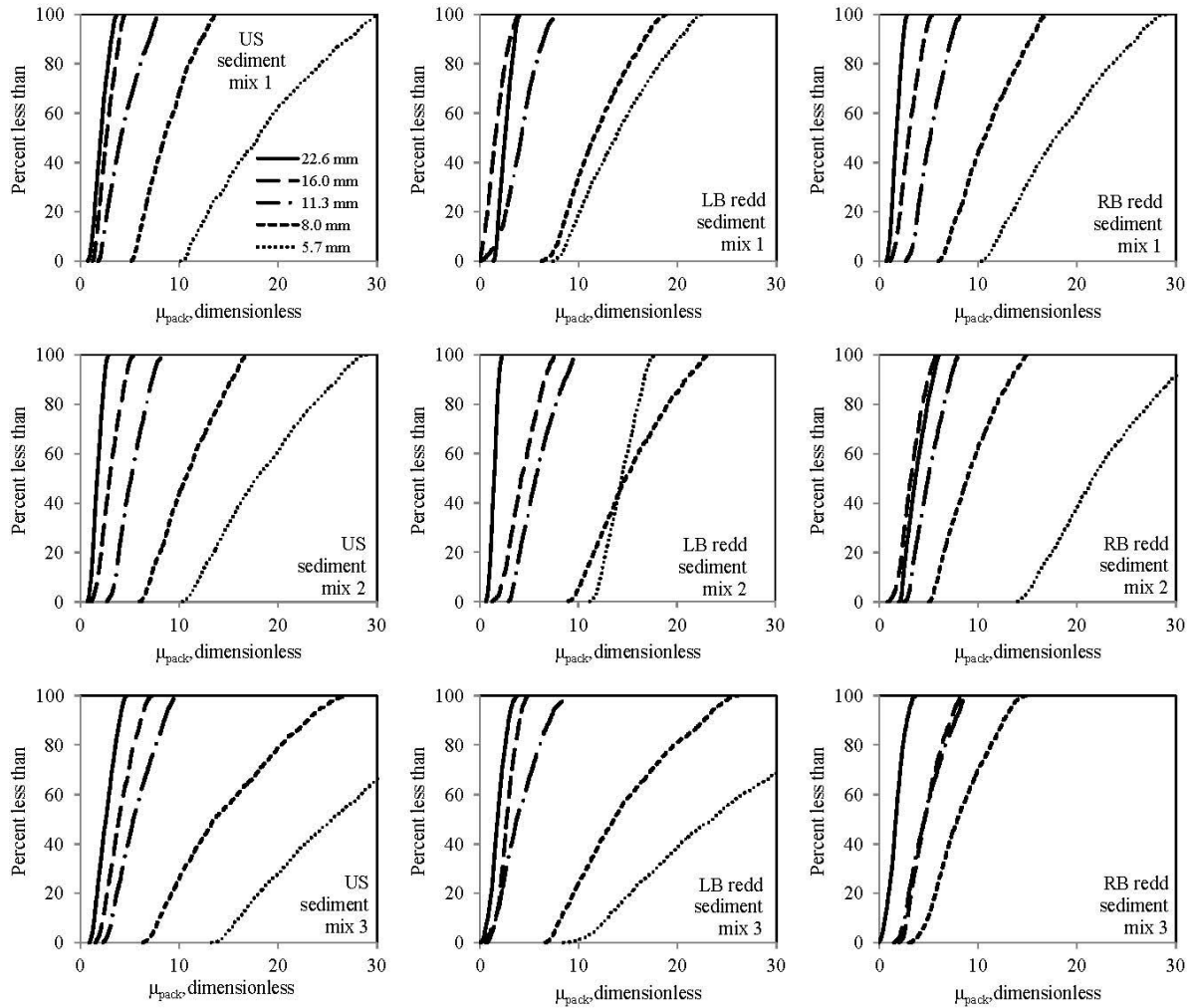


Figure 2.7. Cumulative distributions of packing friction coefficients (μ_{pack}) for grain-size classes on the unspanned beds (US), left bank redds (LB) and right bank redds (RB) for sediment mixtures 1-3. Lines represent half-phi size classes (lower bin size reported in figure key) for each bed.

Table 2.3. Average friction coefficients for total resistance (μ_t), pocket angle resistance (μ_p), and packing resistance (μ_{pack}), and the standard error of the average μ_{pack} by each grain-size class (lower bin size shown) and bed.

Bed	Size class (mm)	Avg grain weight (gram force)	Avg μ_t	Avg μ_p (% of μ_t)	Avg μ_{pack} (% of μ_t)	Standard error of avg μ_{pack} ^a
US mix 1	22.6	19.9	3.1	1.0 (32%)	2.1 (68%)	0.5
	16.0	9.9	3.7	1.0 (27%)	2.7 (73%)	0.6
	11.3	3.5	5.4	1.0 (18%)	4.4 (82%)	0.9
	8.0	1.0	9.6	0.8 (8%)	8.8 (92%)	1.2
	5.7	0.7	19.8	1.2 (6%)	18.6 (94%)	5.5
LB redd mix 1	22.6	26.6	3.5	0.9 (25%)	2.6 (75%)	0.5
	16.0	11.8	3.8	2.2 (59%)	1.6 (41%)	1.0
	11.3	4.1	7.1	2.9 (41%)	4.2 (59%)	2.1
	8.0	0.9	13.5	1.5 (11%)	12.0 (89%)	4.2
	5.7	0.6	15.9	1.7 (11%)	14.1 (89%)	3.5
RB redd mix 1	22.6	21.5	3.0	1.3 (43%)	1.7 (57%)	0.5
	16.0	8.1	4.3	1.3 (28%)	3.1 (72%)	1.2
	11.3	3.7	6.8	1.5 (23%)	5.3 (77%)	1.2
	8.0	1.3	12.4	1.4 (11%)	11.0 (89%)	2.9
	5.7	0.7	19.8	1.4 (7%)	18.5 (93%)	7.9
US mix 2	22.6	16.3	3.5	1.2 (35%)	2.3 (65%)	0.7
	16.0	8.0	4.5	1.6 (35%)	2.9 (65%)	1.3
	11.3	3.0	8.9	1.2 (14%)	7.6 (86%)	1.1
	8.0	1.0	13.2	1.2 (9%)	12.0 (91%)	1.2
	5.7	0.6	18.7	1.3 (7%)	17.3 (93%)	2.5
LB redd mix 2	22.6	18.2	2.6	1.1 (43%)	1.5 (57%)	0.5
	16.0	9.1	6.0	1.6 (27%)	4.4 (73%)	3.1
	11.3	4.4	6.9	1.0 (14%)	5.9 (86%)	2.4
	8.0	0.8	16.8	1.5 (9%)	15.3 (91%)	2.6
	5.7	0.5	15.8	1.3 (8%)	14.4 (92%)	2.7
RB redd mix 2	22.6	16.9	4.7	0.9 (20%)	3.8 (80%)	1.2
	16.0	7.8	4.8	1.5 (31%)	3.3 (69%)	2.5
	11.3	3.6	6.4	1.3 (20%)	5.1 (80%)	1.8
	8.0	0.9	10.3	1.1 (10%)	9.2 (90%)	3.1
	5.7	0.5	23.9	1.6 (7%)	22.3 (93%)	4.3
US mix 3	22.6	24.4	3.9	1.3 (32%)	2.6 (68%)	0.6
	16.0	9.5	5.4	1.3 (24%)	4.1 (76%)	1.3
	11.3	4.7	7.0	1.3 (19%)	5.6 (81%)	1.1
	8.0	1.2	16.2	1.5 (9%)	14.7 (91%)	4.2
	5.7	0.7	27.9	1.6 (6%)	26.3 (94%)	6.2

Table 2.3. (continued)

Bed	Size class (mm)	Avg grain weight (gram force)	Avg μ_t	Avg μ_p (% of μ_t)	Avg μ_{pack} (% of μ_t)	Standard error of avg μ_{pack} ^a
LB	22.6	23.4	3.4	1.5 (45%)	1.8 (55%)	1.3
redd	16.0	10.2	4.4	1.6 (37%)	2.8 (63%)	1.8
mix 3	11.3	4.1	6.0	1.9 (31%)	4.1 (69%)	4.0
	8.0	1.4	16.0	1.5 (9%)	14.5 (91%)	9.1
	5.7	0.6	28.1	2.5 (9%)	25.5 (91%)	10.6
RB	22.6	20.2	3.6	1.9 (53%)	1.7 (47%)	1.1
redd	16.0	9.5	6.4	1.6 (25%)	4.8 (75%)	1.2
mix 3	11.3	4.3	6.1	1.2 (21%)	4.8 (79%)	4.2
	8.0	1.1	10.3	1.9 (18%)	8.4 (82%)	3.6

^aStandard error (SE) of average $\mu_{pack} = \sqrt{(SE_{\mu_t})^2 + (SE_{\mu_p})^2}$, where $SE_i = s_i/\sqrt{n_i}$ and where s is the standard deviation of i and n is the number of measurements of i , with i representing μ_t and μ_p , respectively.

Distributions of μ_{pack} exhibit short, steep tails that resulted from limiting pairings of μ_t and μ_p during our Monte Carlo simulations to distributions truncated at the 30th and 70th percentiles (Figure 2.7). For example, truncating the μ_t and μ_p distributions at the 10th and 90th percentiles causes a nearly three-fold increase in skewness of the predicted μ_{pack} distributions for grain-size classes on the RB redd composed of sediment mix 3. The increase is due to expanding the tails of the μ_{pack} distribution which, in turn, causes μ_{pack} to increase by 26% on average across the grain-size classes. Our Monte Carlo simulations of μ_{pack} are therefore conservative, producing values smaller than what might result if we included the tails of the μ_t and μ_p distributions.

We also note that packing resistance varies inversely with grain size on most beds (Figure 2.7). This occurs because small grains are relatively angular (Table 2.1), which promotes jamming, and they tend to be more embedded (Figure 2.6b), thereby generating higher friction. Exceptions where large grains exhibited higher packing resistance than small

grains over at least a portion of their distribution occurred on the LB redd mix 1 and RB redd mix 2 (22.6 and 16.0 mm size classes), LB redd mix 2 (8.0 and 5.7 mm size classes), and the RB redd mix 3 (16.0 and 11.3 mm size classes; Figure 2.7) because equal or slightly higher pocket resistance was measured for the larger size class of each pair. Percentiles of μ_{pack} (Figure 2.7) ranged wider for smaller grains compared to larger grains because small grains display a higher variability of embeddedness (Figure 2.6b) for generating variable packing resistance.

For the ensemble data, packing resistance exhibits a direct relation with embeddedness (E) and an inverse relation with grain size (D) for values averaged within grain-size classes (Figure 2.8). The fit, however, was less strong between μ_{pack} and E ($R^2=0.66$, Figure 2.8a) than D ($R^2=0.90$, Figure 2.8b) probably because E was not measured directly, but estimated from measurements of protrusion and apparent grain diameter. A unique power relation was measured between μ_{pack} and E for each bed surface ($\mu_{pack} = \alpha(E)^\beta$, Figure 2.8a, Table 2.4), where the coefficient α exhibits a linear relation with skewness of the bed surface grain-size distribution and the exponent β varies as a power function of the bed surface D_{50} (Figure 2.9). In other words, beds with similar E can exhibit different local burial by fines and variable degrees of packing resistance depending on the coarseness of the bed. Exceptions included coefficients for the unspawned bed and left bank redd composed of sediment mix 1 that were outliers from the linear trend for reasons that were not apparent in the data (Figure 2.9).

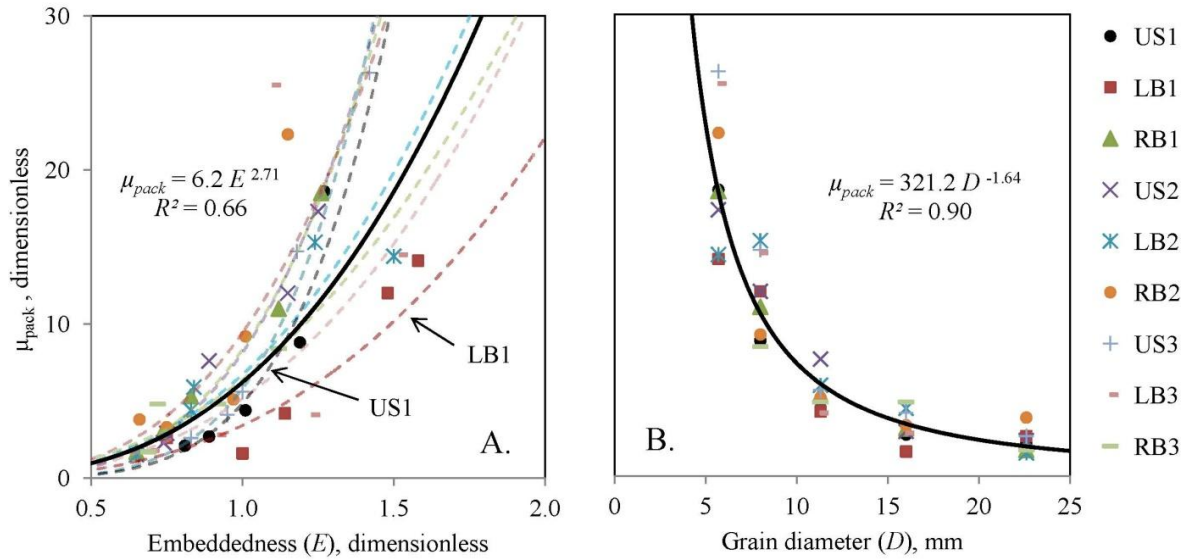


Figure 2.8. Packing friction coefficient (μ_{pack}) as a function of (A.) embeddedness (E) and (B.) grain diameter (D) for unspawned beds (US), left bank redds (LB) and right bank redds (RB) for sediment mixtures 1-3. The solid curves are power regressions of all data in (A.) and (B.). Dotted curves in (A.) are power regressions corresponding to individual beds by color. Friction coefficients and values of E are averaged by grain-size class. Grain diameter represents the lower bin size for classes in half-phi size intervals for each bed. The unspawned bed and left bank redd are labeled in (A.) for reference in Figure 2.9.

Table 2.4. Coefficients (α) and exponents (β) for power law regressions ($\alpha(E)^\beta$) of packing friction coefficients as a function of grain embeddedness (E) for individual beds (see Figure 2.8a).

Sediment mix	1			2			3		
	US	LB redd	RB redd	US	LB redd	RB redd	US	LB redd	RB redd
α coefficient	4.8	3.4	8.3	8.1	6.7	9.4	5.8	6.2	6.4
β exponent	4.60	2.70	3.40	3.54	2.70	2.96	4.53	2.70	2.40
R^2	0.96	0.74	0.98	0.95	0.89	0.75	0.99	0.49	0.66

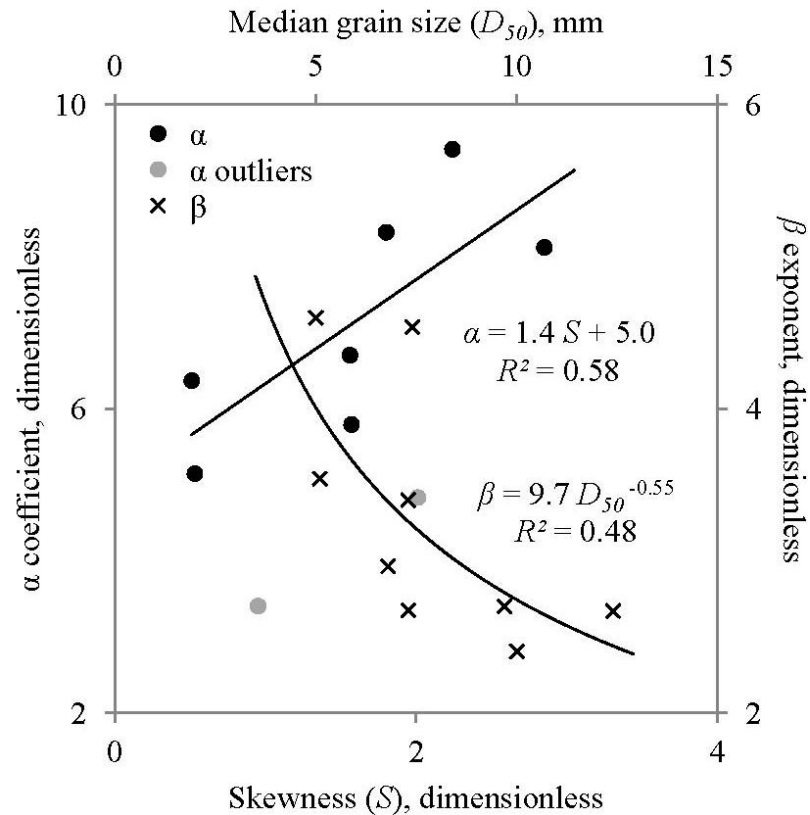


Figure 2.9. Power law coefficients (α) and exponents (β) for regressions of packing friction coefficients (μ_{pack}) and embeddedness (E) for individual beds in Figure 2.8a as a function of the skewness (S) and median grain size (D_{50}) of the bed surface grain-size distributions. Coefficients for the unspawned bed and LB redd composed of sediment mix 1 are shown in the figure, but excluded from the linear regression because they were outliers.

At the bed scale, a power law also related skewness of the bed surface grain-size distribution and bed average μ_{pack} , determined by weighting μ_{pack} averaged within size classes by the proportion of each grain size on the bed (Figure 2.10). This was expected since beds with a higher proportion of fines (increased skewness) will be more tightly packed [Haynes and Pender, 2007] due to grains percolating into the bed [Reid et al., 1985; Schalchli, 1992] and raising the bulk density of the grain mixture [Sohn and Moreland, 1968].

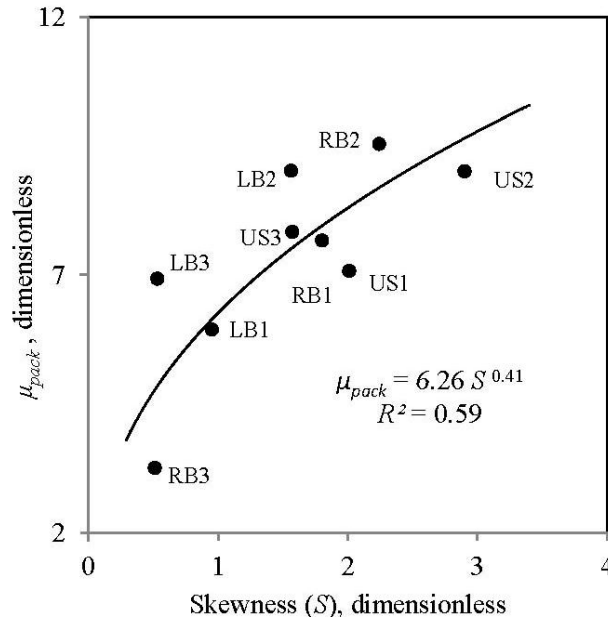


Figure 2.10. Bed average packing (μ_{pack}) as a function of skewness of the bed surface grain-size distributions.

2.4.3 Predictive Equation for Packing Friction Coefficients

We combined data from all beds to develop an equation for predicting μ_{pack} with a multiple regression of the form

$$\mu_{pack_n} = \omega_n E_i^{-\beta_n} D_i^{-\delta_n} S^{-\gamma_n} \quad (2.6)$$

to relate the n^{th} percentile (n) of μ_{pack} to the intercept of the regression (ω), embeddedness (E_i) averaged within the i^{th} grain-size class, the lower boundary of the i^{th} grain-size class (D_i), and skewness of the surface grain-size distribution (S), where α_n , β_n , δ_n , and γ_n are fitted individually with simple linear regressions of E_i , D_i , and S for each value of n (Table 2.5). The multiple regression model and both ω and D_i were significant (with $\alpha=0.05$ for both F and t statistics) for all values of n , but E_i and S were not significant for all percentiles. Insignificance was partly caused by bivariate correlation between D_i and E ($R^2=0.68$). We

examined the effect of bivariate correlation in the model by regressing each covariate against the remaining variables and found the variance inflation factor ($= 1/(1-R^2)$) was <7.4 , indicating that an acceptable level of collinearity existed in the model [Hair *et al.*, 1995; Kutner *et al.*, 2004]. We attempted stepwise removal of E_i then S to improve the model, but doing so failed to improve the significance of the remaining variables and decreased the model's performance. We therefore chose to retain all variables in the multiple regressions (Table 2.5) to avoid producing a model that is not theoretically motivated [O'Brien, 2007], misspecifying the model [Mason and Perreault, 1991], or reducing the model to an artefact that deleting insignificant yet physically meaningful parameters can produce [Freedman, 1983; MacNally, 2000]. Simple linear regressions of the α , β , δ , and γ coefficients for n from 10-90 yielded

$$\omega_n = 1.67n + 262 \quad (2.7)$$

$$\beta_n = -0.13 \ln(n) + 0.63 \quad (2.8)$$

$$\delta_n = -0.13 \ln(n) + 2.18 \quad (2.9)$$

$$\gamma_n = 0.09 \ln(n) - 0.39 \quad (2.10)$$

with R^2 of 0.68, 0.97, 0.96, and 0.98, respectively. Inserting Equations (2.7) through (2.10) in Equation (2.6) gives

$$\mu_{pack_n} = (1.67n + 262)E^{-(0.13\ln(n)+0.63)}D^{-(0.13\ln(n)+2.18)}S^{-(0.09\ln(n)-0.39)} \quad (2.11)$$

We evaluated Equation (2.11) by plotting calculated values of μ_{pack} against μ_{pack} determined from Monte Carlo simulations for each bed (Figure 2.11). Close agreement

occurred for most grain-size classes on all beds, with notable exceptions occurring for 5.7 and 8.0 mm grains on the LB redd composed of sediment mixes 2 and 3 and the US bed composed of sediment mix 3 (Figure 2.11). Discrepancies may result from high standard deviations of pocket angles measured in these size classes on these beds (due to the occurrence of measured angles near 90°) and may reflect the effect of combining data from all beds for Equation (2.11). The 10th percentile of μ_{pack} was also predicted with high error in the 11.3 and 16.0 mm size classes on the LB redd composed of sediment mix 2 because the 10th percentile of embeddedness was near zero in these cases. However, Equation (2.11) accurately predicted μ_{pack} in the majority of comparisons.

Table 2.5. Multiple linear regressions^a of percentiles (n) of packing distributions for all beds combined. The standard error (SE) for regression intercept (ω), embeddedness (E , dimensionless), grain diameter (D , mm), and skewness of the grain-size distributions (S) are listed along with the correlation coefficient (R^2) for each parameter.

n^b	ω^c	SE_i	E^d	SE_E	D^c	SE_D	S^d	SE_S	R^2
10	334	0.29	0.33	0.60	1.91	0.27	-0.19	0.11	0.85
20	294	0.23	0.23	0.49	1.78	0.22	-0.13	0.09	0.89
30	298	0.22	0.18	0.47	1.73	0.21	-0.09	0.09	0.89
40	299	0.21	0.11	0.44	1.68	0.20	-0.08	0.08	0.90
50	317	0.21	0.10	0.43	1.66	0.19	-0.06	0.08	0.90
60	330	0.20	0.05	0.43	1.63	0.19	-0.05	0.08	0.90
70	374	0.20	0.06	0.43	1.64	0.19	-0.03	0.08	0.90
80	409	0.20	0.05	0.43	1.63	0.19	-0.01	0.08	0.90
90	453	0.21	0.05	0.43	1.63	0.19	0.01	0.08	0.90

^a F -statistics for multiple regressions ($n=10-90$) significant at $\alpha=0.05$.

^bDegrees of freedom are 43.

^c P -value significant (<0.05) at $\alpha=0.05$ for $n=10-90$ (two-tailed t -tests).

^d P -value insignificant (>0.05) at $\alpha=0.05$ for $n=10-90$ (two-tailed t -tests).

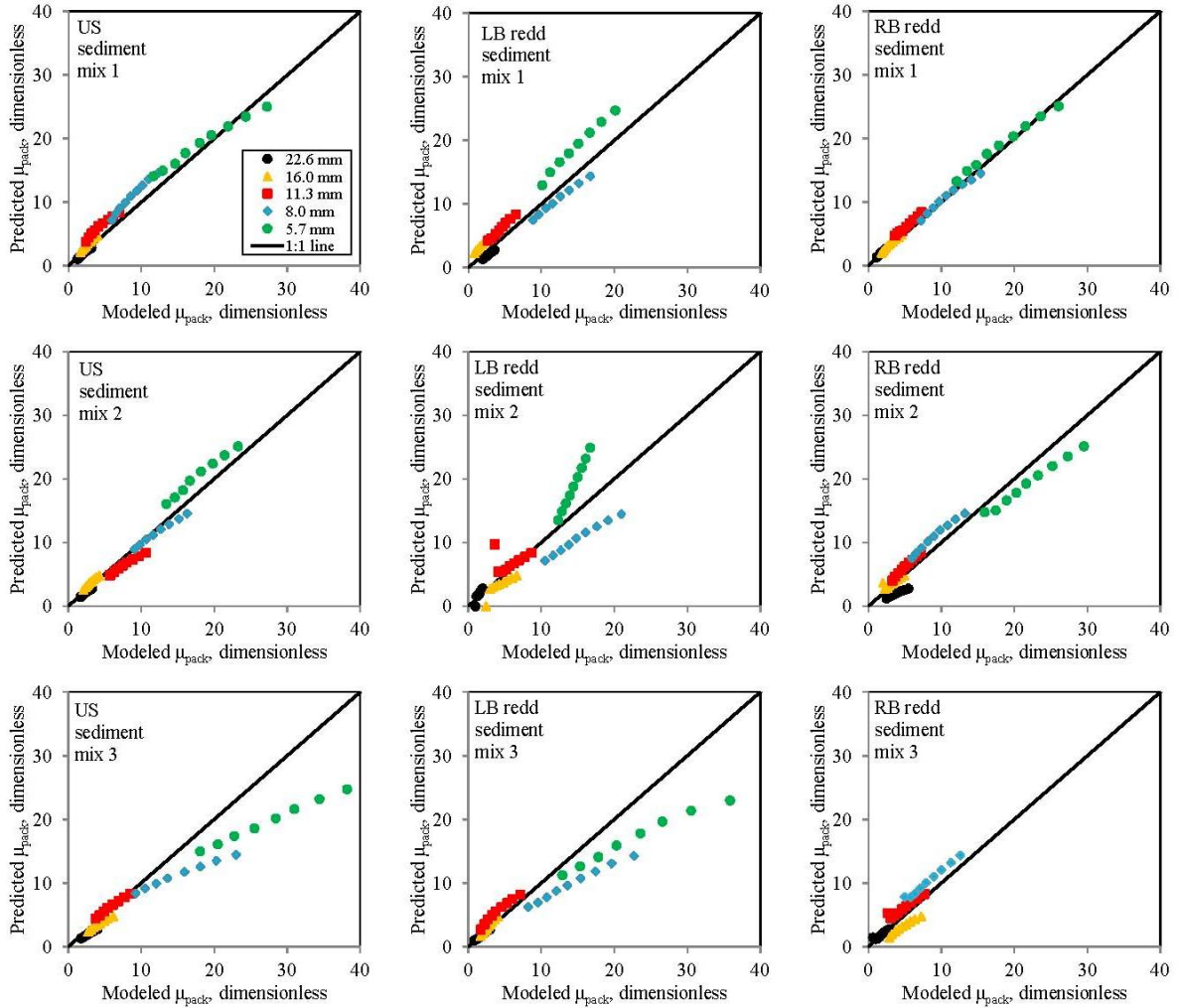


Figure 2.11. Plots of packing predicted with Equation (2.12) versus modeled in Monte Carlo simulations. Symbols and colors represent half-phi size classes (lower bin size reported in figure key) for each bed.

2.4.4 Critical Boundary Shear Stress

We used *Kirchner et al.*'s [1990] modification of the *Wiberg and Smith* [1987] model to evaluate the effect of packing resistance on theoretical values of critical boundary shear stress (τ_{ci})

$$\tau_{ci} = F_g \left\{ \frac{C_D}{2 \tan \phi k^2} \int_{P-e}^P \sqrt{\{D_i^2 - [2z - (2P - D_i)]^2\}} f(z)^2 dz + \frac{\pi C_L}{8k^2} D_i^2 [f(P)]^2 - \right. \\ \left. fP - Di2 - 1 \right. \quad (2.12)$$

where

$$F_g = (\rho_s - \rho) g \pi \frac{D_i^3}{6}$$

$$f(z) = \ln \left(\frac{z}{z_0} \right), \quad z \geq z_0$$

$$f(z) = 0, \quad z < z_0$$

and where ϕ is angle of resistance, e is frontal exposure to flow, g is gravitational acceleration, ρ_s and ρ are the grain and fluid densities (2.65 g cm^{-3} and 1.0 g cm^{-3} , respectively), C_D is the drag coefficient (assumed equal to 0.4), C_L is the lift coefficient (0.2; *Wiberg and Smith*, 1985), κ is von Karman's constant (0.407), D_i the lower boundary of the i^{th} grain-size class, $f(z)$ is the velocity profile function, z is the height above the bed, and z_0 is the roughness height where the velocity profile goes to zero. We define z_0 as $k_s/30$, which is derived from *Nikuradse*'s [1933] results for turbulent flow over rough boundaries, where the equivalent sand roughness (k_s) is taken as $0.4D_{50}$ [*Clifford et al.*, 1992]. To quantify the effect of packing resistance on τ_c , we evaluated Equation (2.12) for each grain size class, D_i ,

on each bed using the 10th percentile total friction angle versus that determined from the 10th percentile pocket angle, with the difference in results representing the effect of packing. The 10th percentile was used because it was shown by *Johnston et al.* [1998] to provide close agreement between predicted and measured values of τ_c at Sagehen Creek. In our calculations, we assume (1) a spherical grain shape (CSF=1.0); (2) the 90th percentile of measured protrusion pairs with the 10th percentiles of total and pocket resistance; and (3) protrusion equals exposure. Item (3) reflects our observation that the average difference between paired measurements of protrusion and exposure varied by only ~1 mm within size classes on the beds [*Buxton, unpublished data*]; item (2) is based on the inverse relationship between total resistance and protrusion [*Hodge et al.*, 2013]; and item (1) was used to simplify the calculations even though measured grains were somewhat elliptical in shape (Table 2.1). However, *Hodge et al.* [2013] note that assuming a spherical shape does not greatly affect calculations of τ_c when the actual shapes of grains are different.

Results show that packing resistance increased τ_{ci} by as much as 72% (30% on average), which represents an increase of up to 48 dyne cm⁻² over τ_{ci} calculated with pocket angles alone (Figure 2.12a). However, as P decreases toward z_0 , τ_{ci} becomes independent of friction angle because the grain is progressively hidden from flow. For example, comparable high values of τ_{ci} were predicted for both the total and pocket resistance angles for the 5.7 mm size class on the LB redd composed of sediment mix 1 (798 vs. 791 dyne cm⁻², respectively) because $P \approx z_0$, indicating the grain was hydraulically hidden from flow. Values of τ_{ci} predicted from total resistance generally increased with grain size, showing a low degree of size-selective transport (Figure 2.12b). Exceptions where greater stability (higher τ_c) was predicted for smaller size classes (5.7, 8.0, and 11.3 mm) occurred on the left

bank redds due to higher values of both embeddedness (Figure 2.6) and packing resistance (Table 2.3), countering the lower inherent instability of particles with less weight.

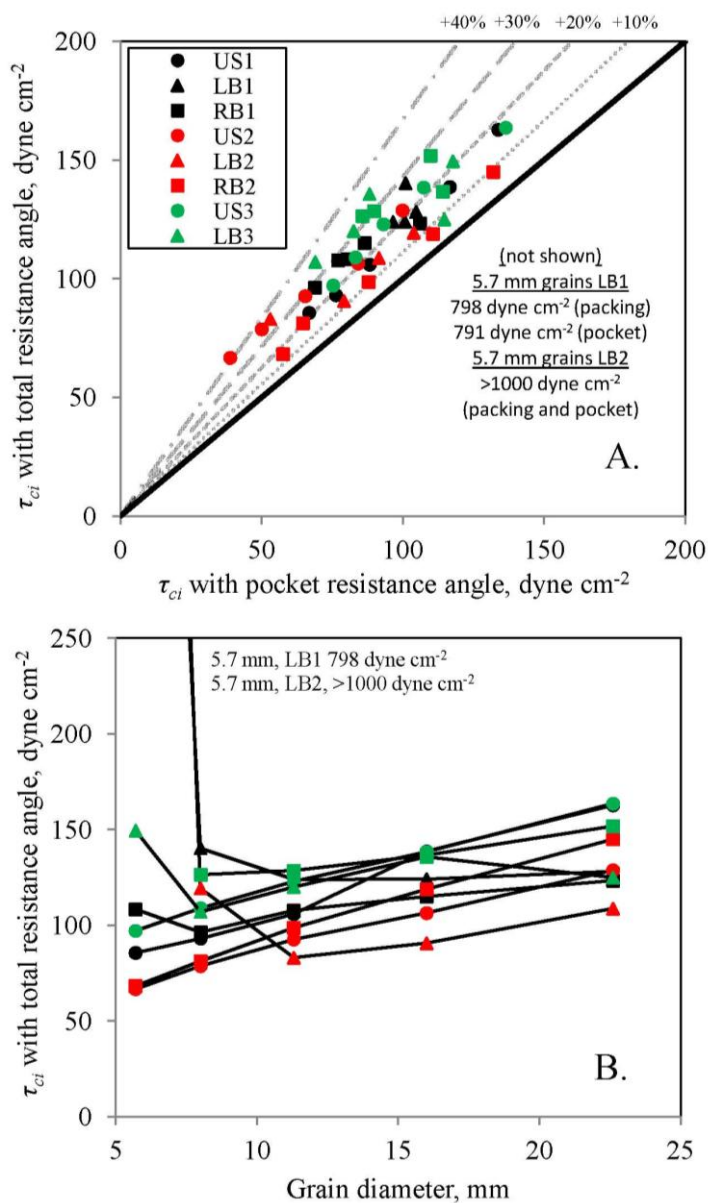


Figure 2.12. Difference in (A.) critical bed shear stress (τ_c) calculated with the total angle of resistance and pocket angle of resistance and (B.) critical bed shear stress calculated for total resistance for grain-size classes on unspawned beds (US) and left bank (LB) and right bank (RB) redds. Values of τ_c computed for the 5.7 mm grains on the LB redd composed of sediment mixes 1 and 2 are not plotted because they far exceeded the other values. Numbers indicate sediment mixtures composing the beds. Grain diameter represents the lower bin size for half-phi size intervals for each.

2.3.5 Grain Hiding Function and Critical Shields Stress

We examined the influence of grain packing on size-selective transport for our bed surfaces using a grain hiding function similar to that of *Parker et al.* [1982]

$$\tau_{ci}^* = \tau_{c50}^* \left(\frac{D_i}{D_{50}} \right)^b \quad (2.13)$$

where τ_{ci}^* and τ_{c50}^* are the critical Shields stresses for D_i and D_{50} , respectively. τ_{ci}^* is defined as

$$\tau_{ci}^* = \frac{\tau_{ci}}{(\rho_s - \rho)gD_i} \quad (2.14)$$

while τ_{c50}^* and b are power law regression values empirically determined for each surface.

At the grain scale, τ_{ci}^* is a function of the fluid stress (drag force per grain area parallel to the bed) and the submerged particle weight. Relatively coarse grains weigh more and protrude farther from the bed than small grains that are subjected to less drag because they are relatively hidden from flow [*Einstein*, 1950; *Egiazaroff*, 1965; *Wiberg and Smith*, 1987; *Kirchner et al.*, 1990]. The competing influence of grain weight and hiding effects are captured in the b -exponent, where a zero value designates fully size-selective entrainment, where small grains are entrained before large grains because transport is solely driven by differences in weight between particle sizes (e.g., no hiding effects). A b -exponent of -1 denotes equal mobility, where size fractions are entrained at the same threshold (uniform τ_{ci}) because differences in grain weight are offset by smaller grains being more hidden from the flow. Between these endpoints, all combinations of grain weight and hiding effects are possible [*Yager and Schott*, 2013], and b -exponents can be lower than -1 [*Buffington and*

Montgomery, 1997], possibly due to high packing (Table 3) and low protrusion (Figure 2.6) for small grains.

We hypothesize that grain packing adds to hiding effects by increasing resistance to motion for small grains, resulting in lower b -values and less size-selective entrainment, thereby promoting conditions that tend toward equal mobility. We test this hypothesis by comparing computed b -values for τ_{ci}^* determined from critical shear stresses for the 10th percentile total and pocket resistance angles, respectively (Section 2.3.4). Results show that packing resistance decreased the b -exponent by up to 43% (14% on average) compared to unpacked grains (in open pockets) (Figure 2.13). The differences were statistically significant (paired two-sample t -test, $\alpha=0.05$), proving our hypothesis that packing substantially lowers the b -exponent and decreases size-selective entrainment.

In addition, simulated spawning caused conditions closer to equal mobility by decreasing the average b -exponent on the tailspill flat on redds (-0.89) compared to unspawned beds (-0.56), suggesting that spawned stream bed surfaces mobilize *en masse* in comparison to unspawned beds. Grain-size fractions were equally mobile on the left bank redds composed of sediment mix 1 (-1.08), 2 (-1.06), and 3 (-1.03), respectively. Exponents for unpacked grains on these beds were also high (-0.96, -0.99, and -0.94, respectively). Taken together, these results suggest that beds with a low standard deviation of grain sizes and low skewness exhibit deep resting pockets that increase hiding effects which are accentuated when fine grains pack particles in their resting pockets (Figure 2.13, Table 2.2). Results also show that critical Shields stresses for median grain sizes (τ_{c50}^*) were up to 73% higher with packing, and were on average 37% higher on all beds (Figure 2.13). These percentages represent increases in τ_{c50}^* from an average of 0.060 (range of 0.044 to 0.075)

for unpacked grains to 0.081 (0.063 to 0.094) for packed grains (Figure 2.13). Our predictions are in the range of τ_{c50}^* values previously reported in the literature, but tend to plot at the upper bounds of the range for a given boundary Reynolds number (Figure 2.14).

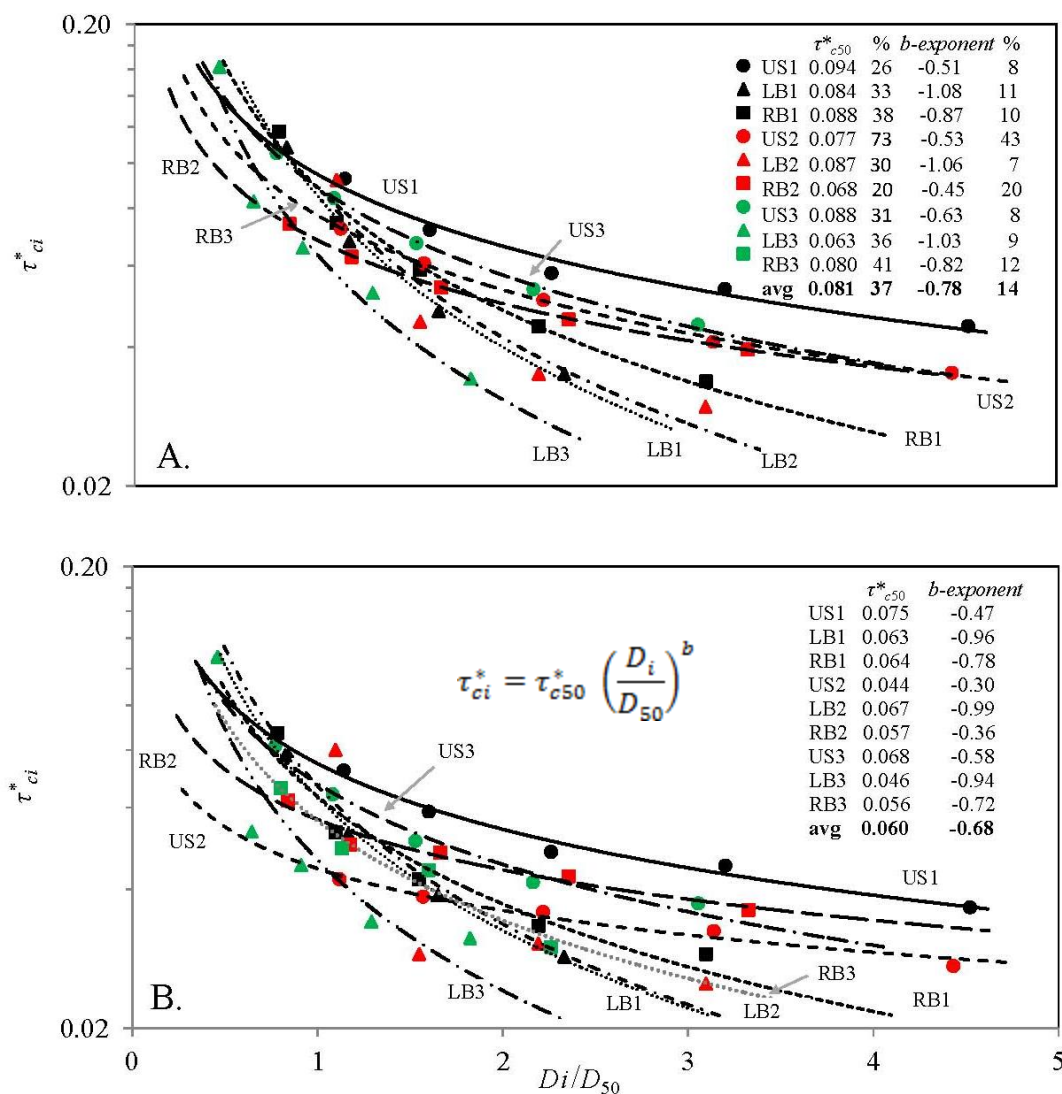


Figure 2.13. Critical dimensionless shear stress (τ_{ci}^*) for grain-size fractions (D_i) calculated with the 10th percentiles of the total resistance angle (A.) and pocket resistance angles (B.) versus relative grain size (D_i/D_{50}) for the unspawed beds (US) and left bank (LB) and right bank (RB) redds composed of sediment mixtures 1-3. Inset tables in both figures indicate critical dimensionless shear stress values for the median grain size (τ_{c50}^*) and the b -exponent in Equation (2.13), which is included in (B.) for reference. The percent increase in τ_{c50}^* and decrease in b due to packing are respectively shown in (A.).

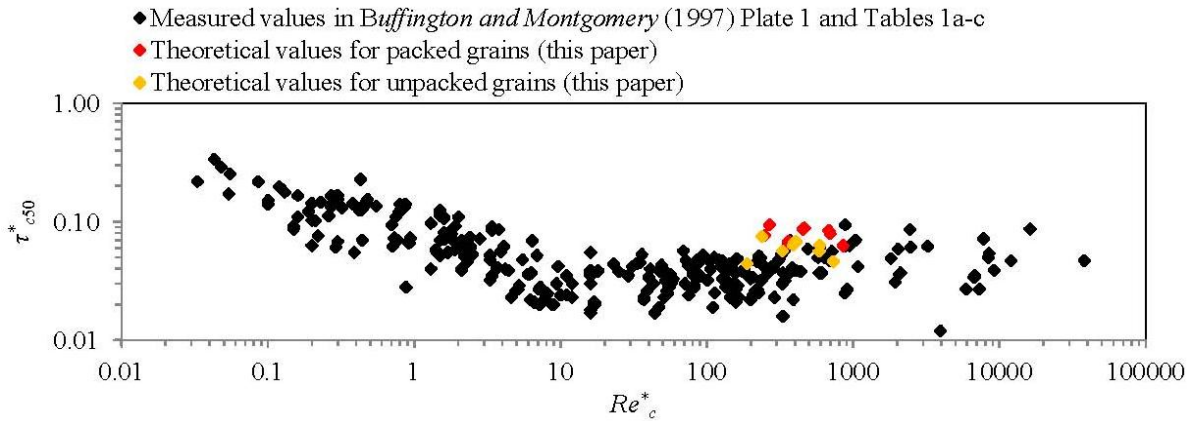


Figure 2.14. Critical dimensionless shear stress for median grain sizes (τ_{c50}^*) versus the critical boundary Reynolds number (Re_c^*) in this study and others. Values obtained from Tables 1a-c in *Buffington and Montgomery (1997)* were measured by visual, reference transport, and competence methods in streams and laboratory channels. Theoretical values for packed and unpacked grains were calculated with Equation (2.13). The critical boundary Reynolds number is defined as $u_c^* D_{50} / \nu$, where u_c^* is the critical shear velocity at incipient motion ($u_c^* \equiv \sqrt{\tau_c / \rho}$) and ν is kinematic viscosity.

2.5 Discussion

Research indicates that τ_{c50}^* typically ranges from 0.030 to 0.086 in gravel-bed rivers due, in part, to variation in turbulent shear stress at the bed and intergranular resistance of particles [*Buffington and Montgomery, 1997*], which is controlled by grain shape, sorting, and packing [*Miller and Byrne, 1966; Li and Komar, 1986; Kirchner et al., 1990; Buffington et al., 1992*]. We further demonstrate that packing resistance is influenced by grain diameter, embeddedness, and skewness of the grain-size distribution. We also show that packing resistance decreases the b -exponent in the grain hiding function [*Parker et al., 1982*], reducing the tendency for size-selective transport and promoting conditions that tend toward equal mobility. Packing may therefore be partially responsible for equal mobility observed by others [*Andrews and Erman, 1986; Lisle and Madej, 1992; Paolo and Seal, 1995*]. In some cases, high packing and low protrusion may combine to decrease the b -exponent

below -1 (Figure 2.13), indicating higher critical shear stresses for smaller grains than larger ones. Since winnowing of fine grains is often required to unpack coarse particles, higher packing resistance for small grains increases the overall stability of the beds so that both large and small grains require higher shear stress for entrainment.

We demonstrate that packing coefficients of friction can be expressed as functions of grain size, embeddedness, and skewness of the grain-size distribution. Of these factors, grain diameter is the most statistically significant variable for predicting packing. However, embeddedness also exerts control on packing (Figure 2.8a) since a grain can only be packed if it is resting at least partially in the bed. As embeddedness increases, skewness of the grain-size distribution plays an increasingly important role in controlling packing because it partially regulates the density of the bed and the points of contact between a grain and the packing matrix. Because of these factors, packing resistance occurred for all grain sizes in our study, reflecting that all stream beds are packed to some degree. Consequently, prior calculations of critical conditions using pocket angles (e.g., *Wiberg and Smith, 1987; Kirchner et al., 1990; Buffington et al., 1992*) underestimate the stress needed for grain motion, as demonstrated here (Figure 2.12a).

Neglecting packing is one of the factors that can make predictions of bed load transport prone to large errors in both steep and low-gradient streams [*Gomez and Church, 1989; Nitsche et al., 2011*] since sediment flux is usually a nonlinear function of the difference between applied and critical shear stresses. Consequently, modification of bed load transport formulae to include packing would likely improve bed load transport predictions. By doing so, our formulation for packing may help to alleviate some of the discrepancy between observations and predictions of sediment transport [*Barry et al., 2004*],

but additional work is needed to improve understanding of packing effects on grain motion. We also recommend that future research quantify packing with paired *in situ* measurements of total resistance and embeddedness given that our values of embeddedness are estimated (Section 2.2.8).

Packing coefficients reported herein may differ from actual values due to our inability to account for dynamic changes in the force acting on a grain when it begins to move from its pocket and alter its protrusion to flow. With increased protrusion in a natural flow, the drag force and torque applied to the grain will increase compared to our load cell measurements that were made at a fixed point on the grain. However, such differences do not apply to grains that move in a sliding motion, which constituted 57% of our total resistance measurements. Furthermore, error in load cell measurements compared to natural fluid forces is probably negligible for the remainder of our measurements due to grain sizes used in this study having short pivot arms and therefore negligible differences in dynamic torque.

Our packing coefficients and calculations of critical shear stress quantitatively support what others have observed in nature; that packing is a significant source of streambed stability [Powell and Ashworth, 1995]. By stabilizing the bed, packing motivates a variety of biological and physical responses in streams that can have a reciprocal effect on bed surface packing. For example, bed stabilization from packing may indirectly increase shear stress on channel banks if sediment transport and associated bed scour do not occur until relatively higher flows. In such cases, the lack of bed scour and hydraulic roughness from mobile sediment [Wiberg and Rubin, 1989] would result in a more rapid increase in flow speeds and depths with discharge, potentially elevating stress on channel banks relative

to mobile bed conditions. These conditions could then lead to bank erosion feeding back to more tightly pack the bed since banks typically exhibit a finer grain-size composition than the bed, providing a source of packing material as the bank erodes. Tight packing may, in turn, affect hyporheic exchange through the bed [Schalchli, 1992], microbial processes [Nogaro *et al.*, 2010], and the availability of interstitial habitat for benthic invertebrates [Gayraud and Phillippe, 2003].

A stream's biology can affect grain packing as well. Just as cohesive sediment mortars bed surfaces [Barzilai *et al.*, 2013], microalgae and macrofauna secrete polymers that bind mineral grains [Patterson, 1997] and increase consolidation and packing of the bed [Stone *et al.*, 2011]. Similarly, silk secretions by net spinning caddisfly (*Hydropsyche* spp.) bind grains and increase critical conditions for particle entrainment [Statzner *et al.*, 1999; Cardinale *et al.*, 2004; Johnson *et al.*, 2009; Albertson *et al.*, in press]. Conversely, a stream's fauna can also have a destabilizing effect on packing. For example, crayfish activity reduces sand in gravel interstices [Statzner *et al.*, 2000] and loosens the bed [Rice *et al.*, 2012]. Similarly, salmon spawning winnows sand and loosens stream beds [Montgomery *et al.*, 1996]. These activities can reset the stress history of a channel and other physical and biologic processes that pack stream beds.

2.6 Summary

We report the first measurements of grain packing resistance to particle motion and calculate packing effects on critical bed shear stress. Our results indicate that packing resistance can be expressed as a function of grain size, embeddedness, and skewness of the grain-size distribution. Embeddedness influences packing resistance because a grain can

only be packed if it is resting at least partially in the bed. As embeddedness increases, skewness of the grain-size distribution plays an increasingly important role in controlling packing resistance by regulating the sediment density of the bed and the points of contact between a grain and the packing matrix. However, grain diameter is the most statistically significant variable due to packing resistance being strongly inversely related to grain size. The inverse relationship results because smaller grains are more embedded (hidden from flow) and in contact with the surrounding bed material; and because small grains tend to be more angular for increasing intergranular jamming. Because winnowing of fine grains is often required to unpack coarse particles, higher packing resistance for small grains may increase the overall stability of the bed, so that both large and small grains require higher shear stresses for entrainment.

Including packing in calculations of shear stress increased critical values by as much as 72% (30% average) over that calculated with pocket angles alone and reduced the degree of size-selective transport on the beds, indicating that packing promotes conditions that tend toward equal mobility. Specifically, the exponent of the grain hiding function was lowered by up to 43% (average 14%) by including packing in calculations of the critical Shields stress. Packing also reduced the critical Shields stress for the median grain size by up to 73% (37% on average).

Due to its stabilizing effect on grains, including packing in calculations of critical bed shear stress and sediment flux will likely improve the accuracy of bed load transport predictions, which are typically nonlinear functions of the difference between applied and critical shear stresses. However, additional work is needed to identify the mechanics of

packing resistance and to better understand ties between grain packing, physical processes, and biology in river channels.

2.7 References

- Albertson, L. K., L. S. Sklar, P. Pontau, M. Dow and B. J. Cardinale (in press), A mechanistic model linking insect (*Hydropsychidae*) silk nets to incipient sediment motion in gravel-bedded streams, *J. Geophys. Res.–Earth Surf.*
- Allan A. F. and L. E. Frostick (1999), Framework dilation, winnowing and matrix particle size: the behaviour of some sand–gravel mixtures in a laboratory flume, *J. Sed. Res.*, 69, 21-26.
- Andrews, E. D. and D. C. Erman (1986), Persistence in the size distribution of surficial bed material during an extreme snowmelt flood, Sagehen Creek, northeastern California, *Water Resour. Res.*, 22, 627-634.
- Barry, J. J., J. M. Buffington, and J. G. King (2004), A general power equation for predicting bed load transport rates in gravel bed rivers, *Water Resour. Res.*, 40, doi:10.1029/2004WR003190.
- Barzilai, R. J., B. Laronne, and I. Reid (2013), Effect of changes in fine-grained matrix on bedload sediment transport in a gravel-bed river, *Earth Surf. Proc. Landforms*, 38, 441-448.
- Brouwers, H. J. H. (2006), Particle size distribution and packing fraction of geometric random packings, *Phys. Rev.*, 74, 1-14.
- Buffington, J. M., W. E. Dietrich, and J. W. Kirchner (1992), Friction angle measurements on a naturally formed gravel streambed: Implications for critical boundary shear stress, *Water Resour. Res.*, 28, 411-425.

- Buffington, J. M. and D. R. Montgomery (1997), A systematic analysis of eight decades of incipient motion studies, with special reference to gravel-bedded rivers, *Water Resour. Res.*, 33, 1993-2029.
- Bunte, K. and S. R. Abt (2001), Sampling surface and subsurface particle-size distributions in wadable gravel- and cobble-bed streams for analyses in sediment transport, hydraulics, and streambed monitoring, *U.S. Forest Service Rocky Mtn. Res. Stn. Gen. Tech. Rep. RMRS-GTR-74*, 426 pp.
- Cardinale, B. J., E. R. Gelmann, and M. A. Palmer (2004), Net spinning caddisflies as stream ecosystem engineers: The influence of Hydropsyche on benthic substrate stability, *Func. Ecol.*, 18, 381-387.
- Carling, P. A. and N. A. Reader (1982), Structure, composition, and bulk properties of upland stream gravels, *Earth Surf. Proc. Landforms*, 7, 349-365.
- Corey, A. T. (1949), Influence of shape on the fall velocity of sand grains, unpub. M.S. thesis, 102 pp., Colorado State University, Fort Collins.
- Church, M. (1978), Paleohydrological reconstructions from a Holocene valley fill, in *Fluvial Sedimentology*, edited by A.D. Miall, Canadian Society of Petroleum Geologists, Calgary, Alberta, pp. 743-772.
- Church, M. A. , D. G. McLean, and J. F. Wolcott (1987), River Bed Gravels: Sampling and Analysis, in *Sediment Transport in Gravel-Bed Rivers*, edited by C. R. Thorne, J. C. Bathurst, and R. D. Hey, John Wiley and Sons, pp. 43-88.
- Clifford, N. J., A. Robert, and K. S. Richards (1992), Estimation of flow resistance in gravel-bedded rivers: A physical explanation of the multiplier of roughness length, *Earth Surf. Proc. Landforms*, 17, 111-126.

- Downes, B. J., P. S. Lake, A. Glaister, and J. A. Webb (1998), Scales and frequencies of disturbance: Rock size, bed packing, and variation among upland streams, *Freshwater Biol.*, 40, 625-639.
- Egiazaroff, I. V. (1965), Calculation of non-uniform sediment concentrations, *J. Hydraul. Eng.*, 91, 225-248.
- Einstein, H. A. (1950), The bedload function for sediment transport in open channel flows, USDA Soil Conservation Service Technical Bulletin 1026, Washington DC, 73 pp.
- Folk, R. L. and W. C. Ward (1957), Brazos River bar: A study in the significance of grain size parameters, *J. Sed. Petrol.*, 27, 3-26.
- Francis, J. R. D. (1973), Experiments on the motion of solitary grains along the bed of a water-stream, *Proc. R. Soc. Lond. A*, 332, 443-471.
- Freedman, D. A. (1983), A note on screening regression equations, *Am. Statistician*, 37, 152-155.
- Frings, R. M., M. G. Kleinhans, and S. Vollmer (2008), Discriminating between pore filling load and bed structure load: A new porosity-based method, exemplified for the River Rhine, *Sedimentology*, 55, 1571-1593.
- Gayraud, S. and M. Phillippe (2003), Influence of bed-sediment features on the interstitial habitat available for macroinvertebrates in 15 French streams, *Internat. Rev. Hydrobiol.*, 1, 77-93.
- Gomez, B. and M. Church (1989), An assessment of bed load sediment transport formulae for gravel bed rivers, *Water Resour. Res.*, 25, 1161-1186.
- Groot, C. and L. Margolis (1991), *Pacific Salmon Life Histories*, 564 pp., University of British Columbia Press, Vancouver, B.C.

- Hair, J. F., R. E. Anderson, R. L. Tatham, and W. C. Black (1995), *Multivariate Data Analysis* (3rd ed), 757 pp., Macmillan, New York.
- Hassan, M. A. (1992), Structural controls of the mobility of coarse material in gravel-bed channels, *J. Earth Sci.*, *41*, 105-122.
- Haynes H. and G. Pender (2007), Stress history effects on graded bed stability, *J. Hydraul. Eng.*, *33*, 343-349.
- Heritage, G. L. and D. J. Milan (2009), Terrestrial laser scanning of grain roughness in a gravel bed river, *Geomorphology*, *113*, 4-11.
- Hodge, R. A., D. A. Sear, and J. Leyland (2013), Spatial variations in surface sediment structure in riffle-pool sequences: A preliminary test of the Differential Sediment Entrainment Hypothesis (DSEH), *Earth Surf. Proc. Landforms*, *38*, 449-465.
- Jepson, R., J. Roberts, and W. Lick (1997), Effects of bulk density on sediment erosion rates, *Water, Air, and Soil Pollution*, *99*, 21-31.
- Johnson, M. F., I. Reid, S. P. Rice, and P. J. Wood (2009), Stabilization of fine gravels by net-spinning caddisfly larvae, *Earth Surf. Process. Landforms*, *34*(3), 413-423.
- Johnston, C. E., E. E. Andrews, and J. Pitlick (1998), In situ determination of particle friction angles of fluvial gravels, *Water Resour. Res.*, *34*, 2017-2030.
- Kirchner, J. W., W. E. Dietrich, F. Iseya, and H. Ikeda (1990), The variability of critical shear stress, friction angle, and grain protrusion in water worked sediments, *Sedimentology*, *37*, 647-672.
- Komar, P. D. and Z. Li (1988), Applications of grain-pivoting and sliding analyses to selective entrainment of gravel and to flow-competence evaluations, *Sedimentology*, *25*, 681-695.

- Kutner, M. H., C. J. Nachtsheim, and J. Neter (2004), *Applied Linear Regression Models* (4th ed), 701 pp., McGraw-Hill/Irwin, New York.
- Li, Z. and P. D. Komar (1986), Laboratory measurements of pivoting angles for applications to selective entrainment of gravel in a current, *Sedimentology*, 33, 413-423.
- Ling, C. H. (1995), Criteria for incipient motion of spherical sediment particles, *J. Hydraul. Eng.*, 121, 472-478.
- Lisle, T. E. and M. A. Madej (1992), Spatial variation in armouring in a channel with high sediment supply, in *Dynamics of Gravel-Bed Rivers*, edited by P. Billi, R.D. Hey, C.R. Thorne, and P. Tacconi. John Wiley, New York, pp. 277-296.
- MacNally, R. (2000), Regression and model-building in conservation biology, biogeography and ecology: The distinction between – and reconciliation of – ‘predictive’ and ‘explanatory’ models, *Biodiversity and Cons.*, 9, 655-671,
- Mason, C. H. and W. D. Perrault (1991), Collinearity, power, and interpretation of multiple regression analysis, *J. Marketing Res.*, 28, 268-280.
- McEwan, I. and J. Heald (2001), Discrete particle modeling of entrainment from flat uniformly sized sediment beds, *J. Hydraul. Eng.*, 127, 588-597.
- Meyer-Peter, E. and R. Müller (1948), Formulas for bed-load transport, in *Proceedings of the 2nd Meeting of the International Association for Hydraulic Structures Research*, Int. Assoc. Hydraul. Res., Delft, Netherlands, pp. 39-64.
- Miller, R. L. and R. J. Byrne (1966), The angle of repose for a single grain on a fixed rough bed, *Sedimentology*, 6, 303-314.

- Montgomery, D. R., J. M. Buffington, N. P. Peterson, D. Schuett-Hames, and T. P. Quinn (1996), Stream-bed scour, egg burial depths, and the influence of salmonid spawning on bed surface mobility and embryo survival, *Can. J. Fish. Aquat. Sci.*, *53*, 1061-1070.
- Nikuradse, J. (1933), Strömungsgesetze in rauhen Rohren, *Verein Deutscher Ingenieure Forschungsheft 361, Forschung auf dem Gebiete des Ingenieur-Wesens, Ausgabe B, Band 4* (English translation, Laws of flow in rough pipes, *National Advisory Committee on Aeronautics, Tech. Memorandum 1292*, Washington DC, 1950, 22 pp.
- Nitsche, M., D. Rickenmann, J. M. Turowski, A. Badoux, and J. W. Kirchner (2011), Evaluation of bedload transport predictions to account for macro-roughness in steep mountain streams, *Water Resour. Res.*, *47*, doi:10.1029/2011WR010645.
- Nogaro, G., T. Datry, F. Blondin, S. Descloux, and B. Montuelle (2010), Influence of streambed sediment clogging on microbial processes in the hyporheic zone, *Freshwater Biol.*, *55*, 1288-1302.
- Ockelford, A. and H. Haynes (2013), The impact of stress history on bed structure, *Earth Surf. Proc. Landforms*, *38*, 717-727.
- O'Brien, R.M. (2007), A caution regarding rules of thumb for variation inflation factors, *Qual. and Quantity*, *41*, 673-690.
- Paolo, C. and R. Seal (1995), Grain size patchiness as a cause of selective deposition and downstream fining, *Water Resour. Res.*, *31*, 1395-1407.
- Parker, G., P. C. Klingeman, and D. L. McLean (1982), Bedload and size distribution in paved gravel-bed streams, *J. Hydraul. Div. Am. Soc. Civ. Eng.*, *108*, 544-571.

- Paterson, D. M. (1997), Biological mediation of sediment erodibility: Ecology and physical dynamics, in *Cohesive Sediments*, edited by N. Burt, R. Parker, J. Watts, Wiley and Sons, New York, pp. 215-229.
- Powell, D. M. and P. J. Ashworth (1995), Spatial pattern of flow competence and bed load transport in a divided gravel bed river, *Water Resour. Res.*, *31*, 741-752.
- Powers, M. C. (1953), A new roundness scale for sedimentary particles, *J. Sed. Petrol.*, *23*, 117-119.
- Quinn, T. P. (2005), *The Behavior and Ecology of Pacific Salmon and Trout*, 378 pp., University of Washington Press, Seattle.
- Reid I., L. E. Frostick, and J. T. Layman (1985), The incidence and nature of bedload transport during flood flows in coarse-grained alluvial channels, *Earth Surf. Proc. Landforms*, *10*, 33-44.
- Rice S. P., M. F. Johnson, and I. Reid (2012), Animals and the geomorphology of gravel-bed rivers, in *Gravel-bed Rivers: Processes, Tools, Environments*, edited by Church M., P. Biron and A. G. Roy, John Wiley and Sons, Chichester, pp. 225-241.
- Sanguinito, S. and J. Johnson (2012), Quantifying gravel overlap and dislodgement forces on natural river bars: implications for particle entrainment, *Earth Surf. Proc. Landforms*, *37*, 134-141.
- Schalchli U. (1992), The clogging of coarse gravel river beds by fine sediment, *Hydrobiologia*, *235*, 189-197.
- Schmeeckle, M. W. and J. M. Nelson (2003), Direct numerical simulation of bedload transport using a local, dynamic boundary condition, *Sedimentology*, *50*, 279-301.

- Sohn, H. Y. and C. Moreland (1968), The effect of particle size distribution on packing density, *Can. J. Chem. Eng.*, *46*, 162-167.
- Statzner, B., M. F. Arens, J. Y. Champagne, R. Morel, and E. Herouin (1999), Silk producing stream insects and gravel erosion: Significant biological effects on critical shear stress, *Water Resour. Res.*, *35*(11), 3495–3506.
- Statzner, B., E. Fievet, J. Champagne, R. Morel, and E. Herouin (2000), Crayfish as geomorphic agents and ecosystem engineers: Biological behavior affects sand and gravel erosion in experimental streams, *Limnol. Oceanogr.*, *45*, 1030-1040.
- Stone, M., M. B. Emelko, I. G. Droppo, and U. Silins (2011), Biostabilization and erodibility of cohesive sediment deposits in wildfire-affected streams, *Water Res.*, *45*, 521-534.
- Wiberg, P. L. and D. M. Rubin (1989), Bed roughness produced by saltating sediment, *Water Resour. Res.*, *94*, 5011-5016.
- Wiberg, P. L. and J. D. Smith (1987), Calculations of the critical shear stress for motion of uniform and heterogenous sediments, *Water Resour. Res.*, *23*, 1971-1480.
- Wiberg, P. L. and J. D. Smith (1985), A theoretical model for saltating grains in water, *J. Geophys. Res.*, *90*, 7341-7354.
- Wolman, M. G. (1954), A method of sampling coarse river-bed material, *Eos Trans AGU*, *35*, 951-956.
- Yager, E. M. and H. E. Schott (2013), The initiation of sediment motion and formation of armor layers, in *Treatise on Geomorphology, Fluvial Geomorphology*, Vol. 9, edited by J. Schroder and E. Wohl, Academic Press, San Diego, pp. 87-102.
- Yalin, M. S. (1972), *Mechanics of Sediment Transport*, 290 pp., Benjamin Press, New York.

Chapter 3. The Relative Stability of Salmon Redds and Unspawned Streambeds

3.1 Abstract

Female salmon build nests (“redds”) in streambeds to protect their eggs from predation and damage by bed scour. During spawning, streambed material is mixed, fine sediment is winnowed downstream, and sediment is moved into a tailspill mound resembling the shape of a dune. Redd surfaces are coarser and better sorted than unspawned beds, which is thought to increase stability of redds because larger grains are heavier and harder to move, and sorting leads to higher friction angles for grain mobility. However, spawning also loosens sediment and creates topography that generates flow accelerations, which increases particle mobility. We address the balance of factors controlling the relative stability of redds and unspawned beds in a series of laboratory flume experiments using simulated salmon redds and water worked (“unspawned”) beds composed of mixed-grain surfaces. Spawning lowered packing resistance to particle mobility on the surface of redds by an average of 32% to 39% compared to unspawned beds. Reductions in packing were sufficient to counter the higher inherent stability of relatively coarse grains on redds, overall reducing critical shear stress by 8% to 20% relative to unspawned beds. In addition, boundary shear stress was 13% to 41% higher on a redd due to flow convergence over the tailspill structure. Finally, redd instability relative to unspawned beds was observed in visual measurements of grain mobility, where bed-averaged shear stress was 22% lower at incipient motion on redds and 29% lower at the discharge that mobilized all grain sizes. Results of these complementary methods along with sediment mass transport rates being nearly five times higher on a redd than an unspawned bed indicate that redds are unstable

compared to unspawned beds. Given these findings, further research is needed to investigate linkages between spawning disturbance and stream bed mobility that may affect salmon reproduction in streams.

3.2 Introduction

The decline of Pacific salmon (*Oncorhynchus* spp.) outside of Alaska in the past century has been met with significant efforts to bolster populations. In the United States alone, billions of dollars have been spent to increase salmon runs through hatcheries, fish passage improvements, stream restoration, and other activities [Montgomery, 2003; Bernhardt *et al.*, 2005]. While several salmon runs have benefitted from these types of approaches, the majority of populations have not improved [Bisson *et al.*, 2009], nor are they expected to in the near future [Battin *et al.*, 2007]. Although a single solution for reversing the salmon's decline is unlikely, stream habitats utilized by salmon, specifically riffles, pools, and the intergravel environment, are thought to be limiting factors due to their influence on early survival of salmonids [Nehlsen *et al.*, 1991; Greig *et al.*, 2005, 2007]. Stream habitats are structured by interactions between sediment transport (e.g., bed mobility, depositional patterns of sediment, bank erosion), channel roughness (e.g., stream banks, large wood, boulders), and the magnitude and grain-size distribution of the sediment supply [Lisle, 1982; Madej, 1999]. The act of salmon building nests ("redds") during spawning modifies stream habitats [Burner, 1951; Everest *et al.*, 1987; Chapman, 1988], sediment transport rates [Hassan *et al.*, 2008], and bed stability [Montgomery *et al.*, 1996].

Spawning salmon build redds to protect their eggs from predation and damage from agitation and bed scour [Smirnova, 1955]. Redd construction proceeds by the female using

rapid undulations of her tail fin to hydraulically excavate a pit in the bed, which flushes a portion of the fine sediment into the water column to be carried downstream [Kondolf *et al.*, 1993] while mobilizing coarser sediment a short distance into a dune-like mound called a tailspill [Burner, 1951]. Grains too large to be moved accumulate in the pit where the female will deposit a portion of her eggs for fertilization once the pit is sufficiently deep (0.10 to 0.50 m; DeVries, 1997). The female then covers the eggs with sediment excavated from the next pit upstream. Excavation is repeated until several egg pits are built, with completed redds exhibiting a tailspill mound and an upstream depression called a pot (Figure 3.1). Redd morphology is similar between species in the genus *Oncorhynchus* [Kondolf, 1988], yet redd structures can range widely in surface area (0.6 to 9.4 m²; Bjornn and Reiser, 1991) depending on compaction of the bed, caliber of substrate, velocity and depth of flow, slope of the channel, and body size of the female [Kondolf and Wolman, 1993; Kondolf *et al.*, 1993]. However, population size is the primary control of bed disturbance area, since mass spawning can disrupt the entire channel bed [Hassan *et al.*, 2008], compared to relatively small populations that tend to spawn in discrete patches of relatively high-quality habitat [Isaak *et al.*, 2007].

Spawning in both high and low densities modifies stream beds by mixing sediment [Gottesfeld *et al.*, 2004], purging fines [DeVries, 2012] coarsening and sorting surface grains [Kondolf *et al.*, 1993; Kondolf and Wolman, 1993], and loosening grain packing [Montgomery *et al.*, 1996; Buxton *et al.*, submitted]. These alterations benefit salmon reproduction by promoting hyporheic flow that oxygenates eggs and transports metabolic waste from the nest [Vaux, 1962; Cooper, 1965; Chapman, 1988; Zimmerman and Lapointe, 2005], arguably at the cost of integrity of the redd. On the one hand, theoretical calculations

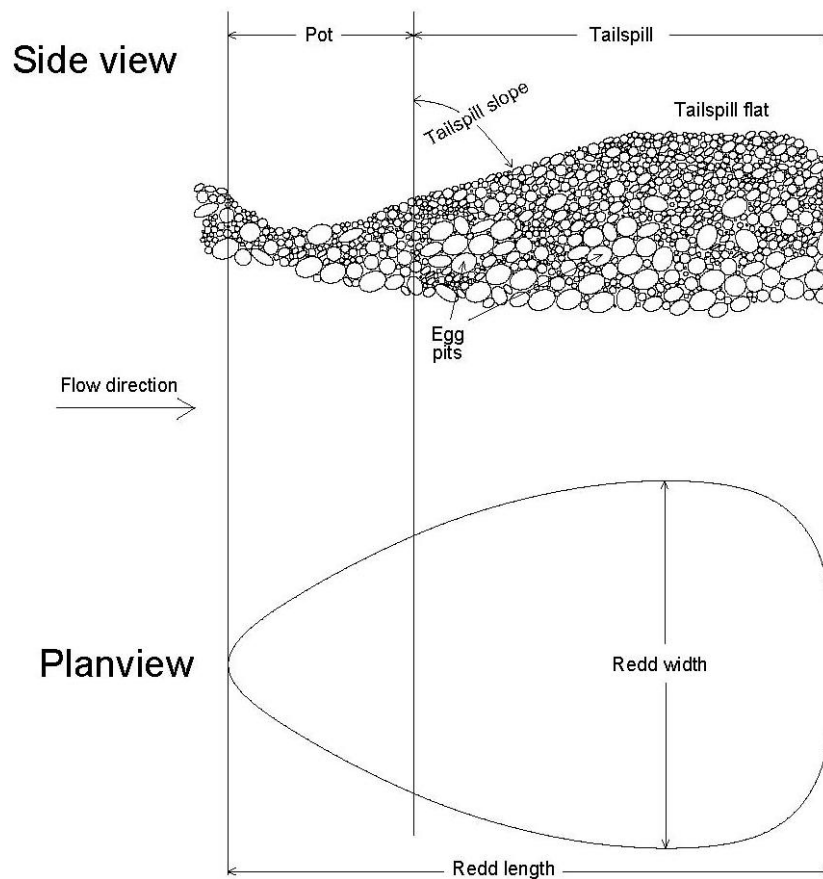


Figure 3.1. Side- and planview diagram of a redd modified from *Buxton et al.* [submitted].

by *Montgomery et al.* [1996] predict that critical conditions for sediment entrainment are around two-times higher on solitary redds than unspawned beds due to spawning coarsening and sorting grains. Coarsening promotes stability because larger grains are harder to move than smaller grains. Sorting tends to stabilize grains by requiring higher pocket friction angles for entrainment [*Buffington et al.*, 1992]. *Montgomery et al.* [1996] also calculated that bed stability is increased an additional 64% by form drag generated by topographic roughness from multiple redds. However, calculations of redd stability have not been supported by observations of scour on solitary redds [*Lisle*, 1989; *Bigelow*, 2003] and redds in high densities [*Rennie and Millar*, 2000], or in numerical models of mass-spawned

reaches [*Hassan and Tonina*, in review]. Disagreement may arise from *Montgomery et al.* [1996] neglecting the destabilizing effects of spawning, which include bed loosening (decreased packing resistance; *Buxton et al.*, submitted) and elevated boundary shear stress due to flow convergence over redd topography, similar to that measured on dunes [*Venditti*, 2007].

Resolving whether redds are more or less stable than unspawned beds is important for linking spawning disturbance to thresholds of sediment mobility, which, in part, govern the structure and availability of stream habitats for salmon reproduction [*Gottesfeld et al.*, 2004]. To further investigate this issue, we conducted several experiments in a laboratory flume using simulated redds and water worked (“unspawned”) beds of mixed-grain sizes to determine the relative stability of spawned and unspawned bed surfaces. Results indicate that the stabilizing effects of spawning (i.e., coarsening and sorting of grains) are offset by destabilizing factors (bed loosening and winnowing of fines that reduce packing resistance). This in combination with flow convergence elevating boundary shear stress over redds causes them to be relatively unstable compared to unspawned beds.

3.3 Materials and Methods

3.3.1 Overview

Three experiments were conducted in a 20 m long, 2 m wide, 1.5 m deep flume at the Center for Ecohydraulics Research at the University of Idaho in Boise to determine the relative stability of salmon redds and unspawned beds. In experiment 1, we used hand measurements (with a load cell) of the downstream force for particle entrainment to compute values of critical shear stress for redds and unspawned beds. We also quantified packing

resistance to particle mobility on redds and unspawned beds following methods in *Buxton et al.* [submitted]. In experiment 2, we measured flow velocity profiles using Particle Image Velocimetry (PIV) to estimate total boundary shear stresses with the log-profile method [e.g. *Wilcock, 1996*] on a redd and an unspawned bed. In experiment 3, we made visual measurements of sediment entrainment and measured bulk transport rates for spawned and unspawned surfaces. Chum salmon (*O. keta*) redd dimensions, grain-size distributions, and the flume slope in the experiments were scaled from field measurements in Kennedy Creek near Olympia, WA. The flume model was generic rather than specific because no other details of Kennedy Creek were reproduced in the experiments.

3.3.2 Field Measurements

We chose Kennedy Creek for field measurements because it has a gravel bed that is typical for streams with salmon and has a large spawning population of chum salmon for locating redds. The study reach is a third-order channel with forced pool-riffle morphology, and has a drainage area of 45 km². The annual hydrograph is rainfall-dominated, with high flows occurring November through March. Chum spawning occurs from September through mid-December, with the highest spawning densities occurring mid-November. Field measurements of redd lengths, widths, and amplitudes, and stream-bed sediments occurred in mid-December, between high flow events on the creek. Measured redds were surrounded by an unspawned bed and were located away from obstructions (large wood, stream banks, boulders) that can distort redds from the common oval or teardrop shape [*Burner, 1951*]. Redd lengths were measured to within ± 0.05 m with a survey rod from the upstream edge of the pot to the downstream edge of the tailspill (Figure 3.1). Redd widths were measured with

the same accuracy at the widest portion of the structure. Redd amplitudes were measured to within ± 0.02 m from the peak height of the redd to the adjacent unspawned bed with a carpenters level and survey rod.

A bulk composite sample (68.6 kg) of sediment was collected on an unspawned portion of a dewatered lateral bar where chum salmon had spawned during a recent high flow event. The depth (0.20 m) of the sample was based on the average depth of 40 egg pockets (0.23 m) measured for chum redds in Kennedy Creek by *Montgomery et al.* [1996]. The maximum particle size in the sample (90.5 mm) was about 1.5% of the total sample weight, which is close to the 1% criterion of *Church et al.* [1987] for requisite sample size. Sampled grains were sieved in half-phi intervals from -1 to -6 (2 to 64 mm) and weighed to the nearest 0.1 kg. A longitudinal profile of the thalweg at the sample location indicated the channel slope was 0.005.

3.3.3 Experimental Scaling

Scaling redd dimensions and flow requires similitude of Froude (Fr) and Reynolds numbers (Re) between the flume and Kennedy Creek. Fr and Re covary with discharge, which forces a decision to scale only one dimensionless parameter. Error introduced by not exactly scaling Re ($=\rho\bar{u}_m h_m/\mu$, with $\rho=1000$ kg m⁻³ and $\mu=1.52 \times 10^{-3}$ kg m*s⁻¹ are the density and dynamic viscosity of water at 4 °C and 5 °C, respectively) is negligible in fully-developed turbulent flow ($Re=4.2 \times 10^4$ in our experiments; *Middleton and Southard*, 1984). Because of this, we used Fr scaling to relate the field prototype (subscript p) to the flume model (subscript m) with $Fr_p=Fr_m$, where $Fr = u/(gh)^{0.5}$, u is flow velocity, g is

gravitational acceleration (9.81 m s^{-2}), and h is flow depth. The model was then related to the prototype with a length factor (L_L)

$$\frac{L_p}{L_m} = \frac{W_p}{W_m} = \frac{\Delta_p}{\Delta_m} = \frac{h_p}{h_m} = L_L \quad (3.1)$$

where L , W , and Δ are the redd length, width, and amplitude, respectively. Redds constructed in the flume were scaled from the average length (2.7 m; standard deviation (s)=0.9 m), width (1.6 m; s =0.5), and amplitude (0.10 m; s =0.04) of 12 redds measured in Kennedy Creek to approximately 0.9 m long, 0.5 m wide, and 0.03 m in amplitude using an L_L of 3 (Table 3.1). Because chum spawned in Kennedy Creek during a wide range of flows up to bankfull discharge, we chose to avoid trampling redds to obtain a representative sample of spawning flow depths and velocities, and instead scaled these parameters from values in the literature. Flow depths for simulated spawning ($h_m=0.10 \text{ m}$) were scaled from the average flow depth that *Smith* [1973] reports chum salmon utilize for spawning in Oregon streams (average $h_p=0.30 \text{ m}$, $s=0.41 \text{ m}$, $n=214$). Data from *Smith* [1973] were also used to scale the flow velocity for simulated spawning ($\bar{u}_m=0.42 \text{ m s}^{-1}$) with the average flow velocity utilized by chum spawners ($\bar{u}_p=0.73 \text{ m s}^{-1}$, $s=0.65 \text{ m s}^{-1}$, $n=214$) using

$$\frac{\bar{u}_p}{\bar{u}_m} = \sqrt{L_L} . \quad (3.2)$$

The average flow depth (0.14 m, $s=0.07 \text{ m}$, $n=8$) and velocity (0.45 m s^{-1} , $s=0.04 \text{ m s}^{-1}$) during simulated spawning were within a standard deviation of scaled chum spawning flow depths and velocities reported by *Smith* [1973]. The average Fr_m (0.39) during simulated spawning was within 10% of the Fr_p (0.43) for chum spawning according to data reported by *Smith* [1973].

Table 3.1. Scaled redd dimensions and median grain sizes (D_{50}) and sorting parameters (σ ; Blatt *et al.*, 1980) for surface particles on redds and unspawned beds (US) in flume experiments 1-3.

Sediment mix	Experiment 1									Experiment 2		Experiment 3	
	1			2			3			1		4	
Bed surface	US	LT ^a redd	RT ^a redd	US	LT ^a redd	RT ^a redd	US	LT ^a redd	RT ^a redd	US	Redd	US	Redd
Length, m	--	0.93	0.97	--	0.86	0.92	--	0.85	0.86	--	0.95	--	0.90
Width, m	--	0.50	0.50	--	0.50	0.54	--	0.52	0.51	--	0.62	--	0.61
Height, m	--	0.04	0.04	--	0.03	0.03	--	0.05	0.05	--	0.07	--	0.06
TS angle ^b	--	11	15	--	13	13	--	12	11	--	16	--	18
D_{50} , mm	5.0	$\frac{9.6}{8.3^c}$	$\frac{7.7}{8.3^c}$	5.1	$\frac{7.6}{7.4^c}$	$\frac{7.3}{7.4^c}$	7.4	$\frac{12.4}{11.9^c}$	$\frac{11.3}{11.9^c}$	8.4	8.6	5.8	6.2
σ , mm	1.1	$\frac{0.9}{0.8^c}$	$\frac{0.8}{0.8^c}$	1.0	$\frac{0.9}{0.8^c}$	$\frac{0.8}{0.8^c}$	1.3	$\frac{0.9}{0.8^c}$	$\frac{0.7}{0.8^c}$	1.2	1.0	1.2	1.0

^aLeft (LT) and right (RT) indicates redds constructed to either side of the unspawned bed.

^bAngles (degrees from horizontal) of the tailspill slope (TS) measured with an electronic level.

^cMedian grain size and sorting parameters determined with grain size distribution combined for the LT and RT redds.

The grain-size distribution from Kennedy Creek was also scaled smaller by a factor of 3, then varied to create four sediment mixtures with slightly different compositions (mix 1-4; Figure 3.2). Mixes 1-3 were used in experiment 1; Mix 1 was used in experiment 2; and Mix 4 was used in experiment 3. In all experiments, the flume slope was set to that of Kennedy Creek (0.005). The use of an undistorted bed slope and Froude-scaled flow depths results in bed shear stress being proportional between the prototype and model, as suggested in concepts proposed by *Einstein and Barbarossa* [1956; see *Wallerstein et al.*, 2001].

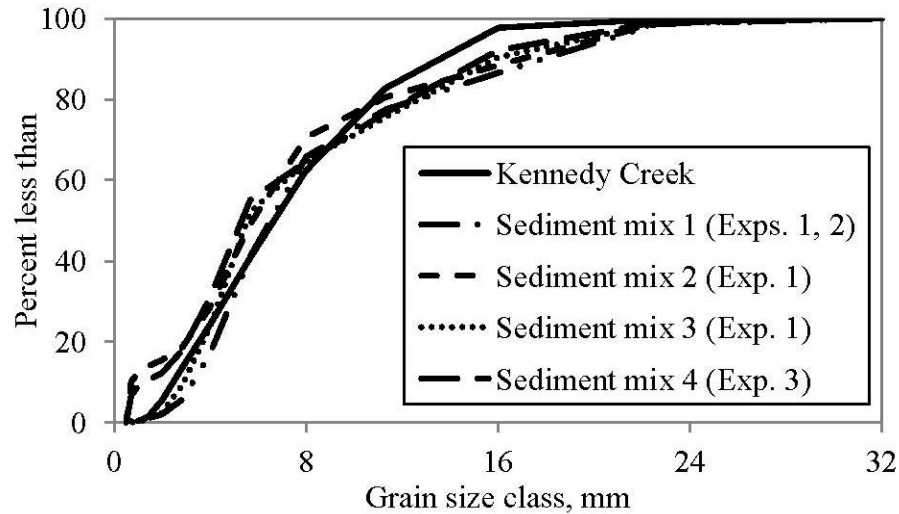


Figure 3.2. Cumulative percentiles for bulk sediment mixtures 1-4 used in the flume experiments (scaled values shown).

Redds were constructed in the flume with a metal spatula that was a scaled model of chum caudal fins measured in Herman Creek near Haines, Alaska, which is a spring-fed channel with a gravel bed that supports a large population of chum spawners. Scaling the metal spatula was an important consideration since the size of redds and the caliber of sediment moved by spawners scales with fish size [*van den Berghe and Gross, 1984*]. We preferred to scale the metal spatula from chum caudal fins in Kennedy Creek, but spawner carcasses were too degraded for these measurements. Instead, we used linear regression to relate paired measurements of caudal fin widths (in mm) to the mid-eye to caudal fork length of female chum (F_L in mm) in Herman Creek (Caudal fin width (mm) = $0.28(F_L) - 0.22$; correlation coefficient (R^2)=0.59, sample number(n)=13). We then used the regression equation with the average female chum fork length measured in Kennedy Creek (602 mm, standard deviation (s)=39 mm, n =27) to estimate an average caudal fin width of 169 mm for Kennedy Creek chum. This value was reduced by a factor of three to set the width of the metal spatula (56 mm) for building redds in the flume.

3.3.4 Experimental Layouts

Experimental layouts varied in the flume to accommodate objectives of experiments 1-3. In all experiments, flow straighteners were installed at the upstream end of the flume to quell flow surges before flow moved up an inclined ramp onto fixed beds of sediment. Fixed beds were installed in the upper 12 m of the flume to generate uniformly rough flow using gravel and sand-sized grains glued to plywood with contact cement. A lumber crib supported fixed beds 0.14 m above the flume bottom for placing sediment mixtures to this depth in the test area, which extended variable distances downstream of the fixed beds. The test area for experiment 1 extended one meter downstream of the fixed beds and was 2 m wide to accommodate beds constructed in three wooden boxes (1.0 m long, 0.64 m wide) installed across the flume. The middle box held an unspawned bed (US), while redds were constructed in boxes to the left (LT redd) and right (RT redd) of the US bed (Figure 3.3a, Table 3.1). The test area for experiment 2 extended 1.4 m downstream and was 1 m wide so that a wooden box with these dimensions was large enough for measuring flow velocities on a compound surface containing both a redd and unspawned bed (Figure 3.3b, Table 3.1). Fixed beds were installed on both sides of the redd and unspawned bed to maintain uniform flow in experiment 2. Beds were constructed in boxes in experiments 1 and 2 for lifting them from the flume to measure grain-size distributions with *Wolman* [1954] pebble counts, and to measure pocket friction angles with a tilt board for beds in experiment 1. In experiments 1 and 2, a fixed bed extended 2 m downstream of the test area to generate roughness that prevented flow from accelerating from the test areas.

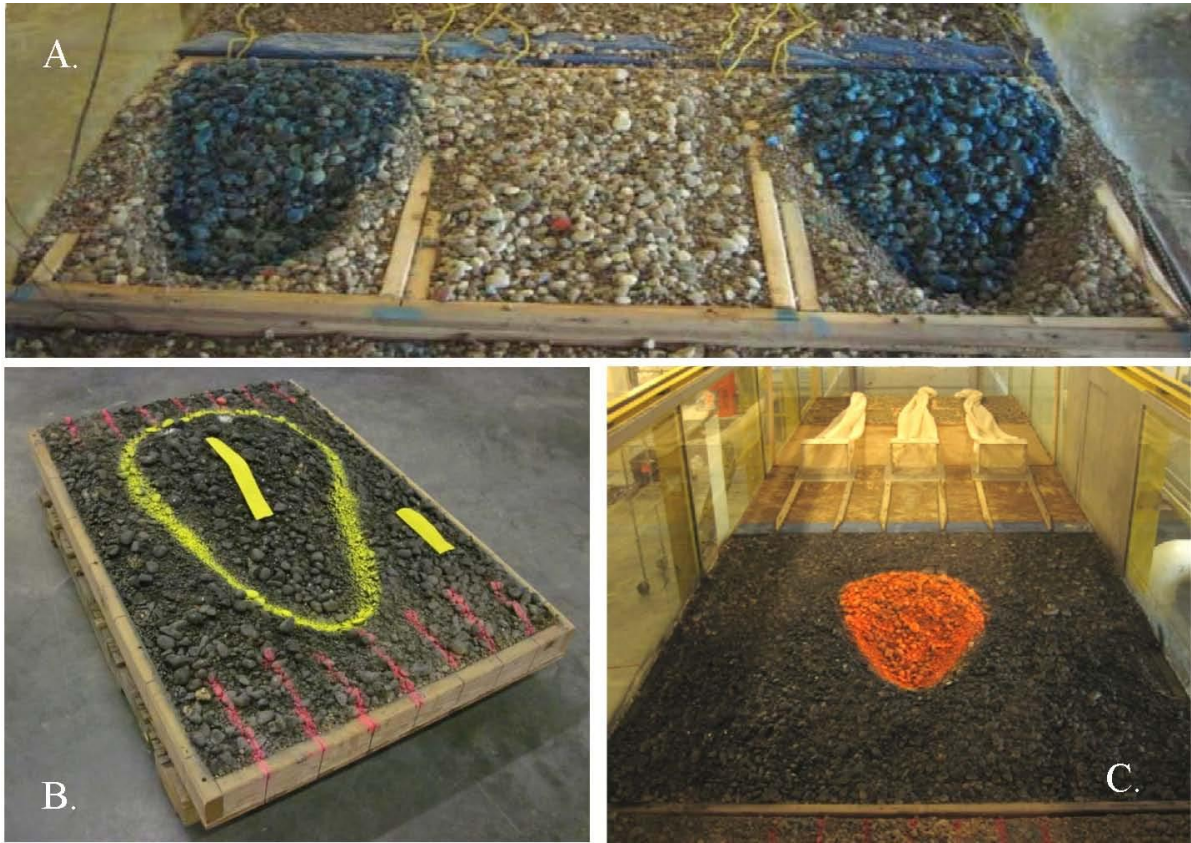


Figure 3.3. Redds and unspawned beds used for (A.) total resistance measurements (F_t) (sediment mix 1 shown), (B.) flow velocity measurements with particle image velocimetry (PIV) and (C.) visual measurements of grain mobility and bed load capture. Beds are spray painted blue in (A.) to discern surface grains from subsurface particles during total resistance measurements; black in (B.) to reduce PIV laser refraction; and in (C.) the redd is painted orange and the unspawned bed is painted black to aide observations of grain mobility and to allow the origin of surface grains to be distinguished in bed load traps that are shown in the upper portion of the figure. The bed in (B.) is shown after removal from the flume, with the outline of the redd and location of PIV transects in yellow (transect on the right is for the unspawned bed). The unspawned bed in (A.) is shown before it was painted to distinguish it from redds in this figure.

The test area for experiment 3 was enlarged to 2 m in the downstream direction by 2 m wide for capturing bed load transport from a redd and unspawned bed (Figure 3.3c, Table 3.1). A smooth plywood bed was installed for 2 m downstream of the test area to provide a platform for fastening bed load traps and to facilitate transport of mobile sediment into the traps. Three bed load traps were installed in equal spacings across the flume at a location

one meter downstream of the test area. To evaluate whether flow accelerated from the test area on the plywood bed, we used an acoustic doppler velocimeter to measure velocity at $0.6h$ for five discharges (0.16 to $0.58 \text{ m}^3 \text{ s}^{-1}$) with measurements at 0.5 m , 1.0 m , and 1.5 m upstream of the middle trap. We did not detect a backwater zone in front of the traps or flow acceleration on the plywood, indicating uniform flow occurred in the test area.

3.3.5 Bed Construction

Redds and unspawned beds were constructed by placing one grain mixture in the test area at a time, screeding sediment flat with a shovel, and slowly wetting the bed, which settled a proportion of the sand and smaller grains into subsurface areas. Flow was then increased to water work beds for a duration that began when five or more grains (usually sand and small gravel) moved at least their diameter downstream. From this point, water working proceeded for a 2 h duration by increasing discharge in increments that maintained a low level of sediment transport for winnowing fines and orienting grains to flow. After water working, flow was adjusted to generate scaled spawning flow depths and velocities. Spawning flow depths were measured to within $\pm 0.8 \text{ cm}$ with a wading rod at the center of locations where redds were constructed. Flow velocities were measured to within $\pm 2\%$ (manufacturer's specification) at six-tenths flow depth for 40 s to 60 s with a pygmy flow meter at these same locations. Spawning flow depths and velocities were measured prior to redd construction. Redds were constructed with the metal spatula by mimicking the spawning action of female salmonids, whereby successive episodes of pit excavation and filling flushed fine grains from larger sediment, loosened grain packing, and moved sediment into the redd tailspill structure. Completed redds exhibited teardrop shapes (Figure 3.1) that were oriented long-axis parallel to flow. As in nature, the longitudinal profile of

redds exhibited a pot depression and tailspill mound with an upstream sloping surface and a flat area (Figure 3.1).

3.3.6 Evaluation of Simulated Spawning

We evaluated the effectiveness of simulating spawning by comparing redd dimensions and grain-size distributions in the flume to those in Kennedy Creek, Herman Creek, and Lilliwaup Creek near Lilliwaup WA. As with Kennedy Creek, Lilliwaup and Herman Creeks were chosen for measurements because they each have a gravel-bed channel that supports spawning populations of chum salmon. Grain-size distributions were measured in the creeks with *Wolman* [1954] pebble counts of approximately 100 grains on redds and unspawned beds each. The intermediate diameters (hereafter grain diameter or D) of sampled grains were measured to 0.1 mm with digital calipers. In experiments 1 and 2, *Wolman* [1954] samples were collected for 150 to 220 apparent grain diameters on redds and unspawned beds by lowering a small pointed stick while looking away. Diameters were apparent because grains were fixed on the bed and often partially buried (see explanation below). In experiment 3, *Wolman* [1954] samples of 100 grains were photographically measured with Sedimetrics software [*Graham et al.*, 2005a, b] to avoid disturbing the beds prior to visual measurements of mobility. We used Sedimetrics because it has been shown to accurately duplicate *Wolman* [1954] pebble counts [*Graham et al.*, 2005a]. We compared the median grain size (D_{50}) and grain sorting parameter (σ , *Blatt et al.*, 1980) for redds in the flume and field

$$\sigma = 3.32 \left(\frac{\log D_{84} - \log D_{16}}{4} \right) + 3.32 \left(\frac{\log D_{95} - \log D_5}{6.6} \right) \quad (3.3)$$

where subscripts indicate percentiles of the grain-size distribution. The length, width, and amplitude of redds in the flume were compared to those of chum redds in Kennedy, Herman, and Lilliwaup Creeks. Redds were measured in the creeks by methods presented in Section 3.3.2. In the flume, we measured the long-axis and width (at the widest portion of the structure) with a survey rod to ± 0.02 m. Redd amplitudes above adjacent unspawned beds were measured in the flume with a ruler and level to the same degree of accuracy.

3.3.7 Experiment 1: Grain Packing Resistance and Critical Shear Stress

3.3.7.1 Mathematical Framework

We computed packing resistance for grains on the tailspill flat of redds and on unspawned beds using

$$\mu_{pack} = \frac{F_t}{F_n} - \tan \phi_p = \mu_t - \mu_p \quad (3.4)$$

where μ_{pack} is the friction coefficient for packing resistance, F_t is the total resistance force, F_n is the normal force on the grain, ϕ_p is the grain's pocket angle, and μ_t and μ_p are friction coefficients for the total and pocket resistance, respectively (see *Buxton et al.*, [submitted] for derivation]. Modifications to Equation (3.4) were necessary for determining μ_{pack} for grains on the sloping portion of the tailspill. Because the angle of the tailspill slopes in the upstream direction (Figure 3.1) and is opposite to that of the slope of the tilt board at grain motion, we subtracted the tailspill slope (ϕ_{ts}) from ϕ_p to avoid conflating angles at grain motion. Values of ϕ_{ts} were measured on redds in the flume with a digital level to the nearest degree. Adjustments to F_t and F_n were also necessary since a component of the grain's

weight acts parallel ($mg \sin \phi_{ts}$) to the sloping bed against F_t , and only a portion of the grain's weight acts perpendicular to the sloping bed surface ($F_n = mg \cos \phi_{ts}$). With these, packing resistance coefficients for grains on the tailspill slope were given by

$$\mu_{pack} = \frac{F_t - mg \sin \phi_{ts}}{mg \cos \phi_{ts}} - \tan(\phi_p - \phi_{ts}) = \mu_t - \mu_p \quad . \quad (3.5)$$

Because F_t measurements disrupt the bed and alter the initial pocket geometry, it is not possible to make paired measurements of total and pocket resistance. Therefore, values of total resistance were measured on half of each redd and unspawned bed before gluing the undisturbed halves and measuring pocket angles (Figure 3.4). From these measurements, we produced distributions of μ_t and μ_p for grain sizes classed in half-phi intervals from -2.5 to -4.5 (5.7 to 22.6 mm). Following the approach of *Buxton et al.* [submitted], we then used Monte Carlo simulations to randomly pair percentiles from each distribution to determine packing resistance distributions for grain-size classes using Equation (3.4) for unspawned beds or Equations (3.4) or (3.5) for redds.

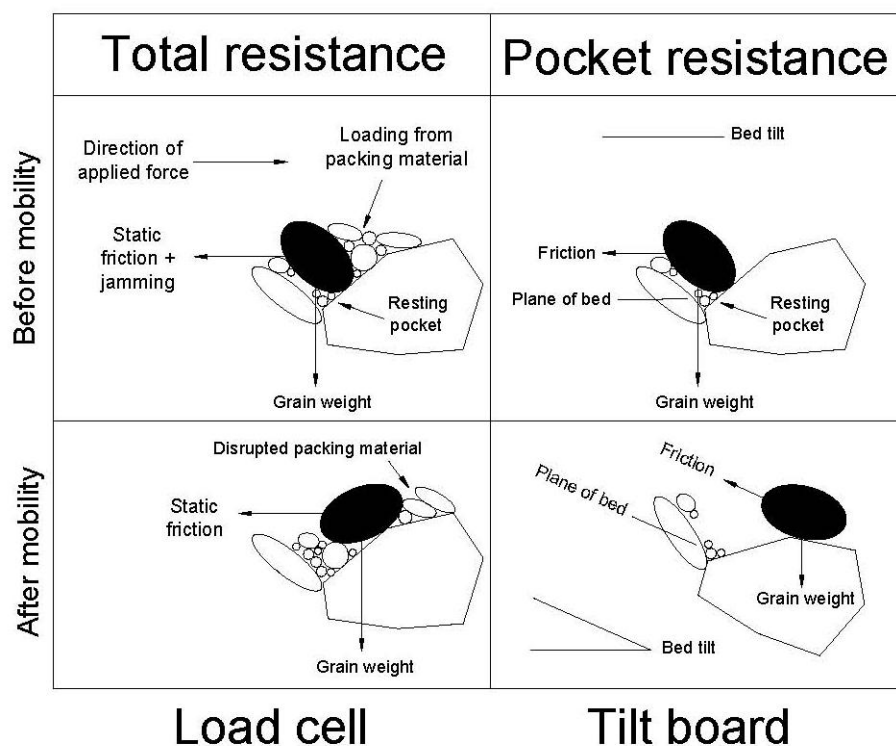


Figure 3.4. Schematic of load cell and tilt board measurements and forces [modified from *Buxton et al.*, submitted]

3.3.7.2 Total Resistance Force Measurements

Total resistance forces were measured with a FUTEK LSB210 load cell. This device was connected to a laptop computer with a FUTEK USB210 that detected the peak applied force at 10 Hz with a nominal accuracy of 0.001% (manufacturers specification). A 3 mm diameter post was inserted in the load cell for applying a push force in a downstream and bed-parallel direction. We pushed at the midpoint of the exposed frontal area of all individual grains that protruded at least partially above the local bed surface [*Johnston et al.*, 1998; *Buxton et al.*, submitted]. Additional criteria for measurements were that grains had to be surrounded by undisturbed sediment. With the slope of the flume set to zero, enough

force was applied to push each grain a distance approximately equal to its diameter, which defined grain movement in our study. Distances of grain movement were approximate because measurements of D could not be made *a priori* without disturbing the grain.

Total resistance measurements proceeded by mobilizing individual grains with the load cell, recording the type of movement (sliding, pivoting/rolling, or tilling), and extracting the grain for weighing to the nearest 0.1 g. We classified the angularity of each grain with the Powers [1953] roundness scale, and measured its three major axes with digital calipers to the nearest 0.1 mm. Grain dimensions were used to calculate planar areas of the grains and to characterize grain shapes with the Corey [1949] shape factor (CSF)

$$\text{CSF} = d_s / \sqrt{d_L d_i} \quad (3.6)$$

where d_s , d_L , and d_i are the short, long, and intermediate grain axes. We excluded tilling motions (movement that plows neighboring grains) because grains in natural channels commonly move in a sliding or pivoting/rolling motion, or some combination of the two [Francis, 1973; Komar and Li, 1988; Ling, 1995]. We restricted analysis to grain sizes classed in half-phi intervals from -2.5 to -4.5 (5.7 to 22.6 mm) since pocket resistance measurements were limited to these grain sizes. The number of total resistance measurements varied with the coarseness of the bed, since large diameter grains cover a relatively large area of the bed compared to small grains and reduced the total number of possible measurements. The number of measurements made in size classes on redds (9 to 90) was less than on unspawned beds (12 to 106) because the latter were less coarse (smaller D_{50} ; Table 3.1). Pooling measurements for the two redds constructed with each sediment mix resulted in 28 to 241 measurements in a given grain-size class on spawned surfaces.

3.3.7.3 Pocket Resistance Measurements

Upon completion of total resistance measurements, contact glue was used to fix the undisturbed halves of the beds so they could be removed from the flume without damage for measuring surface grain-size distributions (*Wolman* [1954] pebble counts) and pocket resistance angles. Glue cemented the bed surfaces without pooling and modifying grain pocket geometries. Glued beds were lifted in their boxes with an overhead crane onto a table for conducting *Wolman* [1954] pebble counts. Beds were then mounted on a tilt board for measuring pocket resistance angles with test grains. Test grains were chosen from the experimental grain mixtures to approximate the average CSF, angularity, and diameter of grains for which total resistance measurements were made (Table 3.2). Pocket resistance angles were measured by dropping a test grain from a low height at random locations on the bed and increasing the angle of tilt until grain movement occurred. Critical pocket angles (ϕ_p) were measured to the nearest degree with an electronic level. Approximately 50 pocket angles were measured with each test grain on each bed. The 50 measurements on redds were apportioned by area between the pot, tailspill slope, and tailspill flat. See *Buxton et al.* [submitted] for additional details and limitations on these pocket angle measurements.

3.3.7.4 Monte Carlo Simulations

Monte Carlo simulations were used to randomly pair percentiles of μ_t and μ_p for determining distributions of μ_{pack} for redds and unspawned beds. Measured distributions of μ_t and μ_p were truncated at the 30th and 70th percentiles to avoid unlikely pairings during the simulations. For example, it is doubtful that a grain in a shallow pocket in a mixed-grain size bed would exhibit high packing resistance or that a grain in a deep pocket would have low

packing. Normal distributions of μ for the simulations were obtained through \log_{10} transformations of measured μ_t and μ_p values. Five thousand individual pairings of μ_t and μ_p (referred to as trials) were used to determine distributions of μ_{pack} for each grain-size class on each bed. Simulations reproduced the mean of measured μ_t and μ_p distributions to within $\pm 1\%$, indicating that μ_t and μ_p could be modeled with acceptable accuracy with log-normal distributions. Hereto, see *Buxton et al.* [submitted] for details regarding the calculations and assumptions in Monte Carlo simulations.

Table 3.2. Approximate equivalence of characteristics of grains used for total resistance measurements and pocket resistance measurements.

Size class ^a (mm)	Diameter (mm)		Grain weight (gram force)		CSF (dimensionless)		Angularity ^c (dimensionless)	
	Total ^b	Pocket	Total ^b	Pocket	Total ^b	Pocket	Total ^b	Pocket
22.6	26.0	28.8	21.6	22.6	0.58	0.56	4.6	4.0
16.0	19.1	19.8	9.3	11.0	0.62	0.60	3.9	4.0
11.3	13.7	15.9	3.8	4.6	0.62	0.60	4.0	4.0
8.0	9.3	8.6	1.1	1.1	0.62	0.69	3.6	3.0
5.7	7.2	7.1	0.6	0.7	0.66	0.78	3.2	3.0

^aLower bin size.

^bValues are means computed from particles used in total resistance measurements.

^cAngularity classified with the *Powers* [1953] roundness scale, where 3 indicates a sub-angular grain, 4 a sub-rounded grain, and 5 a rounded grain.

3.3.7.5 Critical Shear Stress Calculations

Values of critical shear stress (τ_c) were calculated by dividing measurements of F_t by the planar area of grains for which F_t was measured. We assumed grains were aligned with their short-axis perpendicular to the bed and were elliptical in shape, based on the average CSF of 0.62 (grains are increasingly elliptical as CSF decreases from 1.0). Values of τ_c were

weighted by grain-size frequency on each bed surface and pooled for redds as in Section 3.3.7.2.

3.3.8 Experiment 2: Boundary Shear Stress

Flow velocity fields were measured with two-dimensional (2D, streamwise and vertical directions) PIV for making point estimates of boundary shear stress (τ_b) on streamwise transects on a redd and unspawned bed adjacent to the redd (Figure 3.3b). We conducted measurements at two discharges (0.32 and $0.64 \text{ m}^3 \text{ s}^{-1}$) with variable flow depths on the redd (11.0 and 20.1 cm) and unspawned bed (17.5 and 26.6 cm). The relative submergence (h/Δ) of the redd was 1.7 and 3.1 at the 0.32 and $0.64 \text{ m}^3 \text{ s}^{-1}$ discharges, respectively. Bed surfaces were glued to prevent grain movement during velocity measurements. Glue fixed grains without pooling and modifying roughness on the beds. Streamwise transects for velocity measurements were 35.3 cm and 21.1 cm long on the redd and unspawned bed, respectively (Figure 3.3b). The transect was longer on the redd to enable velocity measurements on the flat and sloping portions of the tailspill. The transect on the unspawned bed was located adjacent to the redd, such that flow measurements were likely influenced by flow accelerating around the redd and increasing shear stress relative to what would occur in the absence of the redd.

PIV involved illuminating flocculants in the flow column with a dual pulse 1064 nm laser sheet oriented in the transects positioned in the middle of the flume width. A high-speed camera captured images of flocculants (through the glass sidewall of the flume) at 9 Hz for 120 s at vertical positions from the bed to a height of 12.3 cm. Vertical profiles were composed of 73 interrogation regions, each with an area of 0.22 cm^2 . Instantaneous downstream velocities were calculated in each interrogation region using a cross-correlation

analysis of the distance that flocculants traveled between successive images [e.g., *Adrian, 2005*]. Instantaneous velocities were averaged to give time-averaged velocity for each interrogation region. To save time, only every other vertical profile was used, which increased the streamwise distance between profiles to 0.43 cm, while retaining a sufficiently high spatial resolution of measurements (83 and 53 estimates of τ_b on the redd and unspawned bed, respectively).

We focused on the near-bed region in our estimates of τ_b because the near-bed stress is what affects sediment motion and the log profile is only technically valid in the lower 20% of the flow depth [*von Karman, 1930; Keulegan, 1938; Middleton and Southard, 1984*]. Zero depth in the profiles was set as the highest vertical position before flow speed increased with height above the bed. We disregarded this point and the next to avoid the no-slip condition at the bed [*Munson et al., 2006*] and plotted the next five flow velocities (between 0.43 and 1.3 cm above the bed) against the natural log of heights above the bed. Simple linear regressions indicated that velocities in the near-bed region were strongly logarithmic on the redd and unspawned bed ($R^2 \geq 0.81$ and ≥ 0.77 , respectively). This enabled estimates of τ_b with the slope of the linear regressions and the law of the wall [e.g., *Wilcock, 1996*]

$$\tau_b = \rho \left(\frac{\kappa}{\text{slope}} \right)^2 \quad (3.7)$$

3.3.9 Experiment 3: Measurements of Grain Mobility

Grain mobility was visually measured on a redd and unspawned bed to determine their relative stability during the same time as mobile particles were captured in bed load traps. The redd and unspawned bed surfaces were spray-painted (orange and black,

respectively) to aid observations of mobility and to allow the origin of trapped grains to be discerned (Figure 3.3c). Bed load traps had 0.3 m wide by 0.2 m tall openings and were equipped with 5 m long nets with 3.125 mm mesh openings, which would retain the coarser 89% of bed sediment. Mobility measurements were conducted at 14 successive discharges, each lasting 20 minutes and ranging from 0.12 to 1.05 m³ s⁻¹. The lowest discharge (0.12 m³ s⁻¹) was based on observations of mobility in preliminary experiments with a test bed composed of similar grain sizes. The peak discharge (1.05 m³ s⁻¹) was that which completed erosion of the redd flush with the unspawned bed. Discharge was measured to within ±0.5% with an electromagnetic flow meter in the water supply pipe to the flume. Bed load traps were emptied between flow events and captured sediment was dried and separated by color. Painted grains were weighed to the nearest gram to determine mass transport rates per unit area of the spawned (0.42 m²) and unspawned bed (3.58 m²) for each discharge. We did not include subsurface grains because we could not determine their location of origination.

Visual measurements of entrainment were made for grain diameters we classified as very coarse (>24 mm), coarse (16 to <24 mm), medium (8 to <16 mm), fine (4 to <8 mm) and very fine (<4 mm). Size classes differed from those used in experiments 1 and 2 because we found it difficult to visually measure grain diameters to within half-phi size intervals. We did not quantify uncertainty in our grain-size estimates that are a source of bias in visual measurements of entrainment [Buffington and Montgomery, 1997]. Instead, we used preliminary experiments to practice estimating mobile grain diameters captured in downstream traps, with satisfactory agreement between them. Visual measurements of entrainment were limited to the first half of each flow event because the bed had largely

stabilized by this point. Entrainment was defined as when five or more grains in a size class moved a distance equal to their diameter in 30 s. An exception applied to very-fine grains that were required to evacuate their resting pocket to be classified as mobile, since movement of a lesser distance was difficult to detect. The median diameter of the largest mobile grain and mass transport rates per unit bed area were plotted against the bed averaged shear stress (τ_{avg}) partitioned to remove wall effects (see Appendix A) for each discharge for which visual measurements were made.

3.4 Results

3.4.1 Simulated Spawning, Redds, and Unspawned Beds

Redd surfaces in the flume were coarser (higher D_{50}) and exhibited better sorting (lower σ values) than unspawned beds due to simulated spawning winnowing sand and small grains from larger particles (Table 3.1). We measured comparable effects of spawning in stream channels (Figure 3.5). Moreover, chum redd dimensions in the flume were in the range of redd lengths, widths, and amplitudes in the field after scaling flume redds larger by a factor of three for this comparison (Figure 3.6). This indicates flume redds were properly scaled to chum redds in nature. However, redd dimensions in the flume ranged less than redds in streams. This resulted from the latter being located in a greater diversity of spawning conditions (flow velocity and depth, channel slope, substrate size) than those represented by the flume experiments.

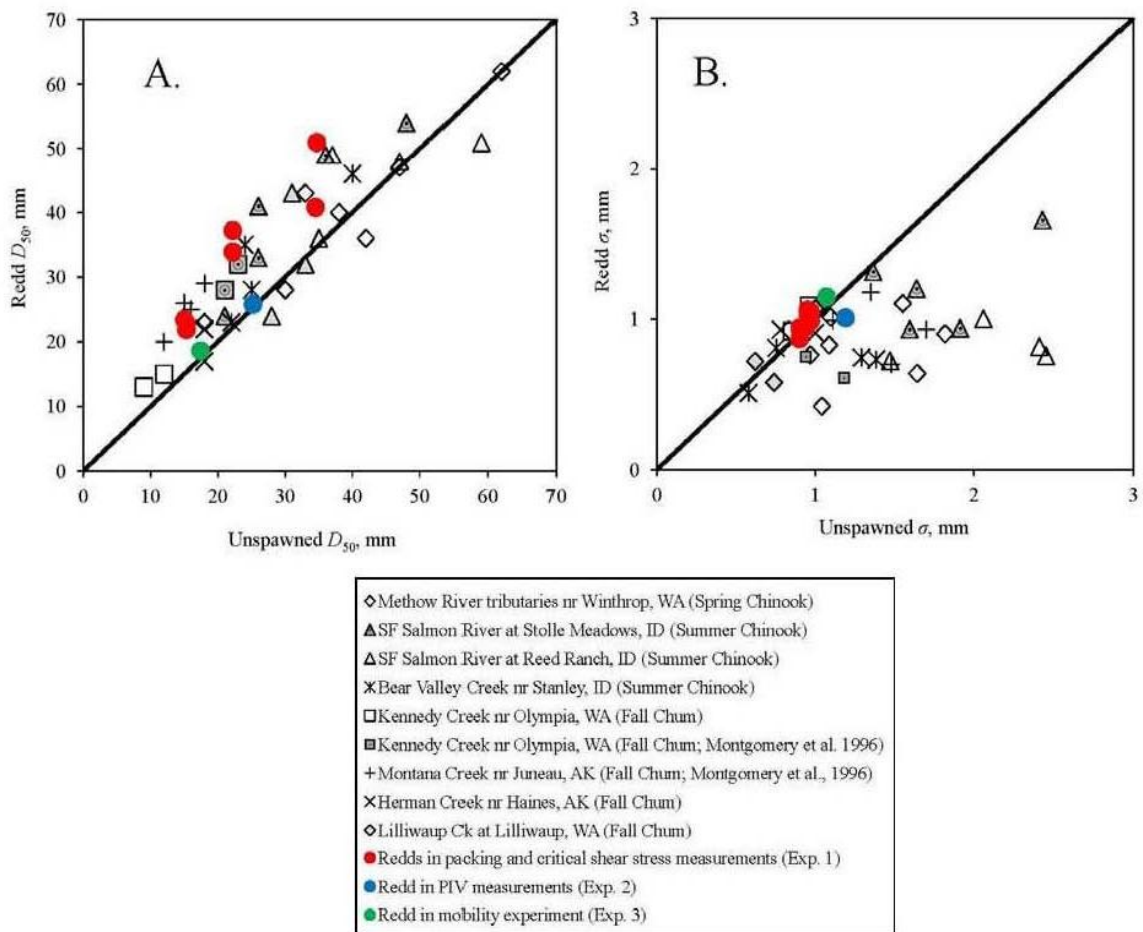


Figure 3.5. Median grain size (D_{50} in A.) and (B.) sorting parameters (σ , *Blatt et al.*, 1980) measured on redds in the flume and on Pacific salmon redds in several Washington and Idaho streams. Median grain sizes in the flume are scaled larger by a factor of 3 for comparison to values of D_{50} in streams.

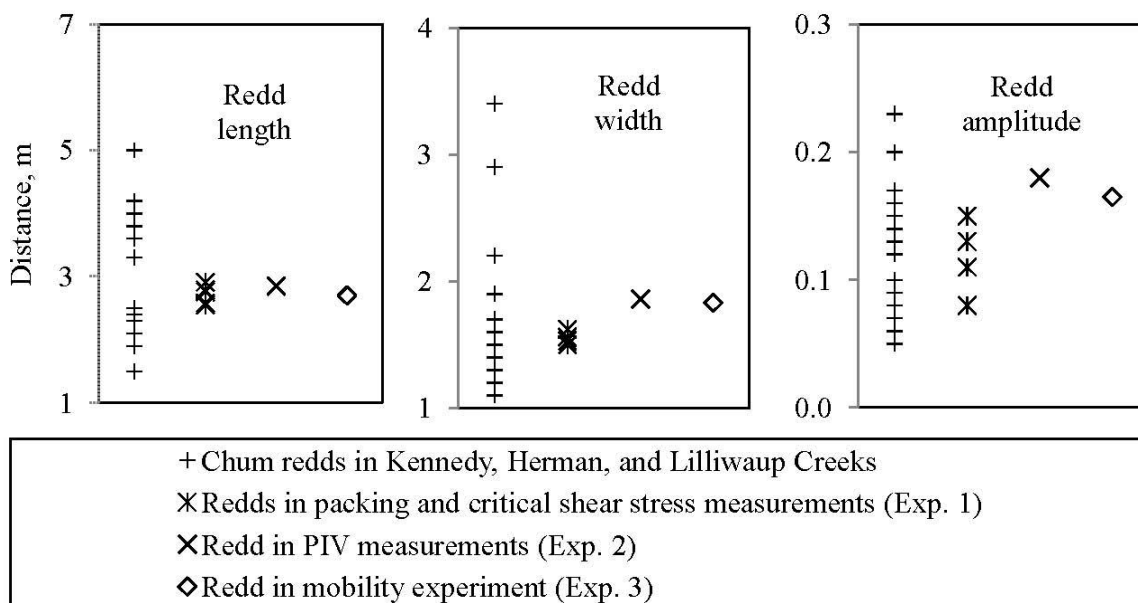


Figure 3.6. Redd dimensions in the flume compared to dimensions of chum salmon redds in Kennedy Creek near Olympia, WA, Herman Creek near Haines, Alaska, and Lilliwaup Creek at Lilliwaup, WA. Redd dimensions in the flume are scaled larger by a factor of 3 in these comparisons.

3.4.2 Packing Friction Coefficients

Results of Monte Carlo simulations for redds and unspawned beds are presented as cumulative percentile distributions of μ_{pack} (Figure 3.7) and as averages for each source of resistance (μ_t , μ_{pack} , and μ_p) within size classes on each bed (Table 3.3). Similar to *Buxton et al.*'s [submitted] findings, packing was the primary form of resistance to grain motion and exceeded pocket angle resistance (μ_p) by up to 88% (Table 3.3). Average values of μ_p were largely constant between grain-size classes and bed surfaces, a result that contradicts prior pocket angle studies [*Kirchner et al.*, 1990; *Buffington et al.*, 1992] due, in part, to small sample sizes and averaging within size classes. In contrast, μ_t and μ_{pack} increased with decreasing grain size (Table 3.3). The inverse relationships with grain size (Figure 3.7,

Table 3.3) resulted because smaller grains were more buried [Buxton *et al.*, submitted] and angular (Table 2), which increased frictional resistance and promoted jamming, respectively. Largely constant values of μ_p were not expected since coarser (larger D_{50}) and better sorted (lower σ ; Table 1) redds should display deeper resting pockets and higher angles for entrainment, and therefore greater μ_p [Buffington *et al.*, 1992]. However, μ_p was only statistically higher (paired two-sample *t*-test, $\alpha=0.05$) on redds composed of sediment mix 1. This may have resulted from sorting spatially varying on the bed, such that bed-averaged sorting was too general for associating with the average μ_p for each size class that was characterized with only around 50 measurements of μ_p .

The relative unavailability of fine sediment for packing large grains on redds caused μ_t to be lower than on unspawned beds (Table 3). This in combination with similar μ_p between bed surfaces, resulted in cumulative distributions of μ_{pack} being lower on redds than unspawned beds for a given grain size and sediment mixture (Figure 3.7). Moreover, the weighted (by grain-size frequency) bed-averaged μ_{pack} on redds was 39% ($\mu_{pack}=7.7$), 32% (8.7), and 36% (7.6) lower than on unspawned beds (12.6, 12.8, 11.8) composed of sediment mixes 1-3, respectively. Additionally, the total weighted average (by grain size frequency on the beds) μ_{pack} was 36% lower on redds as a whole than unspawned beds. For comparison, Buxton *et al.* [submitted] reported the median μ_{pack} was 13% lower on the tailspill flat of redds compared to unspawned beds. Packing resistance on the tailspill flat is somewhat higher because fines that were mobilized during redd construction re-deposited on the tailspill flat, locally increasing μ_{pack} [Buxton *et al.*, submitted].

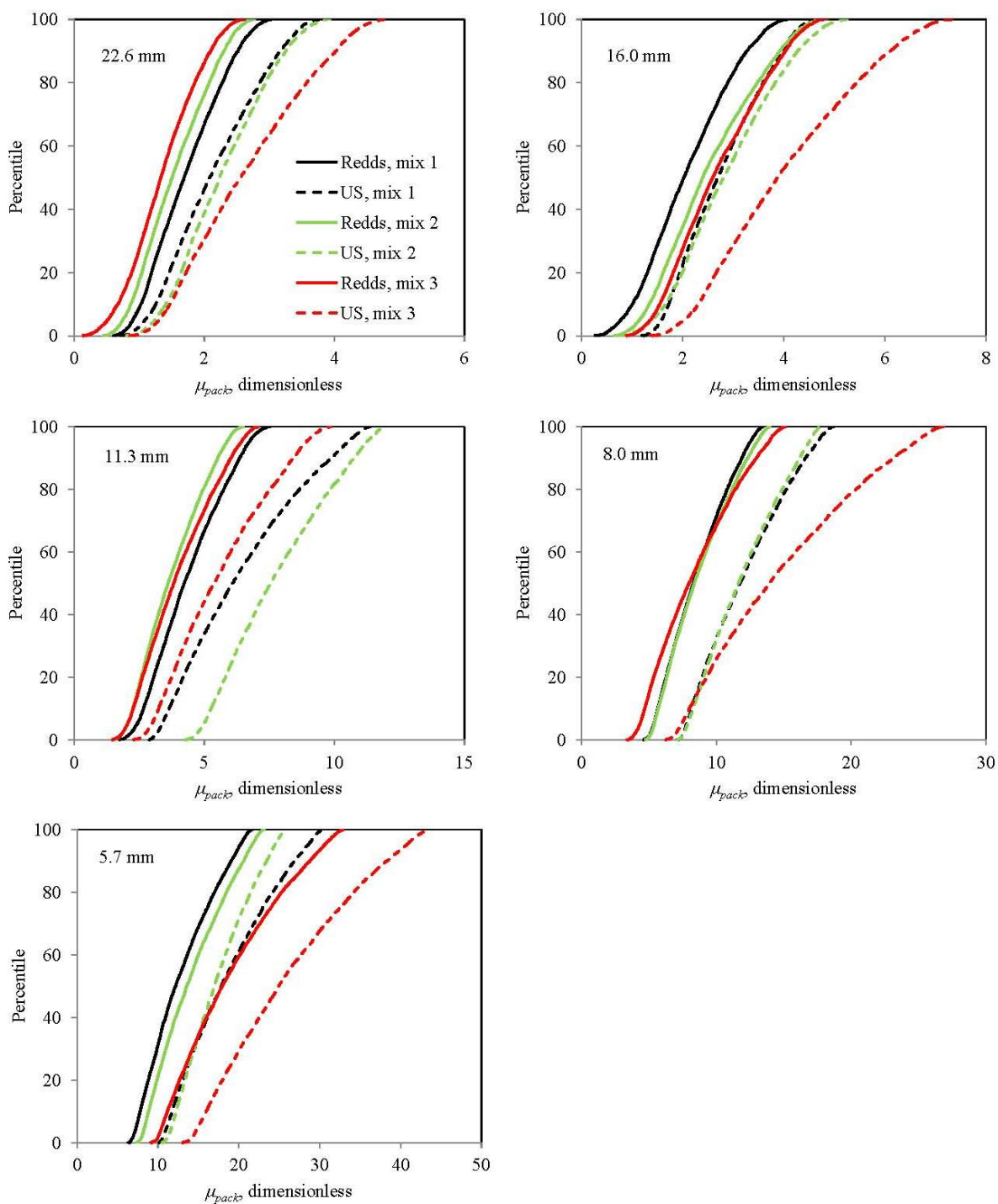


Figure 3.7. Cumulative distributions of packing friction coefficients (μ_{pack}) for grain-size classes (lower bin size reported in figures) on the unspanned beds (US) and redds composed of sediment mixtures 1-3.

Table 3.3. Average friction coefficients for total resistance (μ_t), pocket angle resistance (μ_p), and packing resistance (μ_{pack}), and the standard error of the average μ_{pack} by each grain-size class (lower bin size shown) and bed. Values of bed average μ_{pack} are also listed.

Bed	Size class (mm)	Avg μ_t	Avg μ_p (% of μ_t)	Avg μ_{pack} (% of μ_t)	Standard error of avg μ_{pack} ^a	Bed avg μ_{pack} ^b
US mix 1	22.6	3.1	1.0 (32%)	2.1 (68%)	0.5	12.6
	16.0	3.8	1.0 (26%)	2.8 (74%)	0.5	
	11.3	7.4	1.0 (13%)	6.4 (87%)	0.9	
	8.0	12.9	0.8 (36%)	12.1 (94%)	1.2	
	5.7	19.8	1.2 (6%)	18.6 (94%)	4.0	
Redds mix 1	22.6	2.8	1.0 (37%)	1.7 (63%)	0.3	7.7
	16.0	3.4	1.3 (39%)	2.1 (61%)	0.4	
	11.3	5.7	1.3 (23%)	4.4 (77%)	0.6	
	8.0	9.8	1.2 (12%)	8.5 (88%)	0.8	
	5.7	14.2	1.3 (9%)	12.8 (91%)	2.1	
US mix 2	22.6	3.5	1.2 (35%)	2.3 (65%)	0.7	12.8
	16.0	4.5	1.6 (35%)	2.9 (65%)	0.6	
	11.3	9.0	1.2 (13%)	7.8 (87%)	1.1	
	8.0	13.2	1.2 (9%)	11.9 (91%)	1.0	
	5.7	18.7	1.3 (7%)	17.4 (93%)	2.4	
Redds mix 2	22.6	2.6	1.1 (40%)	1.5 (60%)	0.4	8.7
	16.0	3.7	1.2 (32%)	2.5 (68%)	0.6	
	11.3	5.0	1.2 (25%)	3.8 (75%)	0.6	
	8.0	9.8	1.0 (11%)	8.7 (89%)	0.9	
	5.7	15.3	1.2 (8%)	14.1 (92%)	1.8	
US mix 2	22.6	3.9	1.2 (32%)	2.6 (68%)	0.6	11.8
	16.0	5.4	1.3 (25%)	4.0 (75%)	0.5	
	11.3	6.9	1.3 (19%)	5.6 (81%)	0.8	
	8.0	16.2	1.5 (9%)	14.8 (91%)	3.5	
	5.7	27.8	1.7 (6%)	26.1 (94%)	9.0	
Redds mix 3	22.6	2.3	1.2 (47%)	1.4 (53%)	0.3	7.6
	16.0	4.0	1.3 (32%)	2.7 (68%)	0.4	
	11.3	5.1	1.1 (21%)	4.0 (79%)	0.8	
	8.0	9.7	1.3 (13%)	8.4 (87%)	1.5	
	5.7	20.4	1.4 (7%)	19.0 (93%)	5.5	

^aStandard error (SE) of average $\mu_{pack} = \sqrt{(SE_{\mu_t})^2 + (SE_{\mu_p})^2}$, where $SE_i = s_i/\sqrt{n_i}$ and where s is the standard deviation of i and n is the number of measurements of i , with i representing μ_t and μ_p , respectively.

^bBed average packing calculated as a weighted average by grain-size frequency on each bed.

Distributions of μ_{pack} exhibited short, steep tails that resulted from limiting pairings of μ_t and μ_p in Monte Carlo simulations to the 30th to 70th percentiles (Figure 3.7). If pairings of μ_t and μ_p had been made between a wider range percentiles, distributions of μ_{pack} would have displayed higher skewness and larger average μ_{pack} , as demonstrated by *Buxton et al.* [submitted]. Truncating distributions of μ_t and μ_p at the 30th and 70th percentiles therefore produced relatively conservative values of μ_{pack} [*Buxton et al.*, submitted]. For a given grain size and bed surface, standard errors of μ_{pack} were high relative to values of μ_{pack} averaged within size classes (Table 3.3). This resulted from low numbers of measurements and variability in μ_t and μ_p . Standard errors generally increased with decreasing grain size because standard deviations of μ_t and μ_p were higher for smaller grains and fewer measurements were made for smaller size classes.

3.4.3 Critical Shear Stress

Measured values of τ_c are presented as cumulative distributions by grain-size class on redds and unspawned beds in Figure 3.8. Results are also presented as averages within grain-size classes, as well as averages weighted by grain-size frequency, for each surface in Table 3.4. Weighted average values of τ_c were 8% (387 Pa versus 420 Pa), 15% (384 Pa versus 453 Pa), and 20% (447 Pa versus 559 Pa) lower on redds than unspawned beds composed of sediment mixes 1-3, respectively (Table 3.4). Redd instability resulted from redd construction mixing sediment and flushing fines from larger gravels, which disrupted grains from their stable orientations and loosened packing [Section 3.4.2; *Buxton et al.*, submitted] and re. We hypothesize that reduction in packing on redds was sufficient to counter the greater inherent stability of relatively coarse grains on redds (Table 3.1). Additionally, values of τ_c averaged within grain-size classes generally increased with

decreasing grain diameter (Table 3.4). This resulted from most values of τ_c for a given percentile (e.g. beyond the 10th to 20th percentile) increasing with decreasing grain size (Figure 3.8). Distributions of τ_c therefore suggest that after the least stable particles are mobilized on the beds, a larger proportion of small grains than larger sediment remain stable, perhaps due to packing resistance being higher for smaller grains [Buxton *et al.*, submitted].

Table 3.4. Critical shear stress averaged within grain-size classes (lower bin size shown) and used to calculate the weighted average (by grain size frequency) for each bed.

Grain-size class (mm)	Sediment mix					
	1		2		3	
	Critical shear stress (Pa)					
	Redds	US bed	Redds	US bed	Redds	US bed
22.6	269	260	229	266	245	340
16.0	253	263	296	282	328	384
11.3	315	318	286	436	305	419
8.0	386	310	353	407	438	664
5.7	504	571	493	517	801	818
Weighted average	387	420	384	453	447	559

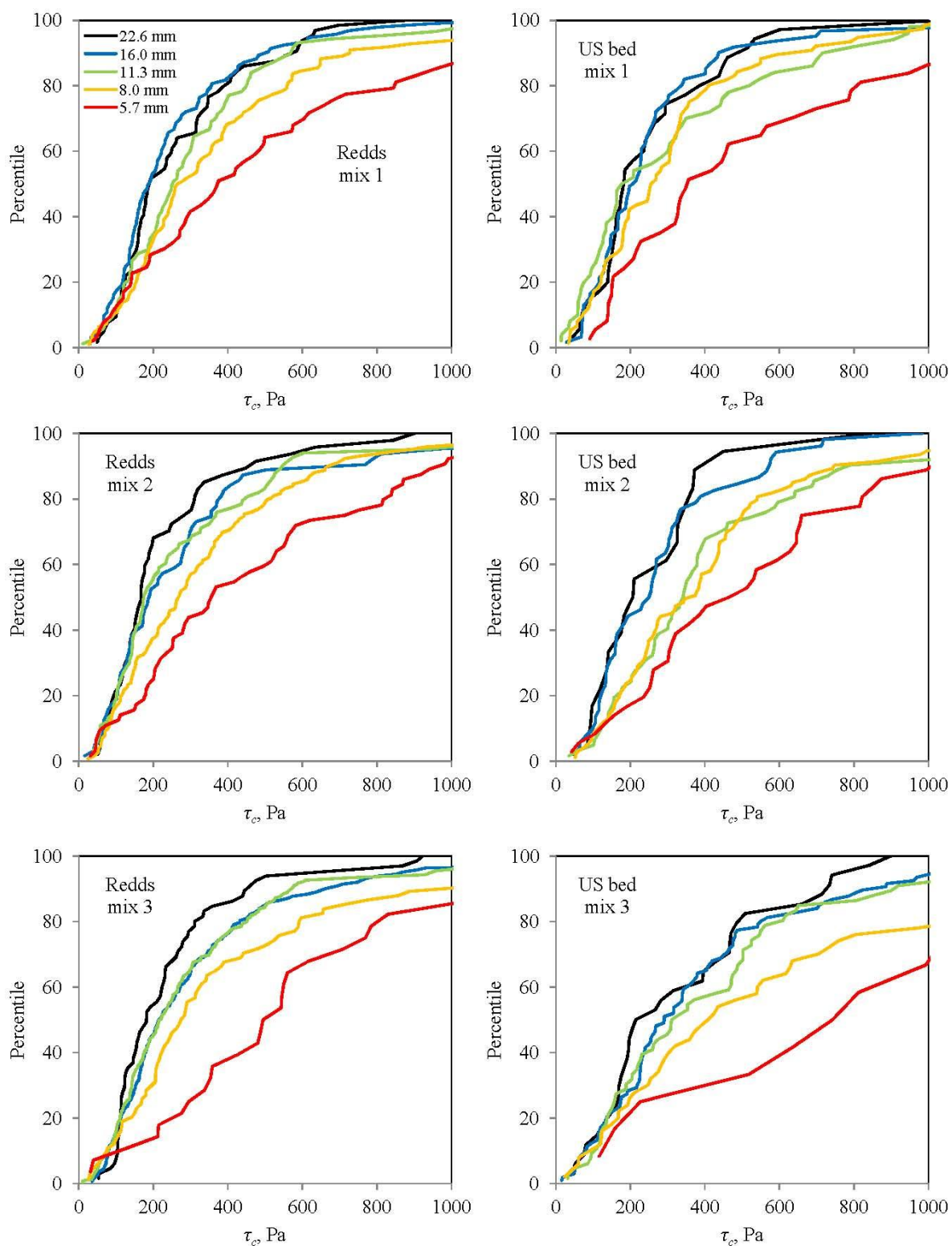


Figure 3.8. Cumulative distributions of critical shear stress (τ_c) grouped by bed surface and plotted for grain-size classes in half-phi intervals (lower bound of each bin size reported in figure key) on reds and unspawned (US) beds composed of sediment mix 1-3.

3.4.4 Boundary Shear Stress

Boundary shear stress estimates are plotted as point-values on the measured transects and as bed-averaged values (Figures 3.9a-d). Large spatial variability in τ_b was captured by the high resolution of PIV measurements on the hydraulically rough surface on the redd. Variability in τ_b was higher on the redd (standard deviation was 64 and 59 Pa at discharges of 0.32 and 0.64 m³ s⁻¹, respectively) than the unspawned bed (standard deviation was 21 and 41 Pa at discharges of 0.32 and 0.64 m³ s⁻¹, respectively). This occurred because the redd's dune-like profile increases topographic roughness from that of the planar bed and because the redd exhibited a coarser surface (Table 3.1) that provided greater topographic variability at the grain scale. We speculate that variability in τ_b on the redd is important for eroding the tailspill, since movement of coarse surface grains by locally high peaks in shear stress would expose relatively fine grains in the underlying structure, further enhancing erosion [Hawke, 1978; Peterson and Quinn, 1996].

As expected, transect-averaged τ_b was higher on the redd (96 Pa; Figure 3.9a) than on the unspawned bed (57 Pa; Figure 3.9c) at low discharge (0.32 m³ s⁻¹) and low relative submergence ($h/\Delta=1.7$). Higher τ_b on the redd resulted from flow convergence and acceleration on the stoss side of the tailspill, similar to that observed over fluvial bed forms [e.g., Nelson et al., 1993; Venditti, 2007; Ojha and Mazumber, 2008; Motamedi et al., 2014]. Moreover, the observed differences in τ_b are conservative because flow acceleration around the flanks of the redd likely increased boundary shear stresses measured on the unspawned bed (Figure 3.3b) compared to those that would occur in the absence of redd topography.

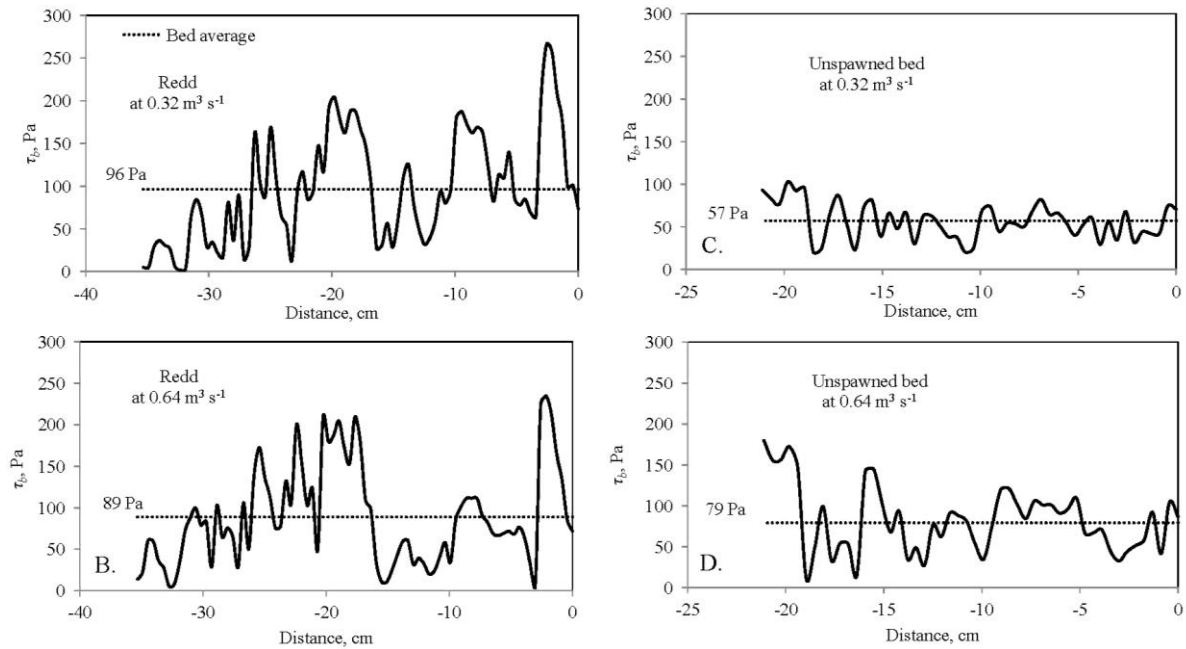


Figure 3.9. Boundary shear stress (τ_b ; solid line) estimated on a redd (A. and B.) and unspawned bed (C. and D.) with the law of the wall using flow velocity profiles measured with Particle Image Velocimetry at flow rates of $0.32 \text{ m}^3 \text{ s}^{-1}$ and $0.64 \text{ m}^3 \text{ s}^{-1}$ in the flume. Values are averaged on both structures (dotted lines). Negative horizontal distances are in the upstream direction. The horizontal distance of the tailspill flat in Figure 3.9a-b is located from 0 to -15.1 cm, and the tailspill slope is located from -15.1 to -36.2 cm.

At a high discharge ($0.64 \text{ m}^3 \text{ s}^{-1}$), the difference in transect-averaged τ_b between the redd (89 Pa; Figure 3.9b) and unspawned bed (79 Pa; Figure 3.9d) decreased to 13% due to the high relative submergence of the redd ($h/\Delta=3.1$) causing the tailspill to be comparatively drowned out. Lower τ_b at higher submergence of the redd is consistent with changes in τ_b measured on dunes [Maddux *et al.*, 2003; Stoesser *et al.*, 2006], which results from less flow acceleration on the redd generating higher slopes of linear regressions of the natural log of height above the bed (y-axis) versus flow velocity (e.g. lower flow velocity near the bed) and lower τ_b as depth increases. Moreover, higher τ_b on redds than unspawned beds at both

flow rates is consistent with values reported by *Venditti* [2007]; he measured boundary shear stress being 22-155% higher on dunes than planar beds.

3.4.5 Mobility Experiment

Results for the grain mobility experiment are presented in a plot of the median diameter in the largest mobile grain-size class versus discharge (Figure 3.10). Results are also presented as surface mass transport rates per unit area of the spawned and unspawned bed versus partitioned bed average shear stress (τ_{avg} ; Figure 3.11). Grain incipient motion was observed on the redd at a τ_{avg} (10.4 Pa) that was 22% lower than on the unspawned bed (13.4 Pa; Figure 3.10). This was expected based on the transect-averaged τ_b being up to 41% higher on the redd (Figures 3.9a-d), and by the lowest measured value of τ_c on redds (32 Pa) being 40% less than on unspawned beds (52 Pa; Figure 3.8, Table 3.4). The τ_{avg} that mobilized all grain sizes occurred within a narrower range on the redd (10.4 to 15.3 Pa for the <4 mm to >24 mm size class) than the unspawned bed (13.4 to 21.5 Pa; Figure 3.10). In addition, τ_{avg} that completed entrainment of all grain-size classes was 29% lower on the redd (15.3 Pa) than on the unspawned bed (21.5 Pa). Observed differences in τ_{avg} may be conservative because flow acceleration around and transverse from the redd may have heightened stresses adjacent to the redd, causing entrainment at a lower shear stress than might occur on unspawned areas located outside the influence of the redd.

Grain mobility on the redd caused downstream translation of the tailspill structure until it dispersed and scoured flush with the unspawned bed. Translation began for flows with $\tau_{avg} \leq 12.0$ Pa, when entrainment was limited to the tailspill crest. The mobile bed area expanded at 13.4 Pa to include unspawned grains adjacent to the redd and grains on the tailspill flat. At this flow, mobile grains on the unspawned bed were transported downstream

while mobile grains on the redd were mainly captured in the lee of the tailspill, promoting translation of the tailspill structure. Sustained mobility on the redd filled the lee area at around 15.3 Pa. At this point, the tailspill began to disburse as mobile grains were transported downstream. As mobility continued, the tailspill lowered in elevation, which reduced the lee area and accelerated downstream dispersion of the tailspill. At 17.9 Pa, unspawned grains that were mobilized upstream of the redd deposited in the pot, partially filling it. From 19.4 Pa through 20.4 Pa, entrainment on the unspawned bed increased to include coarse grains (16 to <24 mm), while the redd tailspill rapidly dispersed downstream between 18.9 Pa and 20.4 Pa. At 21.5 Pa, entrainment of very-coarse grains (>24 mm) concluded mobility of unspawned size classes. At a τ_{avg} of 23.0 Pa, the tailspill was eroded flush with the unspawned bed.

Mass transport rates of surface grains per unit area of spawned and unspawned portions of the bed support observations of redd translation followed by dispersal. Mass transport rates also support our conclusion that redds are more mobile than unspawned beds (Figure 3.11). Although Figure 3.10 gives the impression that the unspawned bed was initially more mobile, this is an artifact of the sequence of events and transient storage of mobilized grains. Whereas incipient motion occurred on the redd at 10.4 Pa, grain capture in the lee of the redd delayed measureable rates of sediment transport by the bedload traps until 15.3 Pa, when the lee filled and grains transported downstream into the traps. In contrast, unspawned grains mobilized later than the redd (13.4 Pa, Figure 3.10), but rapidly traversed the flume and were captured sooner by the bed load traps (14.3 Pa, Figure 3.11). We do not have an explanation for surface transport rates decreasing on both beds at 17.2 Pa. However, at 17.9 Pa, transport rates once again increased and largely equalized between surfaces

(Figure 3.11). At 18.9 Pa, erosion of the tailspill promoted redd dispersion and higher sediment transport rates on the redd than unspawed bed, which was sustained for the remainder of the experiment. This along with average mass transport rates being nearly 5 times higher on the redd ($0.66 \text{ g s}^{-1} \text{ m}^{-2}$) than on the unspawed bed ($0.14 \text{ g s}^{-1} \text{ m}^{-2}$) verifies that redds are unstable compared to unspawed beds.

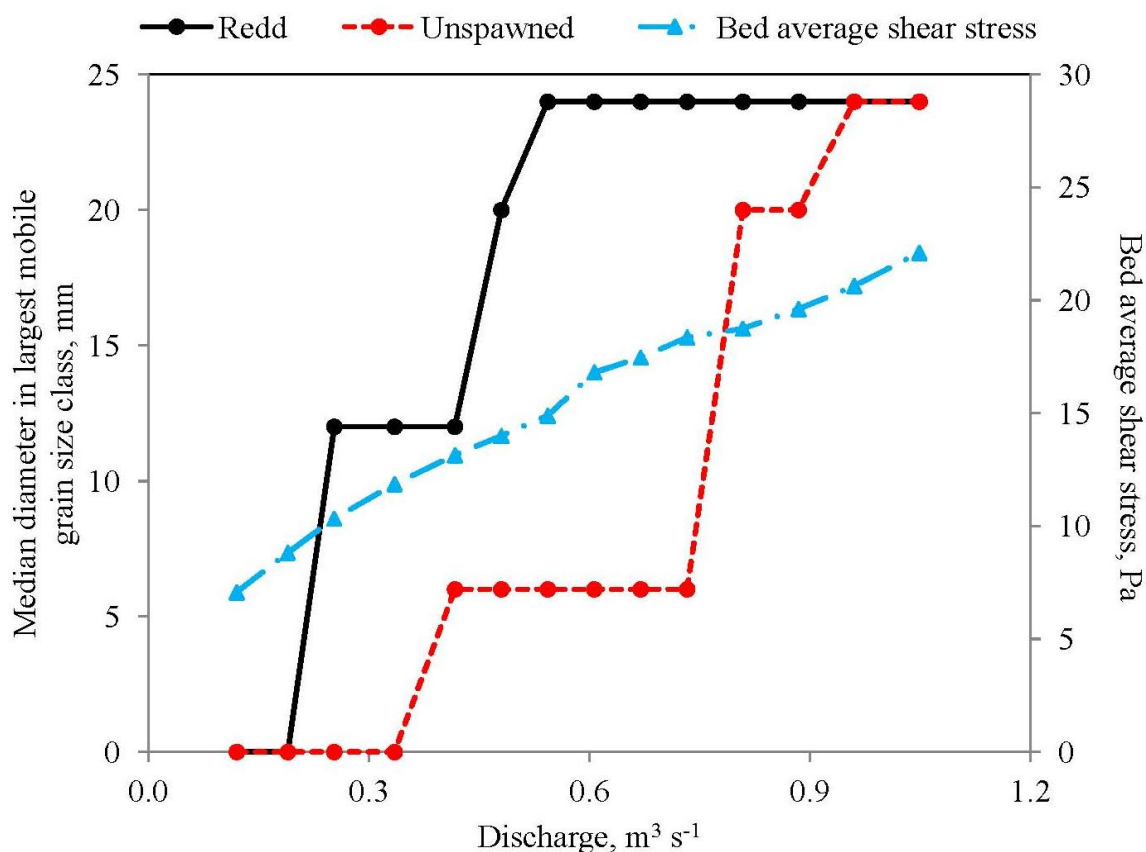


Figure 3.10. Visual measurements of grain mobility on a redd and unspawed bed. Bed-average shear stress is plotted as a function of discharge in the flume for reference.

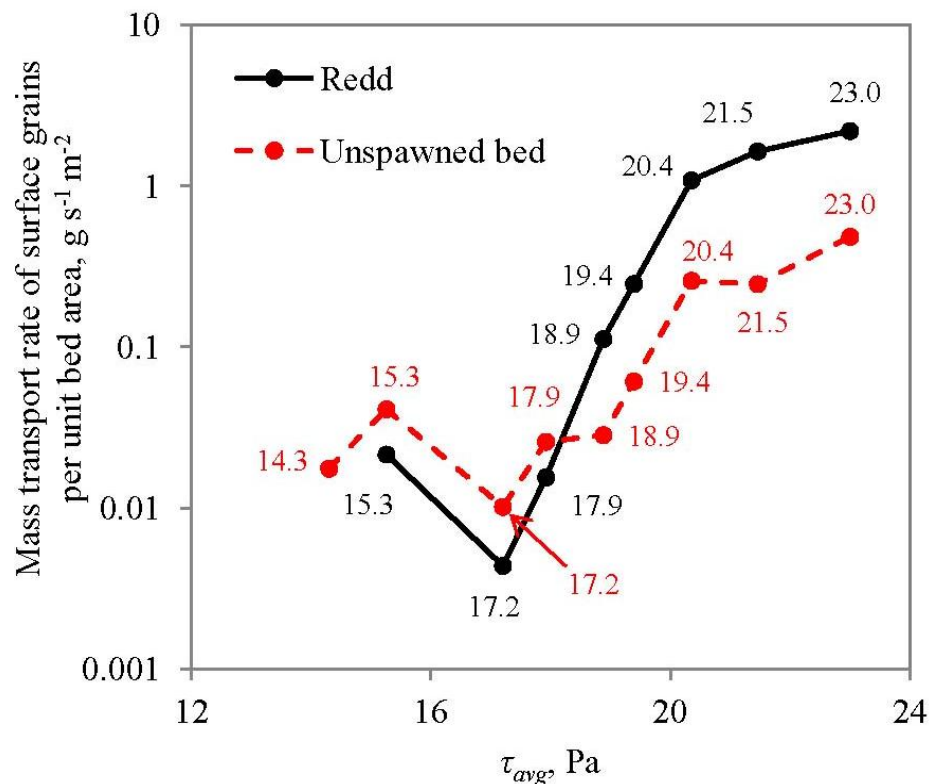


Figure 3.11. Mass transport rates of surface grains mobilized from the spawned and unspawned bed areas in experiment 3. Data labels are values of bed average shear stress (τ_{avg}) in pascals.

3.5 Discussion

Our experiments demonstrating that redds are less stable than unspawned beds support field observations of redd instability by *Lisle* [1989], *Rennie and Millar* [2000], and *Bigelow* [2003] and counter *Montgomery et al.*'s [1996] theoretical calculations indicating that spawning stabilizes solitary redds. Our findings differed from *Montgomery et al.*'s [1996] because we accounted for destabilizing effects of spawning on bed mobility, including 1) bed loosening during redd construction, which decreased packing resistance and critical shear stress, and 2) flow convergence over the redd, leading to relatively higher boundary shear stresses. Our findings most directly apply to redds that are unsheltered by

flow obstructions and nearby redds. However, *Montgomery et al.* [1996] also considered the effect of redd form drag on stability by treating redds as channel-spanning bed forms. Except perhaps in low-order channels, redds only occupy a portion of a channel's width; therefore, in mid- to high-order channels, such as Kennedy Creek, it remains unclear whether form drag from redds extracts sufficient momentum from flow to decrease flow velocity and shear stress and protect downstream redds from erosion.

Redd form drag effects on flow speed are a function of the amplitude and spacing of redds, with higher drag and lower flow velocity associated with redds that are less submerged and in closer spacings. Therefore, form drag from redds varies with the density of spawning and the redd amplitude relative to the range of flow depths that occur throughout post-spawning hydrographs. Additionally, research involving dunes suggests that irregularly spaced redds may suppress turbulent flow structures, leading to 20% less drag on redds [*Venditti, 2007*] compared to regularly spaced redds in unobstructed areas of streams. Flow drag may also be lower on redds in the vicinity of channel banks, vegetation, boulders, or large wood [*Mull and Wilzbach, 2007*] since a proportion of the total drag would be expended on local roughness elements [*Manga and Kirchner, 2000; Bledsoe et al., 2005*] rather than on the bed.

Upstream redds may also protect downstream redds by direct sheltering. However, research involving dunes [*Engel, 1981; Nelson and Smith, 1989; Ojha and Mazumder, 2008*] suggests that redds separated by streamwise distances greater than 4 to 6 times the amplitude of the upstream redd are unsheltered and may experience the relatively high boundary shear stress that we observed on a redd compared to an unspawned bed. Redds built in spacings below this range may also experience elevated boundary shear stress as a result of local

variations in flow, including flow acceleration over and around redds and high turbulence generated by tailspill wakes. Finally, increased boundary shear stress may occur on redds as a result of mass spawning eroding macro-bed forms and smoothing large-scale topography, which can offset momentum losses due to small scale topography from redds [*Hassan and Tonina*, in review].

The size, shape, and orientation of redds also affects the stability of spawned beds. For instance, boundary shear stress on a redd will vary with the redd size, which influences flow convergence on the structure, with larger, taller redds experiencing higher water pressure, shear stress, and flow drag. Redds in teardrop shapes (used in this study) are streamlined and generate the least drag per unit volume when constructed long-axis parallel to flow [*Vogel*, 1994], which is typical in nature. Low drag is associated with increased stability because streamlined forms experience small variations in water pressure and reduced shear stress compared to bluff bodies in flow. The teardrop form of redds results from flow dispersing grains during spawning and possibly also from probing behavior by the female [*Jones and Ball*, 1954] during construction of the redd. Probing behavior relies on the female's sense of flow direction, which she uses to construct a redd in a shape and orientation that maximizes hyporheic flow to eggs. She accomplishes this by flushing fine sediment to increase hydraulic conductivity and by constructing a tailspill mound for topographically forcing flow through the nest. Probing may also direct the female to abandon a nest if the bed is too coarse or too tightly packed for flushing fines from gravels and constructing eggs pits at a suitable depth [*Tautz and Groot*, 1975; *van den Berghe and Gross*, 1984]. Since probing behavior relies on a female's sense of flow, injury and environmental conditions may result in redds that are oddly shaped or angled to flow. We

have observed injured (bear-bitten) female chum building redds with the long-axis angled up to around 30° to flow. Turbidity can also lead to construction of unusual redd shapes by disorienting the female and causing her to wander laterally during spawning [*Lorenz and Eiler, 1989*].

Our finding that redds are unstable compared to unspawned beds does not imply that embryos are overly vulnerable in egg pockets. Grain mobility on redds is unlikely to threaten embryos because redd surfaces are typically sealed by sand, which blocks fine sediment from infiltrating egg pits and suffocating or entombing eggs [*Beschta and Jackson, 1979; Meyer et al., 2005; May et al., 2009*], and such seals tend to reform after erosional events [*Lisle, 1989*]. Tailspill erosion is also unlikely to significantly alter flow for oxygenating eggs and flushing metabolic wastes [*Cooper, 1965; Meehan and Swanston, 1977; Johnson, 1980*] since high hydraulic conductivity in the redd would continue to increase flow to eggs, assuming gravel interstices are not clogged by delivery of excessive fines during redd mobility [*Meyer et al., 2005*]. Moreover, redd erosion in itself is unlikely to threaten egg incubation in the nest. This hypothesis is based on our excavations of redds and those made by others [*Hawke, 1978; Peterson and Quinn, 1996*], indicating the top-down layering in tailspills includes a coarse surface layer, a surface seal of sand and silt, a cover layer of unsorted fines and small gravel, and a bridge of gravel-sized grains overlying egg pockets composed of the largest grains in the area of redd construction (Figure 3.12). With this stratigraphy, tailspill scour following disruption of surface grains would only be prevented by relatively small grains in the cover layer, so that scour would rapidly proceed following initial mobility. However, tailspill scour eventually erodes redds flat with the unspawned bed. At this point, boundary shear stress could equalize between the redd and

unspawned bed, so that erosion exposing egg pockets may only be as likely as when unspawned beds scour as deep, as observed by *Rennie and Millar* [2000] in field experiments involving chum salmon redds. Furthermore, scour of unspawned beds to egg pocket depths may not unduly threaten incubation in the nest since egg pockets are composed of grain sizes that are the largest in the area of redd construction, and therefore are potentially more stable than unspawned beds.

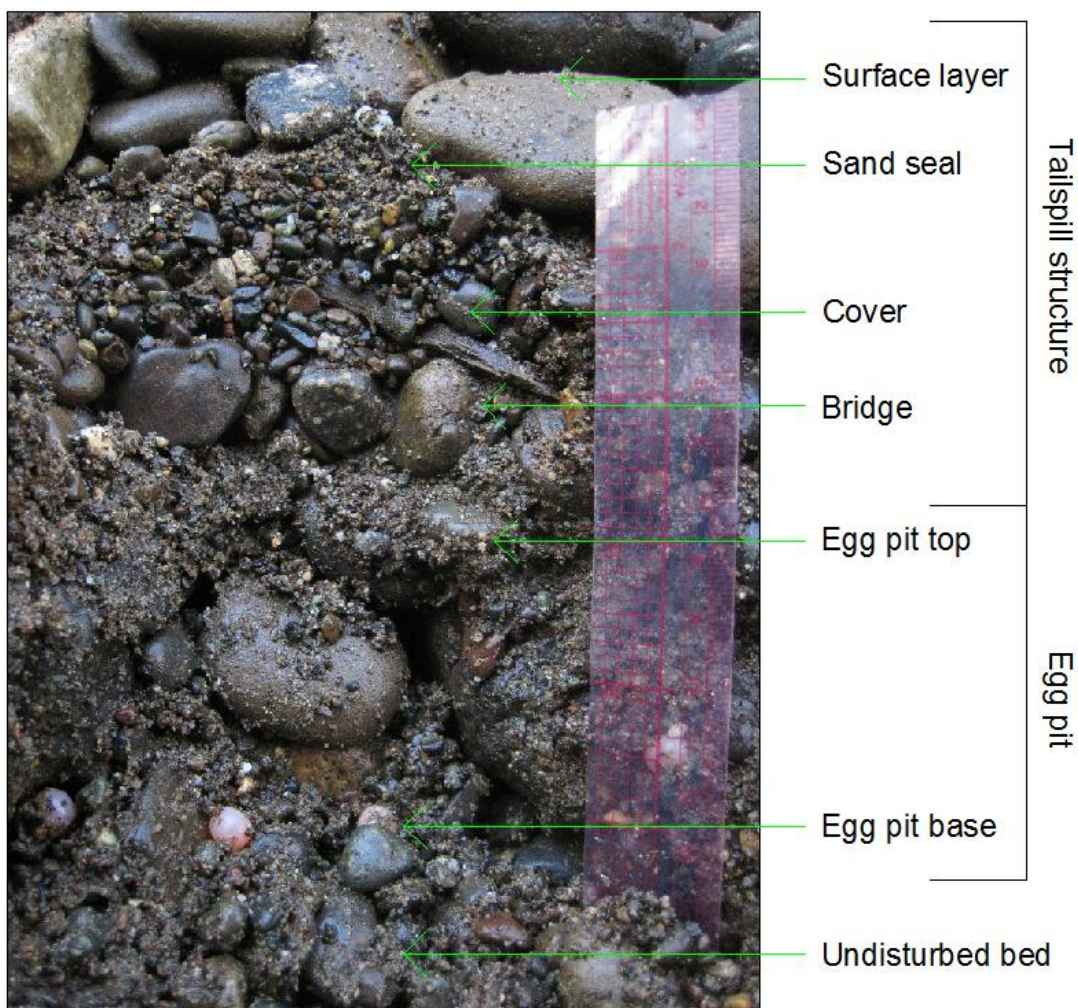


Figure 3.12. Stratigraphy of sediment in a dewatered chum salmon redd in Kennedy Creek, WA.

Low packing resistance on redds can persist for days to months after spawning is complete [DeVries, 1997; Gottesfeld *et al.*, 2004]. Persistence depends on a number of factors, including the density and proximity of upstream spawning activity and the timing of flow events following redd construction [Buffington *et al.*, 2013], both of which mobilize fine sediment for repacking grains. Deposition of fine grains can stabilize redds, but may come at the expense of reduced survival of embryos in the nest. For example, strong negative relationships have been established between concentrations of fine sediment (typically <2 mm) in gravel and embryo survival in laboratory and field studies [Everest *et al.*, 1987; Chapman, 1988]. Fines slow egg development by reducing delivery of oxygenated water to eggs [Cordone and Kelly, 1961], limiting alevin movement in gravel interstices [Phillips *et al.*, 1975], suffocating embryos by obstructing micropores in egg membranes [Greig *et al.*, 2005], or entombing embryos in the nest [Koski, 1966; Vaux, 1968; Sowden and Power, 1985]. Tailspill erosion may therefore be less detrimental to salmon reproduction than sedimentation of the redd.

Our findings are based on a series of flume measurements that were conducted under limited experimental conditions. Results may have differed, for instance, if silt and clay-sized material had been included in the sediment mixtures. This would have generated relatively higher packing resistance and critical shear stress on unspawned beds due to sediment cohesion and grain mortaring [Barzilai *et al.*, 2013] that would have been disrupted by simulated spawning. Higher stability for unspawned beds would also have resulted if beds had been formed by feeding sediment into the flume instead of using screeded beds of hand-placed sediment. Differences in grain stability would have resulted because the former would have deposited grains in relatively stable configurations

throughout the depth of the beds compared to only surface grains being stabilized on the screeded beds [Cooper and Tait, 2009]. Moreover, redds may have exhibited somewhat higher stability in visual observations of entrainment and bed load transport measurements if they had been modeled after species of salmon that construct smaller structures with less amplitude (e.g. pink (*O. gorbuscha*) and sockeye (*O. nerka*) salmon) that generate lower flow convergence and less boundary shear stress [DeVries, 2012]. The opposite may have occurred, however, if redds had been modeled after Chinook salmon (*O. tshawytscha*) that construct larger redds with higher amplitudes than other species of Pacific salmon. Overall, the limited extent of our experiments makes additional studies necessary before our findings can be generally applied to salmon redds in nature.

Another factor left unexamined in our experiments was the three-dimensional (3D) nature of flow interactions with redds, as our velocity measurements were limited to a 2D transect on the centerline of a redd. As a result, velocity measurements on the redd did not show lateral divergence of flow across the top of the redd and accelerations along the flanks of the redd that would be expected to occur. Nor did we measure the hydraulic effects of the pit depression, which likely shelters grains [Hobbs, 1937], recirculates flow [Burner, 1951], and lowers boundary shear stress on this area of the redd. These expectations were supported by our visual observations of bed mobility, which indicated that grains within the pit remained in place and were buried by unspawned grains mobilized upstream of the redd (Experiment 3). Therefore, further investigations are needed to characterize the 3D flow structure associated with redds, adjacent unspawned beds, and unspawned beds at variable distances from redds.

Redd building by salmon can be responsible for movement of around half the annual yield of sediment where spawning occurs in mass densities [*Hassan et al.*, 2008]. This and our finding of the relative instability of redds suggests that chronic reductions in spawning activity may lead to sedimentation of fish habitats, which is a leading cause of decline in salmon populations throughout the Pacific Northwest [*Nehlsen et al.*, 1991; *Kaufmann et al.*, 2009]. Sedimentation impacts salmon reproduction by filling pools that juvenile salmonids use for rearing [*Lisle and Hilton*, 1992] and migrating adult salmon use for resting [*Torgersen et al.*, 1999]. Pools filling may, in turn, lead to conversion of pool-riffle channels to plane-bed channels [see *Montgomery and Buffington*, 1997] that are generally avoided by salmonids [*Montgomery et al.*, 1999]. Reduced spawning activity also lessens the amount of fine sediment that is flushed into the water column during redd building to be carried downstream, which can lead to siltation of the intergravel environment and reduce incubation success [*Chapman*, 1988]. Such changes would negatively impact salmon populations and decrease marine subsidies that salmon spawners provide to aquatic food webs [*Cedarholm et al.*, 1999; *Wipfli and Baxter*, 2010] and riparian ecosystems [*Helfield and Naiman*, 2001; *Bilby et al.*, 2003; *Drake and Naiman*, 2007].

Cascading effects of reduced spawning activity may be prevented or reversed by managing salmon escapements to promote physical, biological, and ecological processes that benefit salmon reproduction and aquatic diversity in streams [*Piccolo et al.*, 2009]. The idea that the natural engineering ability of a species can improve or maintain ecosystem processes is not a new one [*Byers et al.*, 2006]. For example, beaver dams raise water tables that promote willow growth [*Bilyeu et al.*, 2008] and salmon build redds that support egg incubation [*Peterson and Quinn*, 1996]. In particular, the scale of engineering performed by

salmon is impressive, whereby mass spawners reorganize stream beds by eroding macro-topography in stream channels [*Hassan and Tonina*, in review] and building large dunes on mainstem rivers [*Gottesfeld et al.*, 2008]. Salmon spawning may also impact river profiles by increasing bed load transport [*Hassan et al.*, 2008] partly as a result of redds exhibiting lower stability than unspawned beds.

3.6 Summary

Using complementary methods, our analyses show that redds are more mobile than unspawned bed surfaces. This conclusion is derived from 1) Monte Carlo simulations indicating that packing resistance to grain motion was 32% to 39% lower on redds than unspawned beds; 2) measurements of critical shear stress demonstrating that spawned grains were 8% to 20% less stable than unspawned grains; 3) boundary shear stress estimates that were up to 41% higher on redd structures than unspawned beds; 4) bed-averaged shear stress at observed incipient motion that was 22% lower on a redd than an unspawned bed; 5) scour of a redd tailspill structure flush with an unspawned bed at about the same bed-average shear stress that completed entrainment of all grain-size classes on the surface of an unspawned bed; and 6) bed load transport rates that were nearly five-times higher on a redd. Our findings most directly apply to isolated redds in open-channel areas, but may also be relevant to mass spawning conditions where topographic roughness and sheltering from redds in high densities are offset by the erosion of bed forms and smoothing channel topography during spawning. Additional factors that can affect redd stability include 1) location of spawning in the channel; 2) spawning density; 3) the shape, size, and relief of the

redd; 4) timing of high flow events; and 5) fitness of the female salmon constructing the redd.

Redd instability is unlikely to overly threaten eggs in salmon nests because sand seals that block fine sediment from suffocating eggs reform after redd destruction, and tailspill erosion is unlikely to significantly alter flow to eggs unless gravel interstices in redds are clogged by fines. We further propose that redd erosion itself is unlikely to threaten egg incubation since erosion of redds to a level flush with the unspawned bed would equalize boundary shear stress between surfaces. Scour to egg pocket depths may then only be as likely to occur when unspawned beds scour as deep. Our findings combined with prior research, which indicates that redd building by mass spawners can mobilize around half the annual bed load yield where salmon spawn [*Hassan et al.*, 2008], suggest chronically low salmon populations may lead to sedimentation of stream habitats and further declines in fish populations. Future research is needed to quantify this linkage to provide a possible basis for managing salmon populations and promote spawning disturbance that streams may require to sustain fish populations.

3.7 References

- Adrian, R. J. (2005), Twenty years of particle image Velocimetry, *Exp. Fluids*, 39, 159-169.
- Balachander, R., B. S. Hyun, and V. C. Patel (2007), Effect of flow depth on flow over a fixed dune, *Can. J. Civ. Eng.*, 34, 1587-1599.
- Barzilai, R. J., B. Laronne, and I. Reid (2013), Effect of changes in fine-grained matrix on bedload sediment transport in a gravel-bed river, *Earth Surf. Proc. Landforms*, 38, 441-448.
- Battin, J., M. W. Wiley, M. H. Ruckelshaus, R. N. Palmer, E. Korb, K. K. Bartz, and H. Imaki (2007), Projected impacts of climate change on salmon habitat restoration, *Proc. Nat. Acad. Sci.*, 104, 6720-6725.
- Bernhardt, E. S., M. A. Palmer, J. D. Allan, G. Alexander, K. Barnas, S. Brooks, J. Carr, S. Clayton, C. Dahm, J. Follstad-Shah, D. Galat, S. Gloss, P. Goodwin, D. Hart, B. Hassett, R. Jenkinson, S. Katz, G. M. Kondolf, P. S. Lake, R. Lave, J. L. Meyer, T. K. O'Donnell, L. Pagano, B. Powell, and E. Sudduth (2005), Synthesizing U.S. River Restoration Efforts, *Science*, 308, 636-637.
- Beschta, R. L. and W. L. Jackson (1979), The intrusion of fine sediments into a stable gravel bed, *J. Fish. Res. Board Can.*, 36, 204-210.
- Bigelow, P. E. (2003), Scour, fill, and salmon spawning in a northern California coastal stream, M.S. thesis, Dept. of Geol., Humboldt State Univ., Arcata, CA.
- Bilby, R. E., E. W. Beach, B. R. Fransen, J. K. Walter, and P. A. Bisson (2003), Transfer of nutrients from spawning salmon to riparian vegetation in Western Washington, *Trans. Am. Fish. Soc.*, 132, 733-745.

- Bilyeu, D. M., D. J. Cooper, and N. T. Hobbs (2008), Water tables constrain height recovery of willow on Yellowstone's northern range, *Ecol. Appl.*, 18, 80-92.
- Bisson, P. A., J. B. Dunham, and G. H. Reeves (2009), Freshwater ecosystems and resilience of Pacific salmon: habitat management based on natural variability, *Ecol. and Soc.*, 14, 45.
- Bjornn, T. C. and D. W. Reiser (1991), Habitat Requirements of salmonids in streams, in *Influences of forest and rangeland management on salmonid fishes and their habitat*, edited by W. R. Meehan, pp. 83-138, Am. Fish. Soc. Sp. Pub. 19, Bethesda, MD.
- Blatt, H., G. Middleton, and R. Murray (1980), *Origin of sedimentary rocks*, Prentice-Hall, Englewood Cliffs, N.J.
- Bledsoe, B. P., S. K. Carney, and R. J. Anderson (2005), Scale-dependent effects of bank vegetation on channel processes: Field data, computational fluid dynamics modeling, and restoration design, *Geophys. Mono. Series 194*, 151-165.
- Buffington, J. M. and D. R. Montgomery (1997), A systematic analysis of eight decades of incipient motion studies, with special reference to gravel-bedded rivers, *Water Resour. Res.*, 33, 1993-2029.
- Buffington, J. M., T. H. Buxton, A. K. Fremier, M. A. Hassan, and E. Yager (2013), Persistence of salmonid redds: A conceptual analysis, poster presentation at Am. Geophys. Union Fall meeting, San Francisco, CA. American Geophysical Union, Fall Meeting 2013, abstract #EP43A-0827.
- Burner, C. J. (1951), Characteristics of spawning nests of Columbia River salmon, *U.S. Fish and Wldf. Serv. Bull.*, 61.

- Buxton, T. H., E. M. Yager, J. M. Buffington, M. A. Hassan, and A. K. Fremier (submitted), Grain packing resistance to particle mobility, *J. Geophys. Research*.
- Byers, J. E., K. Cuddington, C. G. Jones, T. S. Talley, A. Hastings, J. G. Lambrinos, J. A. Crooks, and W. G. Wilson (2006), Using ecosystem engineers to restore ecological systems, *Ecol. Evol.*, 21, 493-500.
- Cedarholm, C. J., M. D. Kunze, T. Murota, and A. Sibatani (1999), Pacific salmon carcasses: Essential contributions of nutrients and energy for aquatic and terrestrial ecosystems, *Fisheries*, 24, 6-15.
- Chapman, D. W. (1988), Critical review of variables used to define effects of fines in redds of large salmonids, *Trans. Am. Fish. Soc.*, 117, 1-21.
- Cheng, N. S. (2011), Revisited Vanoni-Brooks sidewall correction, *Int. J. Sed. Res.*, 26, 524-528.
- Church, M. A. , D. G. McLean, and J. F. Wolcott (1987), River Bed Gravels: Sampling and Analysis, in *Sediment Transport in Gravel-Bed Rivers*, edited by C. R. Thorne, J. C. Bathurst, and R. D. Hey, pp. 43-88, John Wiley and Sons, New York.
- Cooper, A. C. (1965) The effect of transported stream sediments on the survival of sockeye and pink salmon eggs and alevin, *Int. Pac. Salmon Fish. Comm. Bull.* 18.
- Cooper, J. R. and S. J. Tait (2009), Water-worked gravel beds in laboratory flumes – a natural analogue?, *Earth Surf. Proc. Landforms*, 34, 384-397.
- Cordone, A. J. and D. W. Kelly (1961), The influence of fine sediment on the aquatic life of streams, *Cal. Fish and Game*, 47, 189-228.
- Corey, A. T. (1949), Influence of shape on the fall velocity of sand grains, M.S. thesis, Colorado State University, Fort Collins.

- DeVries, P. (1997), Riverine salmonid egg burial depths: review of published data and implications for scour studies, *Can. J. Fish. Aquat. Sci.*, 54, 1685-1698.
- DeVries, P. (2012), Salmonid influences on rivers: a geomorphic fish tail, *Geomorphology*, 157, 66-74.
- Drake, D. C. and R. J. Naiman (2007), Reconstruction of Pacific salmon abundance from riparian tree-ring growth, *Ecol. Appl.* 17, 1523-1542.
- Einstein H. A. and N. L. Barbarossa (1956), River channel roughness, *Trans. Am. Soc. Civ. Eng.*, 177, 440-457.
- Engel, P. (1981), Length of flow separation over dunes, *J. Hydraul. Div. Am. Soc. Civ. Eng.*, 107, 1133-1143.
- Everest, F. H., R. L. Beschta, J. C. Scrivener, K. V. Koski, J. R. Sedell, and C. J. Cederholm (1987), Fine sediment and salmonid production - a paradox, in *Streamside management and forestry and fishery interactions*, edited by E. Salo and T. Cundy, pp. 98-142, University of Washington, College of Forest Resources, Contribution 57, Seattle, Wash..
- Francis, J. R. D. (1973), Experiments on the motion of solitary grains along the bed of a water-stream, *Proc. R. Soc. Lond.*, 332, 443-471.
- Gottesfeld, A. S., M. A. Hassan, J. F. Tunnicliffe, and R. W. Poirer (2004), Sediment dispersion in salmon spawning streams: the influence of floods and salmon redd construction, *J. Am. Water Resour. Assoc.*, 40, 1071-1086.
- Gottesfeld, A. S., M. A. Hassan, and J. F. Tunnicliffe (2008), Salmon bioturbation and stream processes, in *Am. Fish. Soc. Sym.*, 65, pp 1-19.

- Graham, D. J., S. P. Rice, and I. Reid (2005a), A transferable method for the automated sizing of river gravels, *Water Resour. Res.*, *41*, doi:10.1029/2004WR003868.
- Graham, D. J., I. Reid, and S. P. Rice (2005b), Automated sizing of coarse-grained sediments: image processing procedures, *Mathematical Geol.*, *37*, doi: 10.1007/s11004-005-8745-x.
- Greig, S. M., D. A. Sear, and P. A. Carling (2005), The impact of fine sediment accumulation on the survival of incubating salmon progeny: implications for sediment management, *Sci. Tot. Env.*, *344*, 241-258.
- Greig, S. M., D. A. Sear, and P. A. Carling (2007), A review of factors influencing the availability of dissolved oxygen to incubating salmonid embryos, *Hydrol. Proc.*, *21*, 323-334.
- Hassan, M. A. and D. Tonina (In review) Does sockeye salmon spawning activity enhance bed mobility in small creeks? *J. Geophys. Res. Earth Sci.*
- Hassan, M. A., A. S. Gottesfeld, D. R. Montgomery, J. F. Tunncliffe, G. K. C. Clarke, G. Wynn, H. Jones-Cox, R. Poirer, E. MacIsaac, H. Herunter, and S. J. Macdonald (2008), Salmon-driven bed load transport and bed morphology in mountain streams, *Geophys. Res. Lett.*, *35*, doi:10.1029/2007GL032997.
- Hawke, S. P. (1978), Stranded redds of Quinnat salmon in the Mathias River, South Island, New Zealand, *N. Z. J. Marine Fresh. Res.*, *12*, 167-171.
- Helfield, J. M. and R. J. Naiman (2001), Effects of salmon-derived nitrogen on riparian forest growth and implications for stream productivity, *Ecology*, *82*, 2403-2409.
- Hobbs, D. F. (1937), Natural reproduction of quinnat salmon, brown and rainbow trout in certain New Zealand waters, *N.Z. Marine Dep. Fish. Bull.* *6*, 104 pp.

- Hodge, R. A., D. A. Sear, and J. Leyland (2013), Spatial variations in surface sediment structure in riffle-pool sequences: A preliminary test of the Differential Sediment Entrainment Hypothesis (DSEH), *Earth Surf. Proc. Landforms*, 38, 449-465.
- Isaak, D. J., R. F. Thurow, B. E. Rieman, and D. B. Dunham (2007), Chinook salmon use of spawning patches: Relative roles of habitat quality, size, and connectivity, *Ecol. Appl.*, 17, 352-364.
- Johnson, R. A. (1980), Oxygen transport in salmon spawning gravels, *Can. J. Fish. Aquat. Sci.*, 37, 155-162.
- Johnston, C. E., E. E. Andrews, and J. Pitlick (1998), In situ determination of particle friction angles of fluvial gravels, *Water Resour. Res.*, 34, 2017-2030.
- Jones, J. W. and J. H. Ball (1954), The spawning behavior of Brown trout and salmon. *Brit. J. Anim. Behav.*, 2, 103-114.
- Kaufmann, P. R., D. P. Larson, and J. M. Faustini (2009), Bed stability and sedimentation associated with human disturbances in Pacific Northwest streams, *J. Am. Wat. Resour. Assoc.*, 45, 434-459.
- Keulegan, G. H. (1938), Laws of turbulent flow in open channels, *J. Res. National Bureau Standards*, 21, 707-741.
- Kirchner, J. W., W. E. Dietrich, F. Iseya, and H. Ikeda (1990), The variability of critical shear stress, friction angle, and grain protrusion in water worked sediments, *Sedimentology*, 37, 647-672.
- Komar, P. D. and Z. Li (1988), Applications of grain-pivoting and sliding analyses to selective entrainment of gravel and to flow-competence evaluations, *Sedimentology*, 25, 681-695.

- Kondolf, G. M. (1988), Salmonid spawning gravels: A geomorphic perspective on their size distribution, modification by spawning fish, and criteria for gravel quality, Ph.D. dissertation, Johns Hopkins Univ., Baltimore, Maryland.
- Kondolf, G. M. and M. G. Wolman (1993), The sizes of salmonid spawning gravels, *Water Resour. Res.*, 29, 2275-2285.
- Kondolf, G. M., M. J. Sale, and M. G. Wolman (1993), Modification of fluvial gravel size by spawning salmonids, *Water Resour. Res.*, 7, 2265-2274.
- Koski, K. V. (1966), The survival of coho salmon (*Oncorhynchus kisutch*) from egg deposition to emergence in three Oregon coastal streams, M.S. thesis, Oregon State University, Corvallis.
- Ling, C. H. (1995), Criteria for incipient motion of spherical sediment particles, *J. Hydraul. Eng.*, 121, 472-478.
- Lisle, T. E. (1982), Effects of aggradation and degradation on riffle-pool morphology in natural gravel channels, Northwestern California, *Water Resour. Res.*, 18, 1643-1651.
- Lisle, T. E. (1989), Sediment transport and resulting deposition in spawning gravels, North Coastal California, *Water Resour. Res.*, 25, 1303-1319.
- Lisle, T. E. and S. Hilton (1992), The volume of fine sediment in pools: An index of sediment supply in gravel bed streams, *Am. Water Res. Bull.*, 28, 371-383.
- Lorenz, J. M. and J. H. Eiler (1989), Spawning habitat and redd characteristics of sockeye salmon in the glacial Taku River, British Columbia and Alaska, *Trans. Am. Fish. Soc.* 118, 495-502.

- Maddux, T. B., J. M. Nelson, and S. R. McLean (2003), Turbulent flow over three-dimensional dunes: 1. Free surface and flow response, *J. Geophys. Res.*, *108*, doi:10.1029/2003JF000017.
- Madej, M. A. (1999), Temporal and spatial variability in thalweg profiles of a gravel bed river, *Earth Surf. Proc. Landforms*, *24*, 1153-1169.
- Manga, M. and J. W. Kirchner (2000), Stress partitioning in streams by large woody debris, *Water Resour. Res.*, *36*, 2372-2379.
- May, C. L., B. Pryor, T. E. Lisle, and M. Lang (2009), Coupling hydrodynamic modeling and empirical measures of bed mobility to predict the risk of scour and fill of salmon redds in a large regulated river, *Water Resour. Res.*, *45*, doi:05410.01029/02007WR006498.
- Meehan, W. R. and D. N. Swanstrom (1977), Effects of gravel morphology and fine sediment accumulation on survival of incubating salmon eggs, *USDA Forest Service Res. Paper PNW-220*.
- Meyer, C. B., M. D. Sparkman, and B. A. Klatte (2005), Sand seals in coho salmon redds: Do they improve egg survival?, *N. Am. J. Fish. Mgmt.*, *25*, 105-121.
- Middleton, G. V. and J. B. Southard (1984), Mechanics of sediment movement, Soc. Econ. Paleontologist and Mineralogists, short course no. 3, Providence R.I., 401 pp.
- Montgomery, D. R., J. M. Buffington, N. P. Peterson, D. Schuett-Hames, T. P. Quinn (1996), Stream-bed scour, egg burial depths, and the influence of salmonid spawning on bed surface mobility and embryo survival, *Can. J. Fish. Aquat. Sci.*, *53*, 1061-1070.

- Montgomery, D. R. and J. M. Buffington (1997), Channel-reach morphology in mountain drainage basins, *GSA Bull.* 109, 596-611.
- Montgomery, D. R., E. M. Beamer, G. R. Pess, and T. P. Quinn (1999), Channel type and salmonid spawning distribution and abundance, *Can. J. Fish. Aquat. Sci.*, 56, 377-387.
- Montgomery, D. R. (2003), *King of Fish: The Thousand-Year Run of Salmon*, Westview Press, Boulder, CO.
- Motamedi, A., H. Afzalimehr, V. Singh, and L. Dufresne (2014), Experimental study on the influence of dune dimensions on flow separation, *J. Hydrol. Eng.*, 19, 78-86.
- Mull, K. E. and M. A. Wilzbach (2007), Selection of spawning sites by coho salmon in a northern California stream, *N. Am. J. Fish. Mgmt.*, 24, 1343-1354.
- Munson, B. R., D. F. Young, and T. H. Okiishi (2006), *Fundamentals of Fluid Mechanics*, John Wiley & Sons, New York.
- Nehlsen, W., J. E. Williams, and J. A. Lichatowich (1991), Pacific salmon at the crossroads, stocks at risk from California, Oregon, Idaho, and Washington, *Fisheries*, 16, 4-21.
- Nelson, J. M. and J. D. Smith (1989), Mechanics of flow over ripples and dunes, *J. Geophys. Res.*, 94, 8146-8162.
- Nelson, J. M., S. R. McLean, and S. R. Wolfe (1993), Mean flow and turbulence over two-dimensional bed forms, *Water Resour. Res.*, 29, 3935-3953.
- Ojha, S. P. and B. S. Mazumber (2008), Turbulence characteristics of flow region over a series of 2-D dune shaped structures, *Adv. Water Resour.*, 31, 561-576.
- Powers, M. C. (1953), A new roundness scale for sedimentary particles, *J. Sed. Petrol.*, 23, 117-119.

- Piccolo, J. J., M. D. Adkison, and F. Rue (2009), Linking Alaskan salmon fisheries management with ecosystem-based escapement goals: A review and prospectus, *Fisheries*, 34, 124-134.
- Peterson, N. P. and T. P. Quinn (1996), Persistence of egg pocket architecture in redds of chum salmon, *Oncorhynchus keta*, *Env. Biol. Fishes*, 46, 243-253.
- Phillips, R. W., R. L. Lantz, E. W. Claire, and J. W. Moring (1975), Some effects of gravel mixtures on emergence of coho salmon and steelhead trout fry, *Trans. Am. Fish. Soc.* 104, 461-466.
- Rennie, C. D. and R. G. Millar (2000), Spatial variability of stream bed scour and fill: a comparison of scour depth in chum salmon (*Oncorhynchus keta*) redds and adjacent bed, *Can. J. Fish. Aquat. Sci.*, 57, 928-938.
- Smirnova, I. (1955), The effect of mechanical agitation at different periods of development on the eggs of autumn chum salmon, *Nauk SSSR*, 105, 873-876. (Translated from Russian; Fish. Res. Board Can. Transl. Ser. 370)
- Smith, A. K. (1973), Development and application of spawning velocity and depth criteria for Oregon salmonids, *Trans. Am. Fish. Soc.*, 102, 312-316.
- Smith, G. H. and R. I. Ferguson (1996), The gravel-sand transition: flume study of channel response to reduced slope, *Geomorphology*, 16, 147-159.
- Stoesser, T., D. V. Terzi, W. Rodi, N. R. B. Olsen (2006), Rans simulations and Les of flow over dunes at low relative submergence ratios, paper presented at 7th Intl. Conf. Hydroscience and Engineering, Philadelphia, PA.

- Sowden, T. K. and G. Power (1985), Prediction of rainbow trout embryo survival in relation to groundwater seepage and particle size of spawning substrates, *Trans. Am. Fish. Soc.*, 114, 804-812.
- Tang L. M. and X. K. Wang (2009), Experimental study on three-dimensional movements of Particles - Effects of particle diameter on velocity and concentration distributions, *Int. J. Sed. Res.*, 24, 159-168.
- Tautz, A. F. and C. Groot (1975), Spawning behavior of chum salmon (*Oncorhynchus keta*) and Rainbow trout (*Salmo gairdneri*), *J. Fish. Res. Board Can.*, 32, 633-642.
- Torgersen C. E., D. M. Price, H. W. Li, and B. A. McIntosh (1999), Multiscale thermal refuge and stream habitat associations of chinook salmon in northeastern Oregon, *Ecol. Appl.*, 9, 301-319.
- Tonina, D. and J. M. Buffington (2009), A three-dimensional model for analyzing the effects of salmon redds on hyporheic exchange and egg pocket habitat, *Can. J. Fish. Aquat. Sci.*, 66, 2157-2173.
- van den Berghe, E. P. and M. R. Gross (1984), Female size and nest depth in coho salmon (*Oncorhynchus kisutch*), *Can. J. Fish. Aquat. Sci.*, 41, 204-206.
- Vanoni V. A. and N. H. Brooks (1957), Laboratory studies of the roughness and suspended load of alluvial streams, in *Sediment. Lab. Rep. E68*, 121 pp., Calif. Inst. Technol., Pasadena.
- Vaux, W. G. (1968), Intergravel flow and interchange of water in a streambed. *U.S. Fish and Wldf. Serv. Fish. Bull.*, 66, 479-489.

- Vaux, W.G. (1962), Interchange of stream and intragravel water in a salmon spawning riffle, Spec. Sci. Rep. Fish. No. 405, US Fish and Wldf. Serv., Bureau Comm. Fish., Washington, D.C.
- Venditti, J. G. (2007), Turbulent flow and drag over fixed two- and three-dimensional dunes, *J. Geophys. Res.*, *112*, doi:10.1029/2006JF000650.
- Venditti, J. G., W. E. Dietrich, P.A. Nelson, M. A. Wydzga, J. Fadde, and L. Sklar (2010), Mobilization of coarse surface layers in gravel-bedded rivers by finer gravel bed load, *Water Resour. Res.*, *46*, W07506, doi:10.1029/2009WR008329.
- Vogel, S. (1994), *Life in Moving Fluids: The Physical Biology of Flow*. Princeton University Press, Princeton, New Jersey.
- von Kármán, T. (1930), Mechanische Ähnlichkeit und Turbulenz, Nachrichten von der Gesellschaft der Wissenschaften zu Göttingen, Fachgruppe 1, *Mathematik*, *5*, 58-76
- Wallerstein, N. P., C. V. Alonso, S. J. Bennett, and C. R. Thorne (2001), Distorted Froude-scaled flume analysis of large woody debris, *Earth Surf. Proc. Landforms*, *26*, 1265-1283.
- Wilcock, P. R. (1988), Methods for estimating the critical shear stress of individual fractions in mixed-size sediment, *Water Resour. Res.*, *24*, 1127-1135.
- Wilcock, P. R. (1996), Estimating local bed shear stress from velocity observations, *Water Resour. Res.*, *32*, 3361-3366.
- Wipfli, M. S. and C. V. Baxter (2010), Linking ecosystems, food webs, and fish production: subsidies in salmonid watersheds, *Fisheries*, *35*, 373-387.
- Wolman, M. G. (1954), A method of sampling coarse river-bed material, *Trans. Am. Geophys. Union*, *35*, 951-966.

Zimmermann, A. E. and M. Lapointe (2005), Intergranular flow velocity through salmonid redds: Sensitivity to fines infiltration from low intensity sediment transport events, *River Res. Applic.*, 21, 865-881.

Chapter 4. The Influence of Salmon Spawning on the Residence Time and Flux of Marine Derived Nutrients in Streambeds

4.1 Abstract

Salmon that spawn in streams deliver marine-derived nutrients (MDN) that catalyze trophic productivity and support rearing juvenile salmon. The residence time of MDN in hyporheic zones influences stream productivity since biochemical processing requires a certain amount of time to occur. Another factor is the volumetric exchange rate (flux) of nutrients delivered to the biologically active hyporheic zone since biochemical reactions can increase with the supply of nutrients to the bed. Salmon spawning affects the residence time and flux of MDN in hyporheic zones when the female salmon winnow fines during redd construction, which increases hydraulic conductivity and porosity in the bed and forms topography that pumps water through redds. Using a two-dimensional groundwater model, we evaluate the effect of salmon spawning on residence times ($=\text{hyporheic volume} / \text{hyporheic flux}$) and the flux of MDN in the hyporheic zone of a planar streambed with variable proportions of the bed surface occupied by redds. Predictions indicate the residency of MDN decreases sharply with increased proportions of the bed surface occupied by redds, from 5.79 h on an unspawned bed to 0.11 h with one redd (0.05 of the bed surface occupied by redds), and finally to 0.03 h for a mass spawned bed (1.0 spawning). Shorter residence times with increased spawning results from hyporheic flux increasing over four orders of magnitude with spawning while hyporheic volume increased less than an order of magnitude. Given the considerable influence of redds on hyporheic flow, additional research is needed to determine conditions under which stream productivity is limited by hyporheic

flux governing the supply of nutrients to the bed and residence time giving time for biochemical processing of nutrients to occur.

4.2 Introduction

The decline of Pacific salmon (*Oncorhynchus* spp.) outside Alaska has dramatically reduced spawning disturbance to rivers and delivery of marine-derived nutrients (MDN) to most streams [Gresh *et al.*, 2000]. Cultural, economic, and environmental imperatives for reversing the salmon's decline [Lackey, 2000] are motivating researchers to determine escapements that promote keystone roles of salmon in streams [Michael, 1998, 2003]. Consideration of ecosystem processes in setting salmon escapements is currently limited by few quantitative relationships linking spawning activities to physical and ecological processes that influence salmon reproduction [Piccolo *et al.*, 2009; Holtgrieve and Schindler, 2011]. In particular, little is known about how physical modifications to streambeds by variable numbers of spawners influence the residence time and flux of MDN in streambeds. Given the diverse and foundational influence of MDN in stream ecosystems [Gende *et al.*, 2002; Schindler *et al.*, 2003; and Naiman *et al.*, 2009], addressing this knowledge gap will help guide efforts to restore nutrient dynamics in streams with low salmon returns [Wipfli *et al.*, 2004; Kohler *et al.*, 2008].

Marine derived nutrients, including nitrogen, and phosphorous, are delivered to streams by salmon in the form of excreta, eggs, and carcasses [Rinella *et al.*, 2013]. Eggs and carcasses can be directly consumed [Scheuerell *et al.*, 2007], made soluble through decay or, along with excreta, sequestered by flocculation [binding of nutrients to fine sediments; Rex and Petticrew, 2006, 2008] or stream flora [Verspoor *et al.*, 2010], or

dispersed in flow while in transit downstream [Ensign and Doyle, 2005]. Direct consumption, flocculation, and uptake of MDN by stream organisms benefit stream productivity and salmon reproduction. For instance, Heintz *et al.* [2004] found that juvenile coho salmon (*O. kisutch*) that consume salmon carcasses exhibit elevated levels of triacylglycerides (energy reserves) and increased growth rates [Bilby *et al.*, 1996; Wipfli *et al.*, 2003]. Additionally, Wipfli *et al.* [1999] measured macroinvertebrate densities increasing as a result of direct consumption of salmon carcasses in several Alaskan streams. Moreover, nutrient flocs delivered to streambeds stimulate microbial communities and benthic food webs [Rex and Petticrew, 2008]. This process and soluble MDN increase periphyton [Johnston *et al.*, 2004] for consumption by aquatic invertebrates [Cummins and Klug, 1979], which are common prey for juvenile salmon [Wipfli, 1997]. In these ways, positive loops are created, such that as spawning populations increase, so do nutrient levels for sustaining juvenile salmon, potentially yielding greater returns of adult salmon [Cederholm *et al.*, 1999; Stockner, 2003].

Marine nutrients not sequestered by plants or flocculation are temporarily stored in stream flow and groundwater in the hyporheic zone of stream channels. Research has tended to focus on residence times in surface flow, which increase in still or recirculating areas of water, or where flow velocity is reduced by roughness in the channel, including wood, boulders, vegetation, and streambed sediment [Ensign and Doyle, 2005]. Another location for nutrient sequestering that has received considerably less attention is the hyporheic zone, an area of water-saturated sediment composing stream beds, bars, and riparian areas [White, 1993; Edwards, 1998]. The residence time and flux of water and nutrients in hyporheic zones varies spatially due to surface flow interactions with channel roughness and

topography [*Elliot and Brooks, 1997; Savant et al., 1987*] and variations in porosity and hydraulic conductivity in the bed [*Tonina and Buffington, 2009*].

An even less studied influence on the residence time and flux of MDN in hyporheic zones is redd topography and associated hydraulic conductivity and porosity in redds. Construction of redds proceeds by the female salmon using rapid undulations of her caudal fin to hydraulically dig a pit in the bed. In this process, fine sediment is winnowed from gravel, which is mobilized a short distance into a dune-like mound called a tailspill [*Burner, 1951*]. Grains too large to be moved accumulate in the pit where the female deposits a portion of her eggs for fertilization before covering the eggs with sediment excavated upstream. This sequence is repeated until the redd displays an upstream pot depression, one or more pockets of eggs, and a tailspill (Figure 4.1). Pressure differences across the tailspill pump water into the bed [*Cooper, 1965; Thibodeaux and Boyle, 1987; Worman et al., 2002*], which stores surface water in hyporheic areas. However, the exchange may be rapid due to high hydraulic conductivity within the redd (from winnowing of fines during spawning) and short, shallow flow paths [*Cooper, 1965; Tonina and Buffington, 2009*]. Consequently, the influence of spawning on residence times of MDN is unclear, especially in the context of variable densities of spawning since multiple redds create more variable pressure differences and higher conductivity and porosity for transmitting flow into and through the bed.

Understanding the influence of salmon spawning on the supply and residence time of MDN in streambeds is important for coupling physical habitat modifications by salmon to nutrient dynamics in streams, which can help inform fish-habitat restoration activities. Such couplings are important for their potential affect on stream productivity since biochemical processing can accelerate with the supply of nutrients to the bed [*O'Keefe and Edwards,*

2002; Pinay *et al.*, 2009] or simply require a certain amount of time to occur [Valett *et al.*, 1996; Thomas *et al.*, 2003]. We hypothesize the residence time of MDN in the hyporheic zone is low in the presence of spawning and decreases with a larger proportion of the streambed surface occupied by redds. This would result if hyporheic flux increases at a faster rate with the density of redds than hyporheic volume. We evaluate this hypothesis with two-dimensional (2D) groundwater model simulations of a planar stream bed involving variable densities of redds. Model predictions provide first-order estimates of the influence of spawning density on residence times and hyporheic flux of MDN in stream channels.

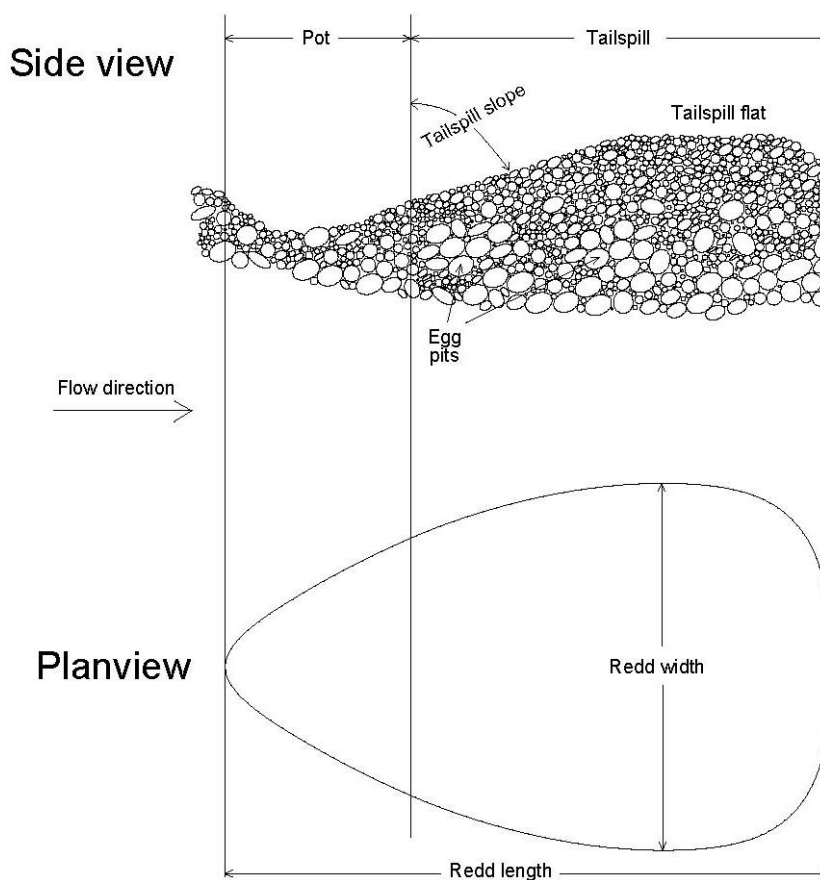


Figure 4.1. Side- and planview diagram of a redd modified from *Buxton et al.* [submitted].

4.3 Methods

4.3.1 Overview

The groundwater model VS2DTI was used to estimate hyporheic volumes and fluxes of MDN as a function of spawning density in an alluvial, spring-dominated stream in southeast Alaska. VS2DTI is a numerical model developed by the U.S. Geological Survey that uses the law of conservation of fluid mass with a non-linear form of Darcy's law to estimate hyporheic flow in porous media (VS2DTI 1.3, *Lappala et al.*, 1987; *Healy*, 1990). VS2DTI has been successfully used in previous investigations of hyporheic flux in stream beds and banks [*Constantz et al.*, 2003; *Cox et al.*, 2007] and laboratory channels [*Hassan et al.*, 2014]. In VS2DTI, the hyporheic zone is coupled to surface water through boundary conditions at the sediment-water interface, including total head (=elevation head+water pressure head) and sediment hydraulic conductivity and porosity. The domain of the model was setup to trace the centerline of Herman Creek near Haines, Alaska (Figure 4.2). Herman Creek was the prototype for modeling because it supports a large population of chum salmon (*O. keta*) and has a planar bed that was simple to represent in VS2DTI's graphical user interface (GUI). Our approach to modeling hyporheic volumes and fluxes of MDN assumes nutrients are in soluble form and fully mixed in surface water at the streambed surface.

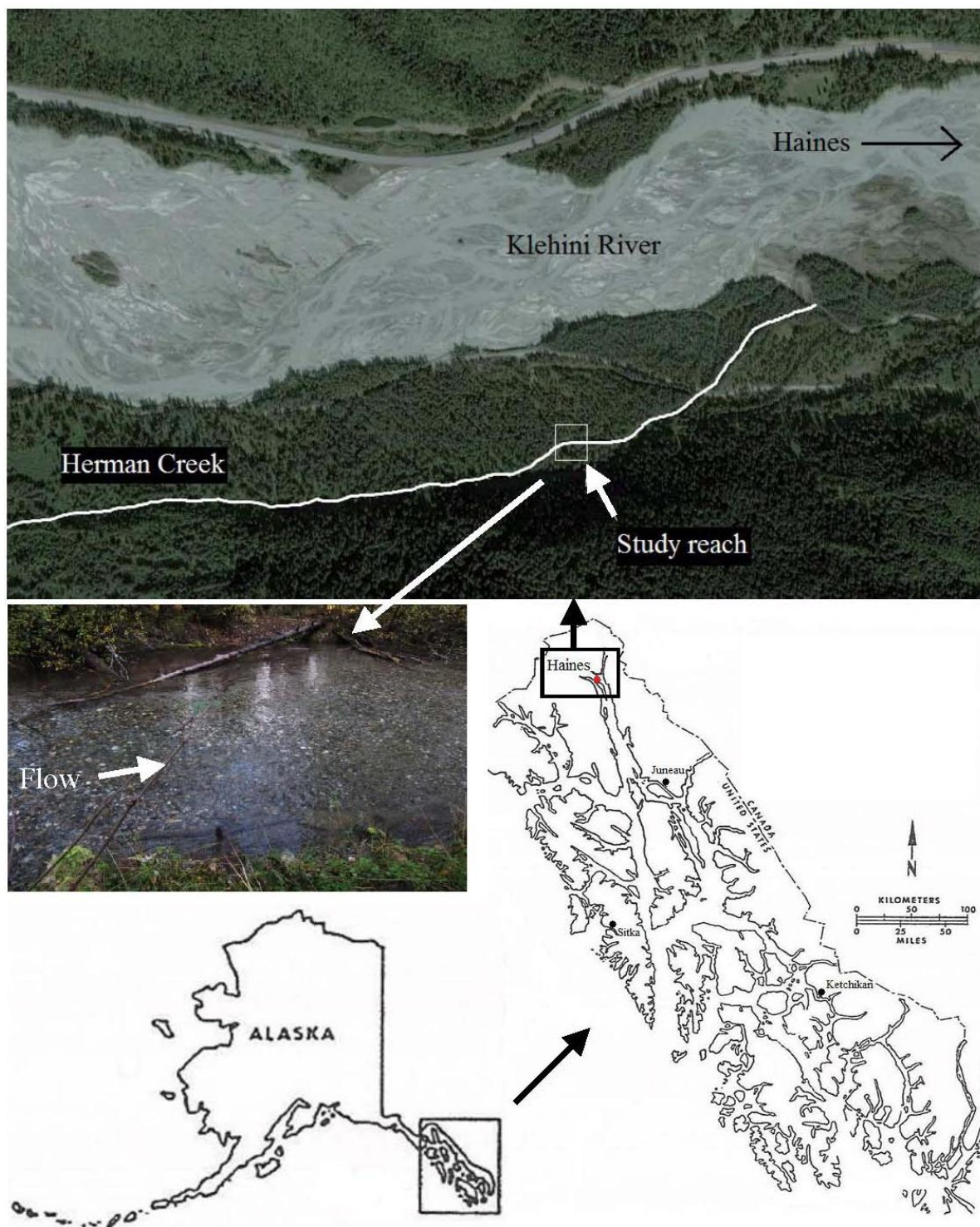


Figure 4.2. Site map for the study reach on Herman Creek near Haines, Alaska.

4.3.2 Field Site

Herman Creek is a pristine, first-order tributary of the Klehini River near Haines, Alaska (Figure 4.2). The study reach is located between 0.6 and 0.7 km upstream of the confluence with the Klehini River, where the surveyed gradient of the channel is 0.003. The study reach is 60 m long, exhibits a gravel bed, planar longitudinal profile, largely uniform channel width of around 25 m, low sinuosity (1.03), and stable, year-round flows (measured annual variation in flow stage is 0.05 m). Channel roughness is primarily from redd topography, although wood in the channel also adds roughness (Figure 4.2). Chum spawning dominates redd construction in the reach, with dispersed spawning by coho salmon and Dolly Varden trout (*Salvelinus malma*). We modeled rather than measured residence times and exchange of MDN in Herman Creek to avoid disturbing spawning beds.

4.3.3 Redds and Unspawned beds in VS2DTI

Surface water exchange with the streambed was modeled in VS2DTI as a function of channel slope decreasing elevation head with downstream distance and redd topography causing variation in water pressure head from the static water head on unspawned beds. We also include the affect of spawning increasing hydraulic conductivity and sediment porosity in redds (Section 2.4). Static water pressure head on unspawned beds was set to the average flow depth (0.25 m) measured where redds occupied approximately 50% of the bed surface. This same average depth was measured on redds, since they tended to be located in deeper portions of the channel, yet exhibited a tailpill surface that extended above unspawned portions of the bed. Near-bed pressure variations on unspawned beds, which depend on surface water hydraulics [Grass, 1971], were not simulated. Water pressure head on redds

was simulated as a dynamic pressure by modeling redds as 2D triangular bed forms using the model of *Elliot and Brooks* [1997]. This treatment simplifies the pressure distribution on redds in nature (Figure 4.1), but we considered this a reasonable approach since it captures the area of high water pressure on the stoss side and low water pressure on the lee side of redds [*Thibodeaux and Boyle*, 1987]. The half amplitude of the dynamic head variation on redds was calculated as

$$h_m = 0.28 \frac{u^2}{2g} \begin{cases} (0.34Y^*)^{-3/8}, & Y^{*-1} \leq 0.34 \\ (0.34Y^*)^{-3/2}, & Y^{*-1} > 0.34 \end{cases} \quad (4.1)$$

where u is the average surface flow velocity, g is gravitational acceleration (9.81 m s^{-2}), and Y^* is dimensionless water depth, defined as flow depth (d) divided by redd amplitude ($d \Delta_{redd}^{-1}$). Values of h_m were then sinusoidally distributed according to h , which estimates periodic drops in pressure due to bed form drag and turbulent energy dissipation [*Tonina*, 2012]

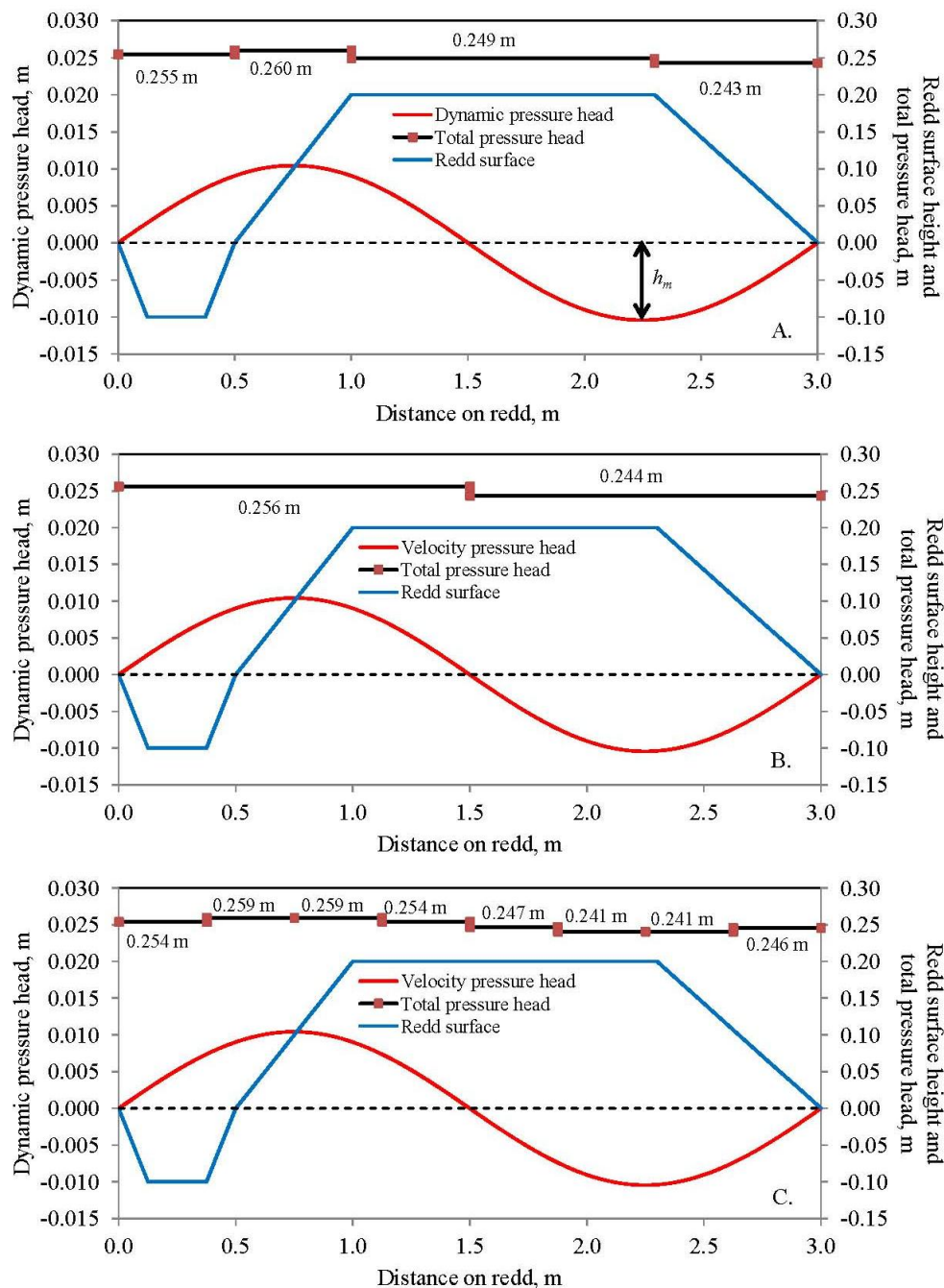
$$h = h_m \sin\left(\frac{2\pi}{\lambda_{redd}} x\right) \quad (4.2)$$

with λ_{redd} is the redd wavelength and x equals the streamwise distance on the redd. Redd wavelengths (λ_{redd}) were measured in Herman Creek from the upstream edge of the pot depression to the downstream end of the tailspill mound. Redd amplitudes (Δ_{redd}) were measured as the difference in elevation between the peak of the tailspill mound and the adjacent unspawned bed. We measured λ_{redd} and Δ_{redd} for five chum salmon redds in the study reach using a survey level and rod. Redd dimensions were taken as average values from each set of measurements (3.0 m and 0.20 m respectively).

Average surface flow velocity (0.45 m s^{-1}) in Equation (4.1) was calculated with *Manning's* [1891] equation using the hydraulic radius (0.25 m), surveyed channel slope (0.003), and *Manning's* [1891] n for the study reach in Herman Creek. *Manning's* [1891] n was estimated with the *Strickler* [1923] equation ($n = 0.015D_{50}^{1/6}$, where D_{50} (in mm) is the median grain size of the bed, equal to 27 mm) to account for grain roughness with an n -value of 0.026. We adjusted this value higher (0.047) to account for redds occupying approximately 50% of the bed surface when flow measurements were made. Adjustment of *Manning's* [1891] n was necessary since values can be up to four-times higher with dunes [*Simons and Senturk*, 1992] that approximate the shape of redds. Although prone to error [*Marcus et al.*, 1992], manual adjustment of *Manning's* [1891] n is common for accounting for sources of roughness that are difficult to quantify or for which roughness values are not available. Two sensitivity runs with n -values of 0.036, approximating roughness associated with one redd, and 0.068, simulating roughness generated by a fully spawned bed, were also examined. The D_{50} of the bed surface (27 mm) was estimated from a *Wolman* [1954] pebble count of 200 grains taken at a station near the middle of the study reach where redds and unspawned beds were equally represented. The intermediate axis of sampled particles was measured with calipers to the nearest millimeter. With a *Manning's* [1891] n of 0.047, surface discharge entering the study reach ($2.84 \text{ m}^3 \text{ s}^{-1}$) was calculated by multiplying average flow velocity, water depth, and channel width.

Values of h were spatially averaged in longitudinal segments on the redd and added to the static water head (0.25 m) to give the modeled distribution of water pressure head on redds. Resulting values of dynamic head were 0.255 m, 0.260 m, 0.249 m, and 0.243 m on the redd pot, upstream sloping tailspill, tailspill flat, and downstream sloping end of the

tailspill, respectively (Figure 4.3a). Spatial averaging reduced the resolution of the pressure head distribution, and was necessary for inputting values in the GUI. We hypothesize the mechanism for pumping surface flow into the bed depends primarily on high and low pressures on the stoss and lee of the redd [Savant *et al.*, 1987]. We test this hypothesis in sensitivity runs with half (2 head values; Figure 4.3b) and double (8; Figure 4.3c) the number of pressure head values on redds compared to the base simulation (4). In the sensitivity run with two head values, values of h were spatially averaged in two longitudinal segments on the redd, one for both the up- and downstream halves of the redd (Figure 4.3b). The sensitivity run with eight head values involved spatially averaging values of h for longitudinal segments depicted in Figure 4.3c. If our hypothesis is correct, hyporheic flux with two pressure heads should be close to the base simulation, and increasing the number of pressure head values to eight should decrease hyporheic flux because the gradient of pressure change between the stoss and lee areas will be more gradual.



Figures 4.3a-c. Depiction of a redd showing the distribution of total water pressure head for base simulations (A.) and in sensitivity runs with half (B.) and twice (C.) the number of total water pressure head values as in the base simulation. Water pressure head was determined by adding the average water depth (0.25 m) to the dynamic pressure head. Dynamic pressure was estimated as h_m (Figure 4.3a) with Equation (4.1) and sinusoidally distributed with Equation (4.2). In the base simulation dynamic pressures were spatially averaged over topographic elements of the redd, including the pot (0.255 m), upstream tailspill slope (0.260 m), tailspill flat (0.249 m), and downstream tailspill slope (0.243 m).

4.3.4 Hyporheic Flow Simulations

The model domain in VS2DTI was 1 m wide and 60 m long and defined by total pressure head at the vertical and top boundaries of the domain and a no-flow boundary simulating an impermeable layer at the base of the domain (Figure 4.4). Elevation head was equal to the depth of alluvium that was set as 3 m at the upstream boundary, and which decreased with the slope of the channel to 2.82 m at the downstream end. Because the actual depth of alluvium underlying Herman Creek was unknown, we used sensitivity runs with 1 m and 2 m depths of alluvium to explore their effect on estimates of hyporheic flux and residency of MDN. The model domain was discretized into a 400 x 200 (horizontal x vertical) grid of cells, each measuring 15 cm long in the streamwise direction by 2 cm tall. Base simulations involved an unspawned bed and beds occupied by variable proportions of redds, including 0.05, 0.15, 0.35, 0.55, 0.75, and mass spawning (1.0), for a total of seven simulations. In simulations with spawning, redds were evenly distributed on the top surface of the domain (Figure 4.4). Simulations were run by allowing solute with the same properties as water to only enter the surface flow-sediment boundary. This effectively isolated surface water exchange with the bed from flow entering through the upstream and downstream ends of the domain.

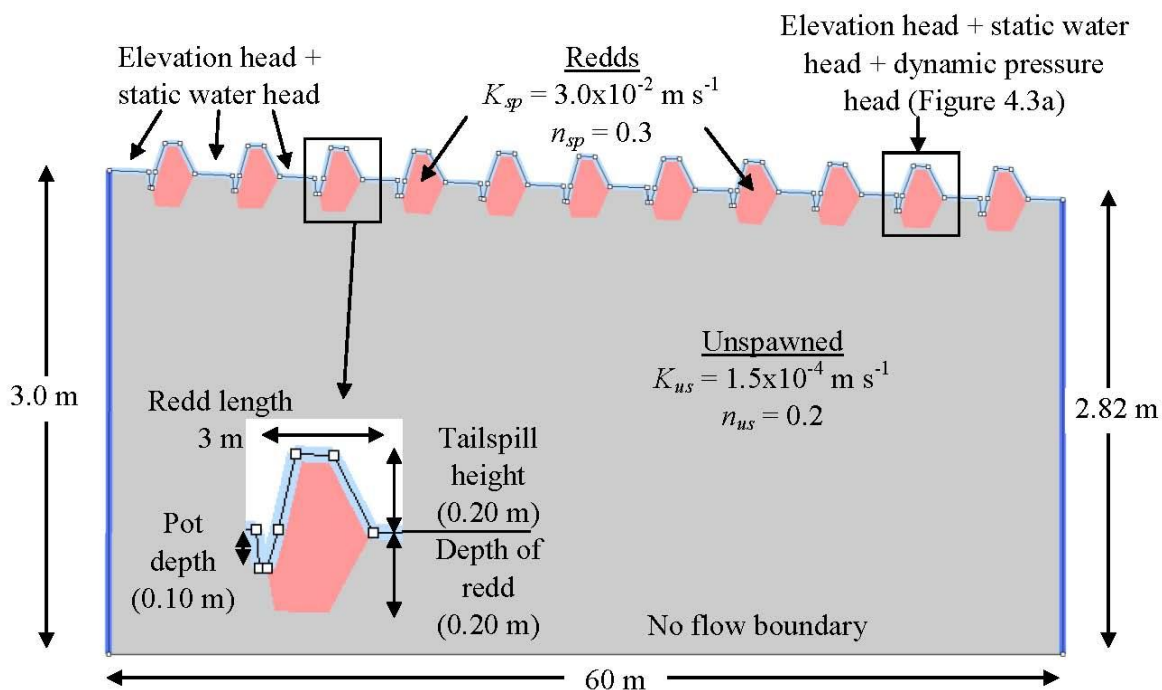


Figure 4.4. Dimensions of the model domain and several parameters included in the simulations. Red areas in the domain represent salmon redds that extend 0.20 m into and above the unspawned area of the domain (grey colored) and exhibit higher hydraulic conductivity (K_{sp}) and porosity (n_{sp}) than unspawned beds (K_{us} and n_{us} , respectively). The lower boundary of the domain represents an impermeable layer. Total pressure head acts on the inlet and outlet boundaries (elevation head+static water head) and on the top boundary as depicted for redds (see Figure 4.3a) and unspawned portions of the bed. Nodes on the pressure inlet boundary are points between which water pressure head is designated in the model.

Spawned and unspawned portions of the domain were delineated by differences in total pressure head at the sediment-water interface (Section 2.3) and by variations in hydraulic conductivity and porosity (Table 4.1, Figure 4.4). In the absence of specific data, parameters are values measured by others or estimates based on material type. Hydraulic conductivity in redds (K_{redd}) was $3.0 \times 10^{-2} \text{ m s}^{-1}$ based on measurements by *Chapman et al.* [1986] and *Zimmermann and Lapointe* [2005] involving Chinook salmon (*O. tsawytschta*) redds and artificial redds on spawning grounds used by Atlantic salmon (*Salmo salar*), respectively. The depth that hydraulic conductivity was altered by spawning (0.20 m) was

set to a value close to egg pit depths measured in chum salmon redds by *Montgomery et al.* [1996]. Hydraulic conductivity in unspawned beds (K_{us}) was set to $1.5 \times 10^{-4} \text{ m s}^{-1}$, which is similar to values measured by *Malcolm et al.* [2004] and *Geist* [2005] in gravel beds prior to disturbance from spawning salmon. Porosity was estimated as 0.3 and 0.2 for spawned (n_{sp}) and unspawned (n_{us}) portions of the bed. Porosity and hydraulic conductivity were higher for redds because spawning flushes fines from gravel and increases grain sorting [*Montgomery et al.*, 1996], which increases intergravel flow speeds and pore space in mixed-grain beds [*Rogers and Head*, 1961]. Dispersivity settings that govern the course of intergravel flow between the longitudinal (streamwise) and vertical (into the bed) directions was set at 0.2 m for redds and unspawned beds. The specific storage parameter was set equal to 0.001 throughout the domain [*Hassan et al.*, 2014]. Simulations lasted 1 d to achieve a steady-state condition (solute into domain = solute out of domain) for estimating hyporheic flux and residence times in the bed. Steady state conditions were established in 3 min or less in all simulations.

Table 4.1. Parameters in base simulations of hyporheic flow.

Parameter	Value	
	Spawned	Unspawned
Specific storage		0.001
Porosity, n	0.3	0.2
Hydraulic conductivity, K	$3.0 \times 10^{-2} \text{ m s}^{-1}$	$1.5 \times 10^{-4} \text{ m s}^{-1}$
Longitudinal and transverse dispersion, m		0.2
Depth of alluvium, m		3 m

4.3.5 Hyporheic Flux and Residence Time of MDN

The duration that MDN is stored in the hyporheic zone was given by dividing the volume of hyporheic pore space by the flux of surface water exchanged with the hyporheic area in the bed. Hyporheic flux was given by the numerical output from the model. To determine hyporheic volumes, we digitized contour plots of solute for each model simulation and measured the hyporheic area associated with redds and unspawned beds with autoCAD software. Hyporheic areas were delineated by the contour indicating a $\geq 10\%$ concentration of solute [Triska *et al.*, 1989; Figure 4.5]. Boundary effects in simulations with 0.75 and 1.0 spawning were excluded by measuring the average area of redds outside the influence of the vertical boundaries of the domain and multiplying by the number of redds. Multiplying hyporheic area by the width of the model domain (1 m) gave hyporheic volume. Hyporheic pore space was then given by multiplying hyporheic volume for redds and unspawned areas of the bed by the porosity associated with each respective volume.

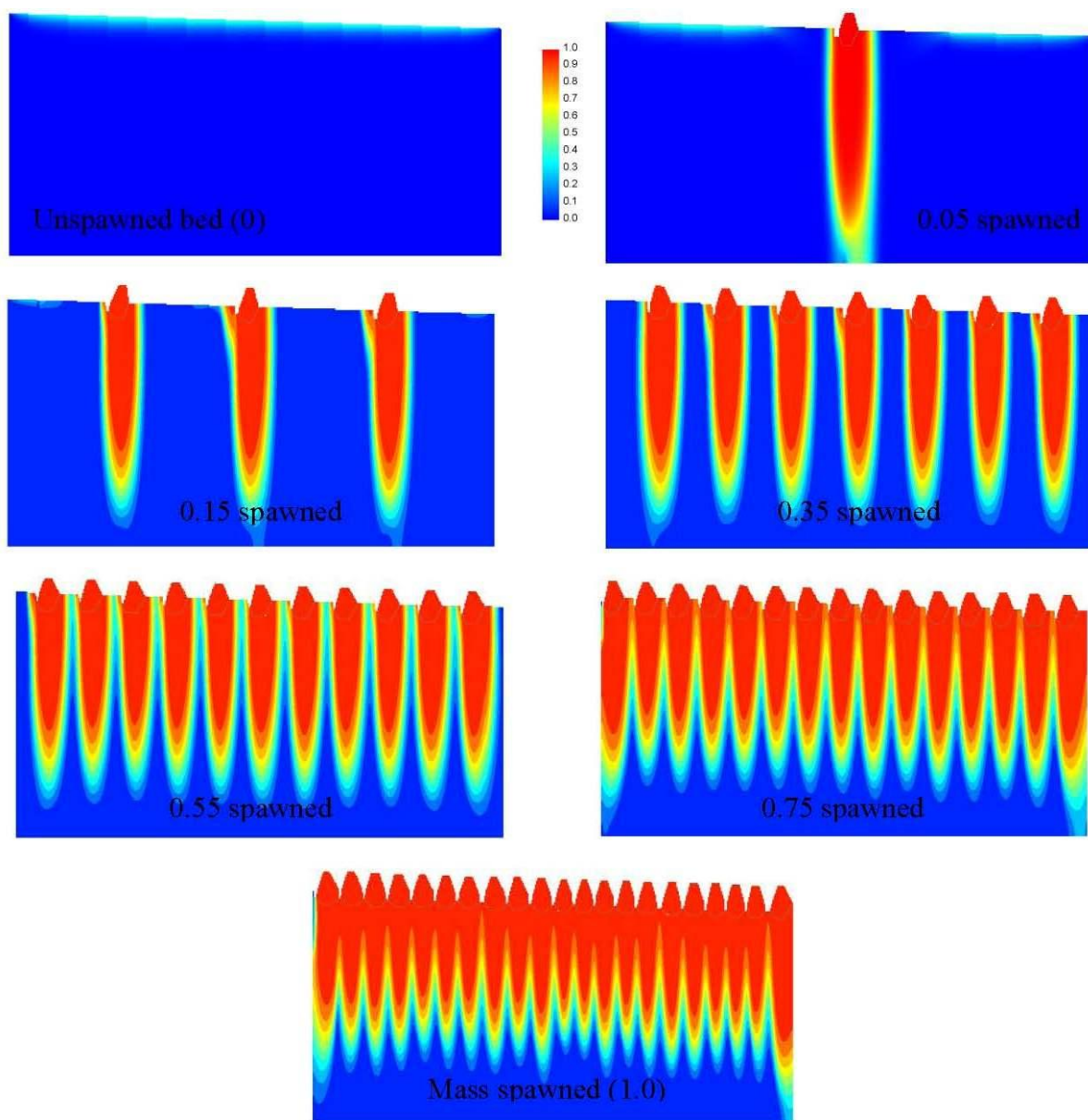


Figure 4.5. Contour plots of solute concentration (indicated in figure key, where 1.0 is 100% concentration) entering the top surface of the domain and exiting the downstream boundary in simulations with an unspawned bed and beds with variable proportions of the surface occupied by redds. Depth of alluvium is 3 m at the upstream (left) end of the domains and 2.82 m at the downstream (right) end of domains. The length of the domains is 60 m, and the width is 1 m.

4.4 Results

4.4.1 Base Simulation

Model results indicate the residence time of MDN in the hyporheic zone decreases sharply with the presence of redds, from 5.79 h on the unspawned bed to 0.11 h with one redd (0.05 spawning), and finally to 0.03 h for the mass spawned bed (1.0 spawning, Table 4.2). In beds with spawning, residence times decreased as a linear function of the proportion of the bed surface occupied by redds (Figure 4.6). Short residence times in the presence of redds resulted from hyporheic volume increasing less than an order of magnitude with spawning while hyporheic flux increased over four orders of magnitude with an increasing proportion of the bed surface occupied by redds (Figure 4.7, Table 4.2). Hyporheic flux and volume increased with spawning due to high hydraulic conductivity (Table 4.1) and divergent water pressure on redds (Figure 4.3) pumping water in the bed at high rates (Figures 4.7) relative to the planar unspawned bed (Table 4.2). Despite static water pressure head on the unspawned bed (no hyporheic pumping from redds), a small amount of hyporheic exchange ($3.6 \times 10^{-5} \text{ m}^3 \text{ s}^{-1}$) probably resulted from the low porosity and hydraulic conductivity of the bed (Figure 4.5, Table 4.1).

Table 4.2. Model results from the base simulations.

Base simulation	Value						
Proportion spawned	0	0.05	0.15	0.35	0.55	0.75	1
Hyporheic pore volume, m^3	0.8	3.5	9.4	19.8	27.3	28.0	29.8
Hyporheic flux, $\text{m}^3 \text{ s}^{-1}$	3.6×10^{-5}	9.1×10^{-3}	2.7×10^{-2}	5.9×10^{-2}	8.3×10^{-2}	1.2×10^{-1}	2.5×10^{-1}
Hyporheic residence time, hrs	5.79	0.11	0.10	0.09	0.09	0.07	0.03

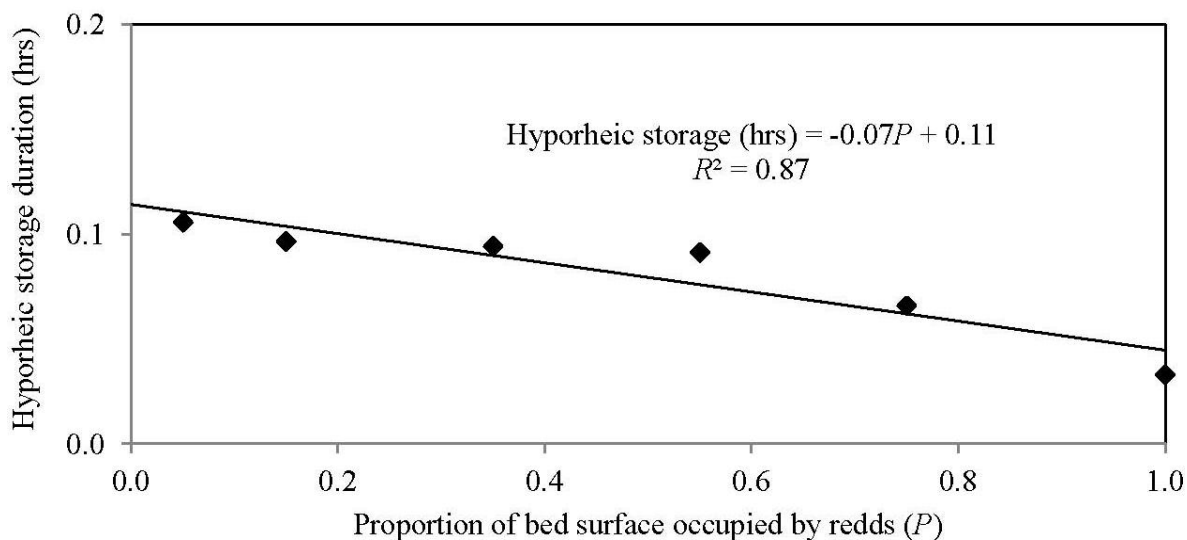


Figure 4.6. Storage duration (hrs) of MDN versus the proportion of the bed surface occupied by redds (P). The curve is a linear regression of the data, indicating an inverse relationship between storage duration and the proportion of the bed surface occupied by redds.

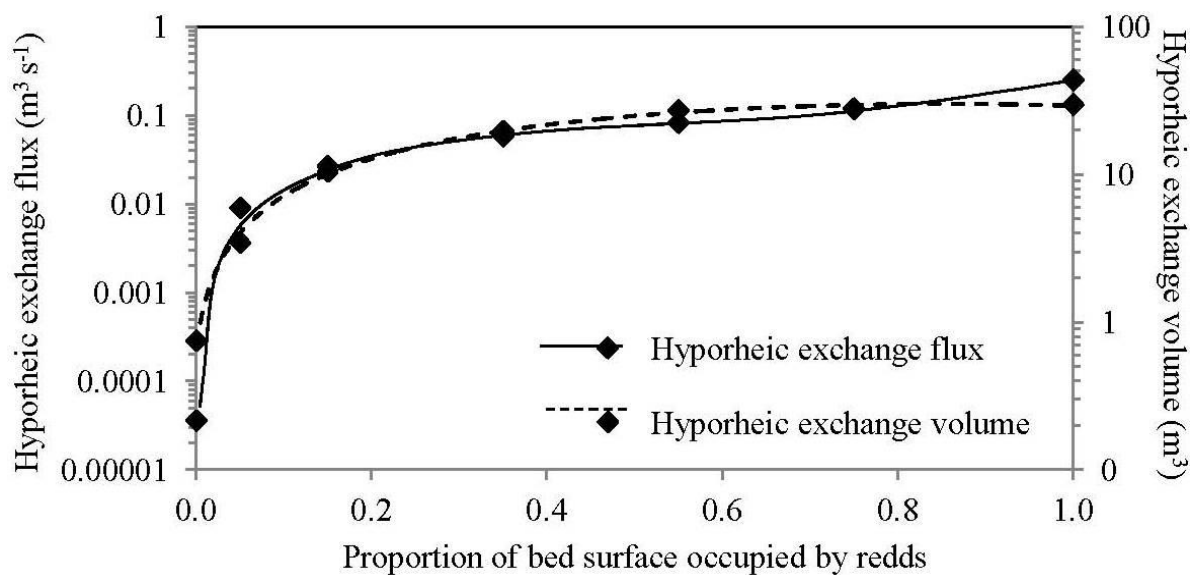


Figure 4.7. Hyporheic flux and volume plotted against the proportion of the bed surface occupied by redds (P). The curves are polynomials that demonstrate the rapid increase in exchange flux and volume from that for an unspawned bed ($P=0$) with the presence of a single redd ($P=0.05$). Thereafter, exchange flux and volume increase linearly with spawning density (P).

Our finding that a single redd significantly increases hyporheic flux in planar channels agrees with *Tonina and Buffington's* [2009] three-dimensional (3D) model results involving a single redd in a simulated pool-riffle channel. However, a conspicuous result in the simulations was depths of exchange generally decreased with increasing spawning density (Figure 4.5). This resulted from increasing proportions of near-surface areas of the bed exhibiting high hyporheic flow speeds with spawning (Figure 4.8), which reduced the depth of solute penetration in the domain (Figure 4.9). Increasingly shallow, yet more intense hyporheic flux with spawning was due to variability in dynamic pressure head and a larger area of the bed surface exhibiting high hydraulic conductivity and porosity [*Tonina and Buffington, 2009*]. In some cases, redds separated by portions of unspawned bed were hydraulically linked via hyporheic flow paths. Such linkages were especially apparent at spawning densities of 0.75 and 1.0 (Figures 4.5, 4.8, 4.9). This suggests where spawning occurs in high densities, interconnecting flow between redds may improve intergravel habitat throughout the reach. As a result, stream reaches with initially low hyporheic flow for supporting egg incubation, may be rendered entirely suitable for spawning when redds occupy three quarters or more of the bed surface.

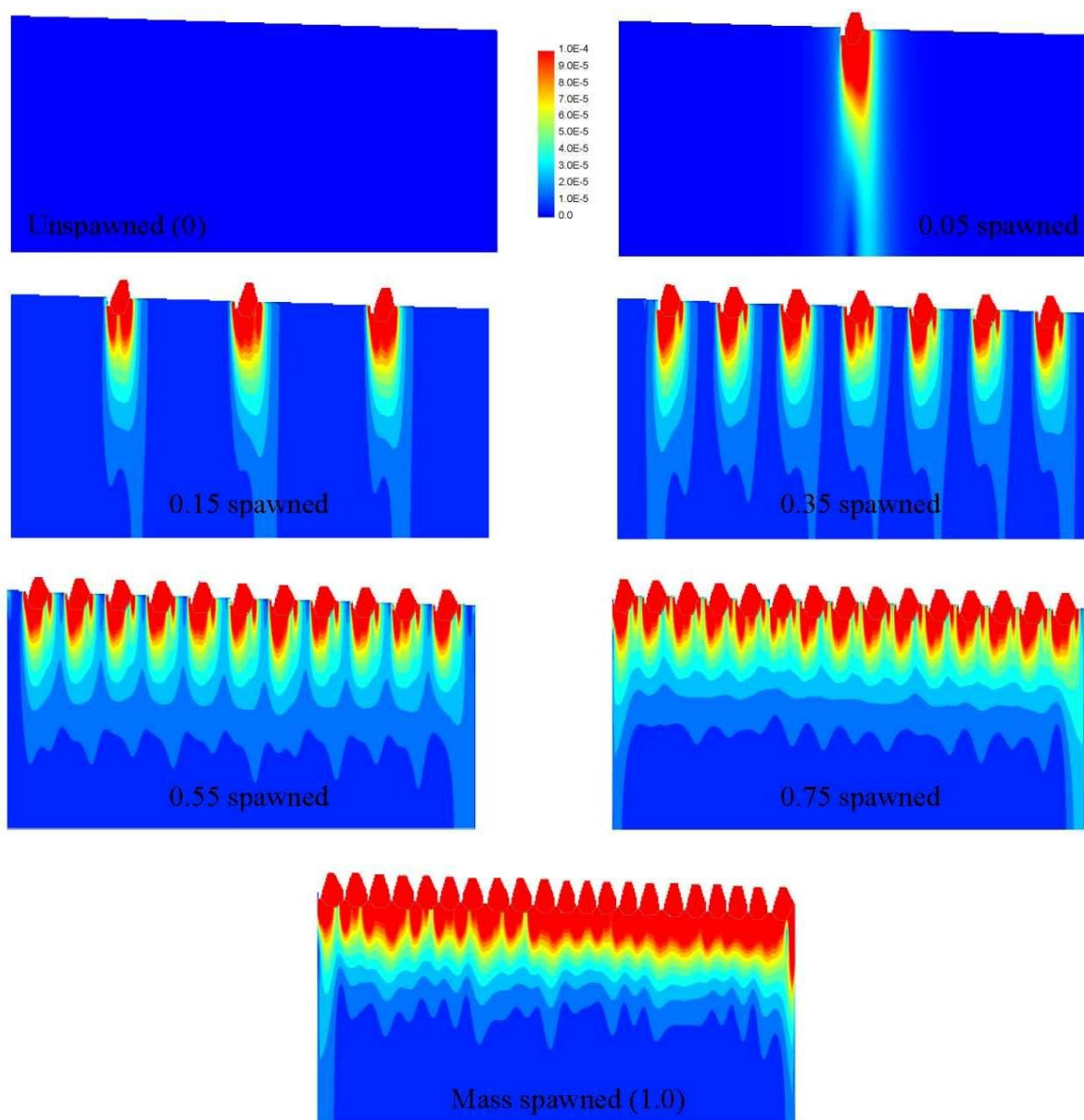


Figure 4.8. Contour plots of hyporheic flow speeds (indicated in m s^{-1} in figure key) in simulations with an unspawned bed and beds with variable proportions of the surface occupied by redds.

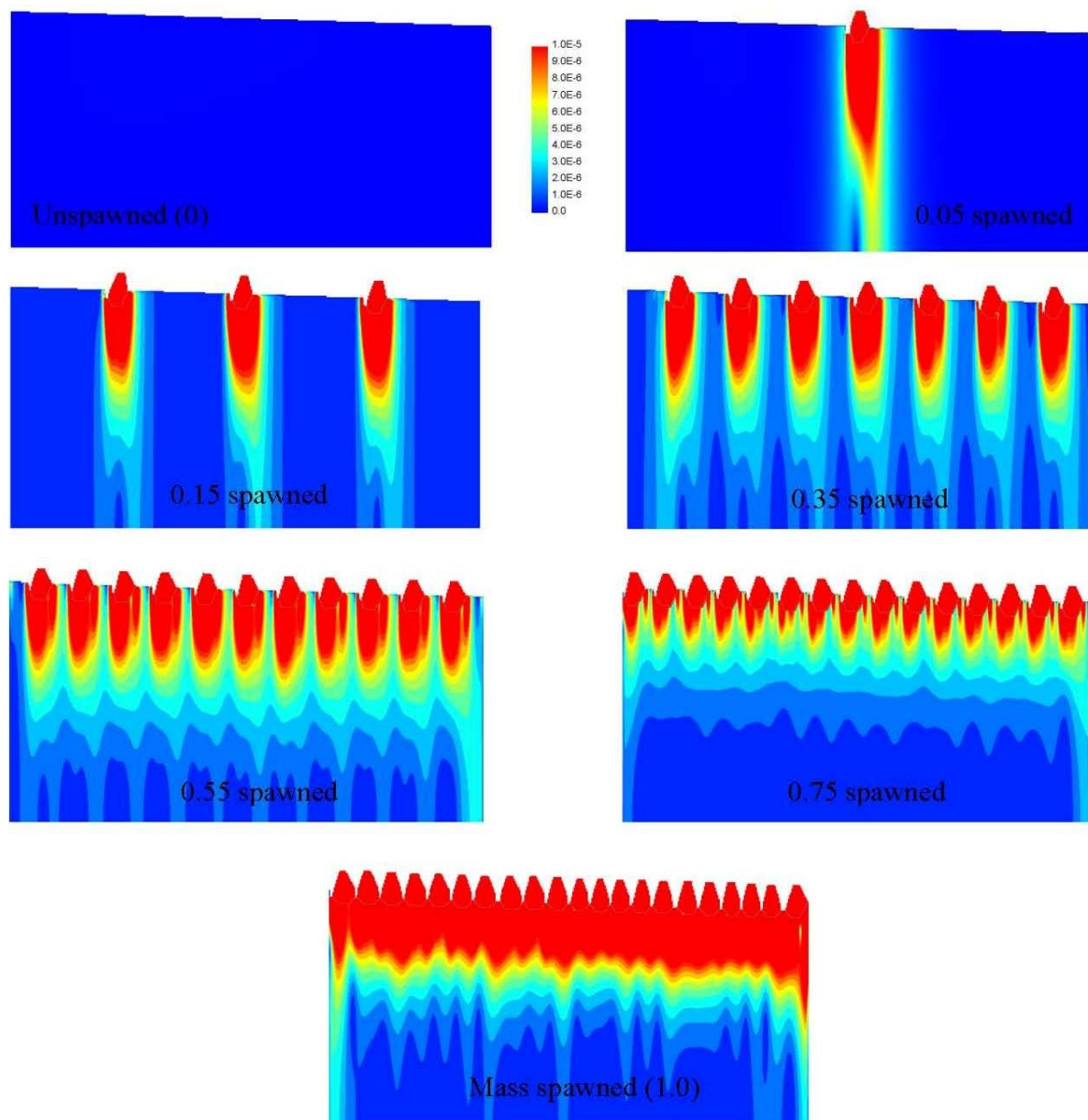
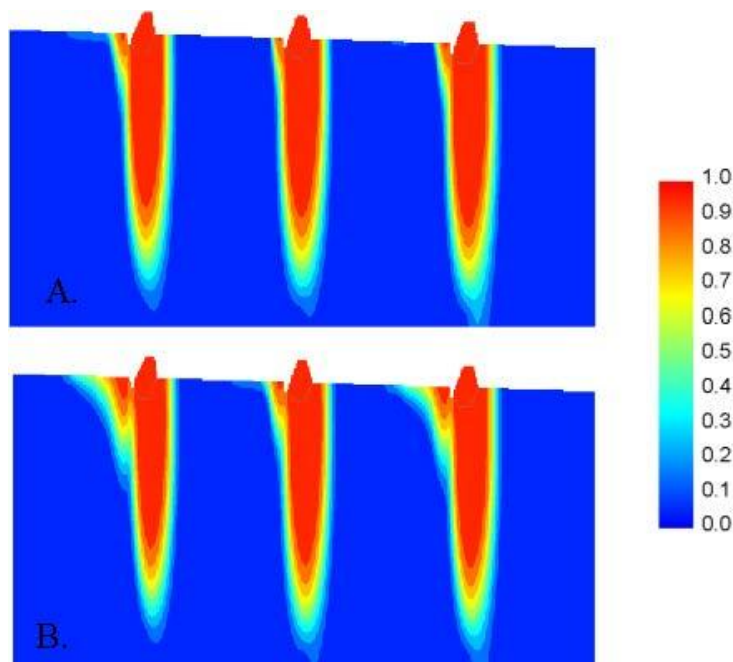


Figure 4.9. Contour plots of hyporheic flux (indicated in $\text{m}^3 \text{s}^{-1}$ in figure key) in simulations with an unspawned bed and beds with variable proportions of the surface occupied by reds.

4.4.2 Sensitivity Runs

Sensitivity runs were used to investigate the influence of several model parameters on estimates of hyporheic flux and residence times of MDN. Sensitivity runs with low (0.036) and high (0.068) values of *Manning's* [1891] n involved beds with 0.05 (one redd) and 1.0 (21 redds) proportions of the bed surface occupied by redds. The bed with 0.15 spawning was used in sensitivity estimates that considered variable alluvial depths (1 and 2 m versus 3 m) and the number of head values on redds (2 and 8 head values versus 4 values of head in the base simulation; Figure 4.3).

Sensitivity results show that doubling the number of head values on redds decreased hyporheic flux 25% from $2.7 \times 10^{-2} \text{ m}^3 \text{ s}^{-1}$ in the base simulation to $2.2 \times 10^{-2} \text{ m}^3 \text{ s}^{-1}$, while flux was lowered only 3% by halving the number of head values ($2.6 \times 10^{-2} \text{ m}^3 \text{ s}^{-1}$). These findings largely support our expectation that hyporheic pumping is primarily driven by the total difference in pressure between the stoss and lee of the redd. However, modifying the pressure distribution also changed the hyporheic volume associated with redds (Figures 4.10a,b). The use of 2 head values limited the area of surface water exchange to the near- vicinity of redds, which lowered the hyporheic volume to 40.8 m^3 (Figure 4.10a) Conversely, with 8 head values, larger areas of surface water exchange occurred near the bed surface in the vicinity of redds, which increased hyporheic volume to 44.0 m^3 from 43.4 m^3 in the base simulation (Figure 4.10b). Changes in hyporheic volume decreased the residence time of MDN 3% to 0.093 hrs with 2 head values from the base simulation (0.096 hrs) while residence time increased 35% to 0.131 hrs with 8 head values. Our decision to use four head values on redds in the base simulations therefore gives conservative estimates of MDN residence times in beds with redds.



Figures 4.10. Contour plots of solute concentration (indicated in figure key, where 1.0 is 100% concentration) in sensitivity runs with two (A.) and eight total head values on redds (B.).

Variable depths of alluvium did not affect spatial patterns of hyporheic flux, which are a function of the distribution of pressure on the streambed (*Tóth, 1963; Tonina and Buffington, 2009*), as modified by redds. As a result, hyporheic flux decreased less than a percent when alluvial depth was reduced from 3 m in the base simulation to 1 m and 2 m in sensitivity runs. However, lower alluvial depth reduced hyporheic flow path lengths and hyporheic volumes, leading to 27% and 55% shorter residence times in the 2 m (0.08 hr) and 1 m (0.05 hr) domains compared to the base simulation (0.11 hr). Base simulations therefore predict substantially longer residency of MDN than would result if shallower alluvium had been assumed in base simulations. Though we did not evaluate the effect of increasing depths of alluvium, our expectation is this would not significantly influence estimates of

hyporheic volume or residence times since only low-intensity exchange extended to a depth of 3 m in simulations with 0.05 and 0.15 spawning.

In sensitivity runs with variable *Manning's* [1891] n , stream discharge and channel width were held constant and water depth was varied to estimate flow speeds in the presence of a single redd ($n=0.036$) versus a mass spawned bed ($n=0.068$). With *Manning's* [1891] $n=0.036$, reach average flow depth was lower (0.21 m) and flow velocity was higher (0.53 m s^{-1}) compared to the base simulation with $n=0.047$ (flow depth=0.25 m; flow velocity= 0.45 m s^{-1}). These changes in flow decreased dynamic water pressure to 0.219 m on the pot, 0.228 m on upstream sloping tailspill, 0.208 m on the tailspill flat, and 0.197 m on the downstream portion of the tailspill. Such changes (relative to the base simulation in Figure 4.3) had little effect on hyporheic flux, hyporheic volume, and residence times, which were 4% lower and 2% and 6% higher compared to the base simulation, respectively.

A similar result was modeled when *Manning's* [1891] n was increased to 0.068 to account for channel roughness from mass spawning (1.0 spawning). In this case, flow depth increased to 0.31 m and flow velocity lowered to 0.36 m s^{-1} . These changes reduced the difference in pressure between the stoss and lee on the redds by largely normalizing dynamic pressure heads to 0.312 m on the pot, 0.315 m on the upstream sloping tailspill, 0.310 on the tailspill flat, and 0.307 on the downstream portion of the tailspill. Slightly lower hyporheic pumping by redds decreased exchange by 10% and reduced the hyporheic volume by 6% over that in the base simulation. Because the reduction in exchange was greater than the reduction in hyporheic volume, residence time increased by 4%. In both sensitivity runs with *Manning's* [1891] n , accounting for roughness in the channel had offsetting effects on hyporheic flux and volume that left hyporheic residence times largely

unchanged. This coupled with exchange flux exhibiting a 10% or less difference in sensitivity runs compared to the base simulations indicate model results are insensitive to flow depths and speeds estimated with variable *Manning's* [1891] *n*-values in Herman Creek.

4.5 Discussion and Conclusions

Our analysis demonstrates residence times of MDN are low in the presence of spawning and decrease as higher proportions of a planar bed surface is occupied by redds. These findings resulted from redds increasing rates of hyporheic flux much more than hyporheic volume, which reduced the residence time of MDN in the bed. Our results further indicate that a single redd increases hyporheic flux more than an order of magnitude above that for a planar unspawned bed, and hyporheic flux was nearly four orders of magnitude higher for a mass spawned bed than a bed without redds. These findings affirm *Tonina and Buffington's* [2009] 3D modeling results that a single redd can significantly increase hyporheic flux. Findings also support *Tonina and Buffington's* [2009] hypothesis that multiple redds strongly influence reach-average hyporheic flux, at least in the context of our simulations.

Our finding that spawning reduces the residence time of MDN in planar channels also likely conservatively applies to channels with pool-riffle morphologies that are preferred by salmon [*Montgomery et al.*, 1999]. Compared to planar channels, hyporheic forcing by pool-riffle topography pumps nutrients deeper into the bed where they reside longer due to extensive travel lengths [*Tonina and Buffington*, 2009]. Travel lengths are longer in pool-riffle channels because hyporheic flow reaches depths that are about 0.7 times

the wavelength of the macro-topography of the bed [*Cardenas and Wilson, 2007; Worman et al., 2002; Tonina, 2012*]. Since redd wavelengths are shorter than wavelengths associated with pool-riffle topography, hyporheic flux associated with redds extends to relatively shallow depths. Therefore elevated hyporheic flux from redds would not be accompanied by an increase in hyporheic volume, which would result in greater reductions in residence times of MDN with spawning density than we modeled for the planar bed in Herman Creek.

By increasing the amount of river water pumped into the bed, redds promote salmon reproduction by oxygenating eggs and removing metabolic wastes, but at the expense of short residence times of MDN in the bed. However, several studies have concluded that hyporheic flux, not residence times, limits nutrient uptake due to high biologic activity in streambeds. For instance, *Bardini et al. [2012]* used a numerical model to simulate hyporheic exchange with dunes and found that hyporheic flux prevails over low residence times since biochemical reactions increase with water velocity in the bed. A similar result was measured by *O'Keefe and Edwards [2002]* and *Pinay et al. [2009]* in sockeye spawning streams in Alaska where MDN were rapidly removed from solution upon entering the metabolically active hyporheic zone [*Duff and Triska, 2000; Larned et al., 2004*]. Hyporheic flux that enhances delivery of nutrients also increases deposition of fines and nutrient flocs in streambeds [*Rex and Petticrew, 2008*], both of which promote biotic growth that can further clog pore spaces [*Orr et al., 2009; Nogaro et al., 2010*]. The resulting decrease in hyporheic flux allows more time for processing of nutrients, such that a positive association is often reported between residence times and nutrient uptake [*Valett et al., 1996; Thomas et al., 2003; Ensign and Doyle, 2005; Ryan et al., 2007*]. However, high efficiency processing nutrients under conditions of limited nutrient supply may come at the expense of the total

amount of nutrients that are processed since most studies do not account for supply limitations on nutrient sequestering. Therefore, on balance, the relative importance of hyporheic flux and residence times controlling biotic uptake and stream productivity largely remains an open question.

Spawning-generated modifications to hyporheic flux extended between redds in high densities to improve water circulation in adjoining nests and throughout the model reach, suggesting a reproductive advantage from mass spawning. Evolution may have led chum and pink salmon (*O. gorbuscha*) to exploit this linkage since their fry migrate to sea upon exiting the nest. Under conditions where biotic uptake of nutrients is limited by the duration of nutrient storage, short-residency of MDN associated with mass spawning is unlikely to impact the reproductive success of chum and pink salmon because fry are not reliant on MDN increasing the prey-food base in streams for salmonid rearing [Wipfli, 1997]. Instead, egg-to-fry survival may benefit from high-density spawning increasing intergravel flow, possibly resulting in larger future returns of salmon due to greater spawning success and higher numbers of fry migrating to sea. However, such reproductive advantage may be countered where superimposition of redds results in eggs being dug from nests by successive waves of spawners [McNeil, 1964; Fukushima *et al.*, 1997]. Redd superimposition can also modify redd topography and mobilize fines that can deposit on or infiltrate into downstream redds [Macdonald *et al.*, 2010]. These outcomes would decrease intergravel flow, as Tonina and Buffington [2009] demonstrated, and possibly affect embryo development by reducing dissolved oxygen in egg pockets [Greig *et al.*, 2007].

Elevated hyporheic flux from spawning activity may also have negative impacts on salmon reproduction by decreasing residence times of MDN, which can lower primary

productivity [Mathison *et al.*, 1988] and the food base for salmon rearing [Gende *et al.*, 2002]. Perhaps in avoidance of such a case, coho and Chinook salmon typically spawn in low densities, conceivably as an adaptation that helps ensure progeny have sufficient food resources for the one to three years they rear in streams before migrating to estuaries as fry [Koski, 2009] or to sea as smolt. Other researchers have explained variations in spawning density with physical factors, such as habitat availability [Isaak and Thurow, 2006] or the timing and depth of channel bed mobility [Montgomery *et al.*, 1999], or with biological influences, including territoriality [Mathison, 1962] and fish size [Quinn and Foote, 1994]. Another possible explanation is spawning density effects on residence times of MDN, since species whose fry rear in the ocean favor mass spawning that reduces residence times, while species with fry that rear in streams favor dispersed spawning that has less impact on the residence time of MDN in streambeds.

Our model results are based on redds that persist in their initial condition after spawning, which is unlikely in many streams [Lisle, 1989; Rennie, 1998; Butler, 1999; Bigelow, 2003]. Modifications to redds that reduce their ability to induce hyporheic flux include colonization by aquatic algae and macrophytes [Merz *et al.*, 2008], infiltration of fine sediment mobilized by flow and upstream spawners [Zimmermann and Lapointe, 2005], and tailspill erosion by stream flow [Montgomery *et al.*, 1996] and fish migration [DeVries, 2012], to name a few. Though common, post-spawning reduction in hyporheic flux from erosion of tailspill structures is not assured, as researchers have also noted redd topography [DeVries, 1997] and spawning-related coarsening of sediment [Gottesfeld *et al.*, 2004] persisting long after spawning is complete. Buffington *et al.* [2013] hypothesized that redd persistence is a function of basin lithology, bedload supply, stream hydrology, and

characteristics of the spawning fish, including population size, redd dimensions, and the timing of spawning relative to high flows. We add that redd persistence is also influenced by spawning mobilizing fine sediments, which can stabilize redds by increasing packing resistance on grains [Buxton *et al.*, submitted]. However, this manner of stabilizing redds reduces hydraulic conductivity and porosity in redds and hyporheic pumping, as a result. We encourage future studies to consider site-specific conditions such as these when evaluating spawning effects on hyporheic flux and residence times of MDN in streambeds.

Our findings can be refined by more robustly including the influence of physical features in streams on water pressure acting on the bed and by considering residence times of MDN in surface flow. In addition to redds, irregularities in channel banks and bed surfaces, and the presence of channel steps, wood, vegetation, boulders and other roughness elements can decrease flow velocity and form slackwater areas, which increase residence times of MDN in surface flow. As an example, *Ensign and Doyle* [2005] found that experimental removal of vegetation and wood from an agricultural channel and blackwater stream reduced transient storage areas by 61% and 41% and nutrient uptake in surface flow by 88% and 38%, respectively. Channel roughness may also increase hyporheic flux and volume by creating variation in dynamic pressure head on streambeds [Roberts *et al.*, 2007]. In these ways, physical features are important for coupling hydrologic, biotic, and abiotic processes [Orr *et al.*, 2009] that promote the capability of streams to process and store nutrients [Ensign and Doyle, 2005].

Overall, our findings offer insight into areas for further exploration and provide first-order estimates of spawning effects on hyporheic flux and residence times of MDN in streambeds. Low estimates of MDN residency in hyporheic areas in the presence of

spawning suggest that other pathways are likely more important for retaining MDN in stream ecosystems. One such pathway involves microbial processes that fix MDN to fine sediments that are stored as flocculents until release by bacterial processing [*Rex and Petticrew, 2008; Petticrew et al., 2011*] or mobilization of stream bed sediments by spawning or floods [*Gottesfeld et al., 2004; Hassan et al., 2008*]. Nutrients are also stored in floodplain soils when salmon carcasses are transported from streams by birds and mammals [*Quinn et al., 2009; Field and Reynolds, 2011*] or overbank floods [*O'Keefe and Edwards, 2002*]. Carcasses delivered to riparian areas provide MDN for uptake by trees and other vegetation, which then grow quicker and provide larger structural complexity in stream channels [*Bilby and Bisson, 1998; Helfield and Naiman, 2001; Drake and Naiman 2007*]. Channel complexity resulting, in part, from MDN accelerating plant growth can increase the quantity and quality of rearing habitat for juvenile salmon [*McMahon and Hartman, 1989; Whiteway et al., 2010*]. This can increase salmon reproductive success and lead to larger future returns of salmon spawners and higher amounts of MDN being delivered to streams.

4.6 References

- Bardini, L., F. Boano, M. B. Cardenas, R. Revelli, and L. Ridolfi (2012), Nutrient cycling in bedform induced hyporheic zones, *Geochimica et Cosmochimica Acta*, 84, 47-61
- Bigelow, P. E. (2003), Scour, fill, and salmon spawning in a northern California coastal stream, M.S. thesis, Humboldt State Univ., Arcata, CA.
- Bilby, R. E., B. R. Fransen, and P. A. Bisson (1996), Incorporation of nitrogen and carbon from spawning coho salmon into the trophic system of small streams: evidence from stable isotopes, *Can. J. Fish. Aquat. Sci.*, 53, 164-173.
- Bilby, R. E. and P. A. Bisson (1998), Function and distribution of large woody debris, in *River ecology and management*, edited by R. J. Naiman and R. E. Bilby, pp 324-346, Springer-Verlag, New York.
- Buffington, J. M., T. H. Buxton, A. K. Fremier, M. A. Hassan, and E. Yager (2013), Persistence of salmonid redds: A conceptual analysis, poster presentation at Am. Geophys. Union Fall meeting, San Francisco, CA. American Geophysical Union, Fall Meeting 2013, abstract #EP43A-0827.
- Burner, C. J. (1951), Characteristics of spawning nests of Columbia River salmon, *U.S. Fish and Wldf. Serv. Bull.* 61.
- Butler, J. (1999), Redd Washout Project Report, Winter 1998-99, Western Ross Fisheries Trust, 6pp.
- Buxton, T. H., E. M. Yager, J. M. Buffington, M. A. Hassan, and A. K. Fremier (submitted), Grain packing resistance to particle mobility, *J. Geophys. Res.*

- Cardenas, M. B., and J. L. Wilson (2007), Hydrodynamics of coupled flow above and below a sediment–water interface with triangular bedforms, *Adv. Water Resour.*, *30*, 301-313.
- Cederholm, C. J., M. D. Kunze, T. Murota, and A. Sibatani (1999), Pacific salmon carcasses: essential contributions of nutrients and energy for aquatic and terrestrial ecosystems, *Fisheries*, *24*, 6-15.
- Chapman, D. W., D. E. Weitkamp, T. L. Welsh, M. B. Dell, and T. H. Schadt (1986), Effects of river flow on the distribution of chinook salmon redds, *Trans. Am. Fish. Soc.*, *115*, 537-547.
- Constantz J., M. H., and G. W. Su (2003), Comparison of heat and bromide as ground water tracers near streams, *Ground Water*, *41*, 647-656.
- Cooper, A. C. (1965), The effect of transported stream sediments on the survival of sockeye and pink salmon eggs and alevin, Intl. Pac. Salmon Fish. Comm. Bull. 18, New Westminster, B.C., Canada.
- Cox, M. H., G. W. Su, and J. Constantz (2007), Heat, chloride, and specific conductance as ground water tracers near streams, *Ground Water*, *45*, 187-195.
- Cummins, K. W. and M. J. Klug (1979), Feeding ecology of stream invertebrates, *Ann. Rev. Ecol. System.*, *10*, 147-172.
- DeVries, P. (1997), Riverine salmonid egg burial depths: review of published data and implications for scour studies, *Can. J. Fish. Aquat. Sci.*, *54*, 1685-1698.
- DeVries, P. (2012), Salmonid influences on rivers: a geomorphic fish tail, *Geomorphology*, *157*, 66-74.

- Drake, D. C. and R. J. Naiman (2007), Reconstruction of Pacific salmon abundance from riparian tree-ring growth, *Ecol. Appl.*, 17, 1523-1542.
- Duff, J. H., and F. J. Triska (2000), Nitrogen biochemistry and surface-subsurface exchange in streams, in *Streams and groundwaters*, edited by J. B. Jones and P. J. Mulholland, pp. 197-220, Academic Press, San Diego, CA.
- Edwards, R. T. (1998), The hyporheic zone, in *River Ecology and Management: Lessons from the Pacific coastal ecoregion*, edited by R. J. Naiman and R. E. Bilby, pp. 399-429, Springer, New York.
- Elliott, A. and N. H. Brooks (1997), Transfer of nonsorbing solutes to a streambed with bed forms: Laboratory experiments, *Wat. Resour. Res.*, 33, 137-151.
- Ensign S. H. and M. W. Doyle (2005), In-channel transient storage and associated nutrient retention: Evidence from experimental manipulations, *Limn. Ocean.*, 50, 1740-1751.
- Field, R. D. and J. D. Reynolds (2011), Sea to sky: Impacts of residual salmon-derived nutrients on estuarine breeding bird communities, *Proc. Roy. Soc. B*, doi:10.1098/rspb.2010.2731.
- Fukushima, M., T. J. Quinn, and W. W. Smoker (1997), Estimation of eggs lost from superimposed pink salmon (*Oncorhynchus gorbuscha*) redds, *Can. J. Fish. Aquat. Sci.*, 55, 618-625.
- Geist, D. R. (2005), Conceptual spawning habitat model to aid in ESA recovery plans for Snake River fall Chinook salmon, 2002–2003 Annual Rep., Bonneville Power Administration, Portland, OR.
- Gende, S. M., E. D. Edwards, M. F. Willson, and M. S. Wipfli (2002), Pacific salmon in aquatic and terrestrial ecosystems, *BioScience*, 52, 917-928.

- Gottesfeld, A. S., M. A. Hassan, J. F. Tunnicliffe, and R. W. Poirer (2004), Sediment dispersion in salmon spawning streams: the influence of floods and salmon redd construction, *J. Am. Water Res. Assoc.*, *40*, 1071-1086.
- Grass, A. J. (1971), Structural features of turbulent flow over smooth and rough boundaries, *J. Fluid Mech.*, *50*, 233-255.
- Greig, S. M., D. A. Sear, and P. A. Carling (2007), A review of factors influencing the availability of dissolved oxygen to incubating salmonid embryos, *Hydro. Process.*, *21*, 323-334.
- Gresh, T., J. Lichatowich, and P. Schoonmaker (2000), An estimation of historic and current levels of salmon production in the Northeast Pacific ecoystem: Evidence of a nutrient deficit in the freshwater systems of the Pacific Northwest, *Fisheries*, *25*, 15-21.
- Hassan, M. A., A. S. Gottesfeld, D. R. Montgomery, J. F. Tunnicliffe, G. K. C. Clarke, G. Wynn, H. Jones-Cox, R. Poirer, E. MacIsaac, H. Herunter, and S. J. Macdonald (2008), Salmon-driven bed load transport and bed morphology in mountain streams, *Geophys. Res. Lett.*, *35*, doi:10.1029/2007GL032997.
- Hassan, M. A., D. Tonina, R. D. Beckie, and M. Kinnear (2014), The effects of discharge and slope on hyporheic flow in step-pool morphologies, *Hydro. Proc.* DOI: 10.1002/hyp.10155
- Healy, R. W. (1990), Simulation of solute transport in variably saturated porous media with supplemental information on modifications to the U.S. Geological Survey's Computer Program VS2D, U.S. Geol. Surv. Wat. Res. Inv. Rep. 90-4025.

- Helfield, J. M. and R. J. Naiman (2001), Effects of salmon-derived nitrogen on riparian forest growth and implications for stream productivity, *Ecology*, 82, 2403-2409.
- Heintz, R. A., B. D. Nelson, M. Larsen, L. Holland, and M. S. Wipfli, and J. P. Hudson (2004), Effects of salmon carcasses on the lipid class and fatty acid composition of juvenile coho Salmon, *Trans. Am. Fish. Soc.*, 133, 559-567.
- Holtgrieve, G. W. and D. E. Schindler (2011), Marine-derived nutrients, bioturbation, and ecosystem metabolism: reconsidering the role of salmon in streams, *Ecology*, 92, 373-385.
- Isaak, D. J., R. F. Thurow, B. E. Rieman, and D. B. Dunham (2007), Chinook salmon use of spawning patches: Relative roles of habitat quality, size, and connectivity, *Ecol. Appl.*, 17, 352-364.
- Johnston, N. T., E. A. MacIsaac, P. J. Tschaplinski, and K. J. Hall, (2004), Effects of the abundance of spawning sockeye salmon (*Oncorhynchus nerka*) on nutrients and algal biomass in forested streams, *Can. J. Fish. Aq. Sci.*, 403, 384-403.
- Kohler, A. E., A. Rugenski, and D. Taki (2008), Stream web food response to a salmon carcass analog addition in two central Idaho, USA streams, *Fresh. Biol.*, 53, 446-460.
- Koski, K. V. (2009), The fate of coho salmon nomads: the story of an estuarine-rearing strategy promoting resilience, *Ecol. and Soc.*, 14, 4 [available at <http://www.ecologyandsociety.org/vol14/iss1/art4/>]

- Lackey, R. T. (2000), Restoring wild salmon to the Pacific Northwest: chasing an illusion? in *What We Don't Know about Pacific Northwest Fish Runs - An Inquiry into Decision-Making*, edited by P. Koss and M. Katz, pp. 91-143, Portland State Univ., OR.
- Lappala, E. G., R. W. Healy, and E. P. Weeks (1987), Documentation of computer program VS2D to solve the equations of fluid flow in variably saturated porous media, U.S. Geological Survey Wat. Res. Inv. Rep 83-4099.
- Larned, S. T., V. I. Nikora, and B. . F. Biggs (2004), Mass transfer-limited nitrogen and phosphorus uptake by stream periphyton: A conceptual model and experimental evidence, *Limnol. Oceanogr.*, 49, 1992-2000.
- Lisle, T. E. (1989), Sediment transport and resulting deposition in spawning gravels, North Coastal California, *Water Resour. Res.*, 25, 1303-1319.
- Macdonald, J. S., C. A. King, and H. Herunter (2010), Sediment and salmon: the role of spawning sockeye salmon in annual bed load transport characteristics in small, interior streams of British Columbia, *Trans. Am. Fish. Soc.*, 139, 758-767.
- Malcolm, I. A., C. Soulsby, A. F. Youngson, D. M. Hannah, I. S. McLaren, and A. Thorne (2004), Hydrological influences on hyporheic water quality: implications for salmon egg Survival, *Hydrol. Proc.*, 18, 1543-1560.
- Manning, R. (1891), On the flow of water in open channels and pipes, *Trans. Inst. Civ. Eng. of Ireland*, 20, 161-207.
- Marcus, W. A., K. Roberts, L. Harvey, G. Tackman (1992), An evaluation of methods for estimating Manning's n in small mountain streams, *Mtn. Res. Dev.*, 12, 227-239.

- Mathison, O. A. (1962), The effect of altered sex ratios on the spawning of red salmon, in *Studies of Alaska Red Salmon*, edited by T. S. Y. Koo, pp. 137-245, Univ. Washington Press, Seattle.
- Mathisen, O. A., P. L. Parker, J. J. Goering, T. C. Kline, P. H. Poe, and R. S. Scalan (1988), Recycling of marine elements transported into freshwater systems by anadromous salmon, *Verh. Internat. Verein. Limnol.*, 23, 249-258.
- McMahon, T. E. and G. F. Hartman (1989), Influence of cover complexity and current velocity on winter habitat use by juvenile coho salmon (*Oncorhynchus kisutch*), *Can. J. Fish. Aquat. Sci.*, 46, 1551-1557.
- McNeil, W. J. (1964), Redd superimposition and egg capacity of pink salmon spawning beds, *J. Fish Resour. Board Can.*, 21, 1385-1396.
- Merz, J. E., J. R. Smith, M. L. Workman, J. D. Setka, and G. Mulchaey (2008), Aquatic macrophyte encroachment in chinook salmon spawning beds: lessons learned from gravel enhancement monitoring in the lower Mokelumne River, California, *N. Am. J. Fish. Mgmt.*, 28, 1568-1577.
- Michael, J. H. (1998), Pacific salmon spawner escapement goals for the Skagit River watershed as determined by nutrient cycling considerations, *Northwest Sci.*, 72, 239-248.
- Michael, J. H. (2003), Toward new escapement goals: integrating ecosystem and fisheries management goals, in *Nutrients in salmonid ecosystems: sustaining production and biodiversity*, edited by J. G. Stockner, pp. 277-282, Am. Fish. Soc. Sym. 34, Bethesda, MD.

- Montgomery, D. R., E. M. Beamer, G. R. Pess, and T. P. Quinn (1999), Channel type and salmonid spawning distribution and abundance, *Can. J. Fish. Aquat. Sci.*, 56, 377-387.
- Montgomery, D. R., J. M. Buffington, N. P. Peterson, D. Schuett-Hames, T. P. Quinn (1996), Stream-bed scour, egg burial depths, and the influence of salmonid spawning on bed surface mobility and embryo survival, *Can. J. Fish. Aquat. Sci.*, 53, 1061-1070.
- Montgomery, D. R., E. M. Beamer, G. R. Pess, and T. P. Quinn (1999), Channel type and salmonid spawning distribution and abundance, *Can. J. Fish. Aquat. Sci.*, 56, 377-387.
- Naiman, R. J., J. M. Helfield, K. K. Bartz, D. C. Drake, and J. M. Honea (2009), Pacific salmon, marine-derived nutrients, and the characteristics of aquatic and riparian ecosystems, *Am. Fish. Soc. Symp.*, 69, 395-425.
- Nogaro, G., T. Datry, F. Mermillod-Blondin, S. Descloux, and B. Montuelle (2010), Influence of streambed sediment clogging on microbial processes in the hyporheic zone, *FreshwaterBiol.*, 55, 1288-1302.
- O'Keefe, T. C. and R. T. Edwards (2002), Evidence for hyporheic transfer and removal of marine-derived nutrients in a sockeye stream in southwest Alaska, *Am. Fish. Soc. Symp.*, 33, 99-107.
- Orr, C. H., J. J. Clark, P. R. Wilcock, J. C. Finlay, and M. W. Doyle (2009), Comparison of morphological and biological control of exchange with transient storage zones in a field-scale flume, *J. Geophys. Res.*, 114, doi:10.1029/2008JG000825.

- Petticrew, E. L., J. F. Rex, and S. J. Albers (2011), Bidirectional delivery of organic matter between freshwater and marine systems: the role of flocculation in Pacific salmon streams, *J. N. Am. Benthol. Soc.*, 30, 779-786.
- Piccolo, J. J., M. D. Adkison, and F. Rue (2009), Linking Alaskan salmon fisheries management with ecosystem-based escapement goals: A review and prospectus, *Fisheries*, 34, 124-134.
- Pinay, G., T. C. O'Keefe, R. T. Edwards, and R. J. Naiman (2009), Nitrate removal in the hyporheic zone of a salmon river in Alaska, *Riv. Res. Appl.*, 25, 367-375.
- Quinn, T. P. and C. J. Foote (1994), The effects of body size and sexual dimorphism on the reproductive behavior of sockeye salmon, *Oncorhynchus nerka*, *Anim. Behavior*, 4, 751-761.
- Quinn, T. P., S. M. Carlson, S. M. Gende and H. B. Rich (2009), Transportation of Pacific salmon carcasses from streams to riparian forests by bears, *Can. J. Zool.*, 87, 195-203.
- Rex, J. F. and E. L. Petticrew (2008), Delivery of marine derived nutrients to streambeds by Pacific salmon, *Nat. Geosci.*, 1, 840-843.
- Rennie, C. D. (1998), Bed mobility of gravel rivers: Mobilization (scour) depth of chum salmon redds, and equilibrium bedload transport, M.S. thesis, Univ. British Columbia, Vancouver.
- Rex, J. F. and E. L. Petticrew (2008), Delivery of marine-derived nutrients to streambeds by Pacific Salmon, *Nat. Geosci.*, 1, 840-843.

- Rex, J. F. and E. L. Petticrew (2006), Pacific salmon and sediment flocculation: nutrient cycling and intergravel habitat quality, in *Sediment Dynamics and the Hydromorphology of Fluvial Systems*, edited by J. S Rowan, R. W. Duck, and A. Werritty, pp. 434-411, Int. Assoc. Hydrol. Sci. Press, Wallingford, U.K.
- Rinella, D. J., M. S. Wipfli, C. M. Walker, C. A. Stricker, and R. A. Heintz (2013), Seasonal persistence of marine-derived nutrients in south-central Alaskan salmon streams, *Ecosphere*, 4, 122. <http://dx.doi.org/10.1890/ES13-00112.1>.
- Roberts B. J., P. J. Mulholland, and W. R. Hill (2007), Multiple scales of temporal variability in ecosystem metabolism rates: results from 2 years of continuous monitoring in a forested headwater stream, *Ecosystems*, 10, 588-606
- Rogers, J. J. W. and W. B. Head (1961), Relationships between porosity, median size, and sorting coefficients of synthetic sands, *J. Sed. Petrol.*, 31, 467-470.
- Ryan R.J., A. I. Packman, and S. S. Kilham (2007), Relating phosphorus uptake to changes in transient storage and streambed sediment characteristics in headwater tributaries of Valley Creek, an urbanizing watershed, *J. of Hydrol.*, 336, 444-457.
- Savant, A. S., D. D. Reible, and L. J. Thibodeaux (1987), Convective transport within stable river sediments, *Water Resour. Res.*, 23, 1763-1768.
- Scheuerell, M. D., J. W. Moore, and D. E. Schindler (2007), Varying effects of anadromous sockeye on the trophic ecology of two species of resident salmonids in southwest Alaska, *Fresh. Biol.*, 52, 1944-1956.
- Schindler, D. E., M. D. Scheuerell, J. W. Moore, S. M. Gende, T. B. Francis, and W. J. Palen (2003), Pacific salmon and the ecology of coastal ecosystems, *Frontiers Ecol. Env.*, 1, 31-37.

- Simons D. B. and F. Sentürk (1992), *Sediment transport technology, water and sediment Dynamics*, BookCrafters, Inc., Chelsea, MI.
- Stockner, J. (Ed.) (2003), *Nutrients in Salmonid Ecosystems: Sustaining Production and Biodiversity*, American Fisheries Society, Bethesda, MD.
- Strickler, A. (1923), Beitrage zur Frage der Geschwindigkeits-formel und der Rauhegkeitszahlen fur Strome, Kanale und geschlossene Leitungen, Bern, Switzerland, Mitt. Eidgenossischen Amtes Wasserwirtschaft, no. 16.
- Thomas S.A., H. M. Valett, J. R. Webster, and P. J. Mulholland (2003) A regression approach to estimating reactive solute uptake in advective and transient storage zones of stream ecosystems, *Adv. Wat. Resour.*, 26, 965-976.
- Thibodeaux L. J. and J. D. Boyle (1987), Bedform-generated convective transport in bottom sediment, *Nature*, 325, 341-343.
- Tonina, D. (2012), Surface water and streambed sediment interaction: The hyporheic exchange, in *Fluid mechanics of environmental interfaces*, edited by C. Gualtieri and D. T. Mihailović, pp. 255-294, CRC Press, Taylor & Francis Group, London, UK.
- Tonina, D. and J. M. Buffington (2009), A three-dimensional model for analyzing the effects of salmon redds on hyporheic exchange and egg pocket habitat, *Can. J. Fish. Aquat. Sci.*, 66, 2157-2173.
- Tóth, J. (1963), A theoretical analysis of groundwater flow in small drainage basins. *J. Geophys. Res.*, 68, 4795-4812.
- Triska, F. J., V. C. Kennedy, R. J. Avanzino, G. W. Zellweger, and K. E. Bencala (1989), Retention and transport of nutrients in a third-order stream in Northwestern California: Hyporheic processes, *Ecology*, 70, 1893-1905.

- Valett H. M., J. A. Morrice, and C. N. Dahm (1996), Parent lithology, groundwater-surface water exchange and nitrate retention in headwater streams, *Limn. Oceanol.*, *41*, 333-345.
- Verspoor, J. J., D. C. Braun, and J. D. Reynolds (2010), Quantitative links between Pacific salmon and stream periphyton, *Ecosystems*, DOI: 10.1007/s10021-010-9371-0.
- White D. S. (1993), Perspectives on defining and delineating hyporheic zones, *J. N. Am. Bentho. Soc.*, *12*, 61-69.
- Whiteway, S. L., P. M. Biron, A. Zimmermann, O. Venter, and J. W. A. Grant (2010), Do in-stream restoration structures enhance salmonid abundance? A meta-analysis, *Can. J. Fish. Aquat. Sci.*, *67*, 831-841.
- Wipfli, M. S. (1997), Terrestrial invertebrates as salmonid prey and nitrogen sources in streams: contrasting old-growth and young-growth riparian forests in southeastern Alaska, USA, *Can. J. Fish. Aq. Sci.*, *54*, 1259-1269.
- Wipfli, M. S., J. P. Hudson, and J. P. Caouette (2004), Restoring productivity of salmon-based food webs: Contrasting effects of salmon carcass and salmon carcass analog additions on stream-resident salmonids, *Trans. Am. Fish. Soc.*, *133*, 1440-1454.
- Wipfli, M. S., J. P. Hudson, J. P. Caouette, and D. T. Chaloner (2003), Marine subsidies in freshwater ecosystems: Salmon carcasses increase the growth rates of stream-resident salmonids, *Trans. Am. Fish. Soc.*, *132*, 371-381.
- Wipfli, M. S., J. Hudson, D. T. Chaloner, and J. P. Caouette (1999), Influence of salmon spawner densities on stream productivity in Southeast Alaska, *Can. J. Fish. Aq. Sci.*, *56*, 1600-1611.

Wolman, M. G. (1954), A method of sampling coarse river-bed material, *Eos Trans AGU*, 35, 951-956.

Worman A., A. I. Packman, H. Johansson, and K. Jonsson (2002), Effect of flow-induced exchange in hyporheic zones on longitudinal transport of solutes in streams and rivers, *Water Resour. Res.*, 38, 1-15.

Zimmermann, A. E. and M. F. Lapointe (2005), Intergranular flow velocity through salmonid redds: sensitivity to fines infiltration from low intensity sediment transport events, *Riv.Res. Appl.*, 21, 865-881.

Appendix A

Shear Stress Partitioning

We determined τ_{avg} by partitioning roughness between the flume walls and granular bed with a modification of the sidewall correction procedure of *Vannoni and Brooks* [1957]. In this analysis, the Darcy-Weisbach friction factor (f) and the Reynolds number (Re) are used with a modification of the Colebrook-White equation by *Cheng* [2011] to estimate friction from the hydrodynamically smooth walls of the flume (f_w)

$$f = \frac{8gRS}{\bar{u}^2} \quad (\text{A1})$$

$$Re = \frac{4R\bar{u}}{\nu} \quad (\text{A2})$$

$$\frac{1}{\sqrt{f_w}} = -2\text{Log} \left(2.51 / \frac{Re}{f} f_w^{1.5} \right) \quad (\text{A3})$$

where R is the hydraulic radius ($wh / (w+2h)$), S is the flume slope, and ν is kinematic viscosity ($1.52 \times 10^{-6} \text{ m}^2 \text{ s}^{-1}$ at 5°C). Measurements of h were within ± 2 cm of the mean value due to the water surface fluctuating during experiments. Values of f and f_w are used to isolate friction on the granular bed (f_b)

$$f_b = f + \frac{2h}{w}(f - f_w) \quad (\text{A4})$$

where w is flow width. Values of f_b , f , and R are then used to determine the hydraulic radius associated with grain roughness (R_b)

$$R_b = \frac{f_b}{f}R \quad (\text{A5})$$

which allows determination of τ_{avg} on the bed

$$\tau_{avg} = \rho g R_b S. \quad (\text{A6})$$